A Diffuse Interface Model of Transport Limited Electrochemistry in Two-Phase Fluid Systems with Application to Steelmaking

by

David Dussault

M. S., Mechanical Engineering (2002)

Submitted to the Department of Mechanical Engineering
in Partial Fulfillment of the Requirement for the Degree of
Master of Science in Mechanical Engineering

at the

Massachusetts Institute of Technology

February 2002

Signature of Author . . . . . .
Department of Mechanical Engineering
Jan 11, 2002

Certified by. . . . . .
Adam C. Powell
Assistant Professor of Materials Engineering

Accepted by. . . . . .
Ain A. Sonin
Chairman, Department Committee on Graduate Students

Abstract

Electric Field-Enhanced Smelting and Refining is a process for accelerating the rate of carbon removal from steel in a steelmaking reactor. It is proposed as an alternative or a complement to the basic oxygen process. Electrodes are inserted into the metal and slag phases. The carbon is removed from the steel to form CO gas at the anodic interface, and the Fe^{2+} in the slag is removed to form Fe at the cathodic interface. The overall reaction rate is limited by the transport of Fe^{2+} to the cathode. To accelerate the reaction, the overall cathode mass transfer coefficient must be increased, and to do so requires an understanding of the kinetics surrounding the cathode.

An Fe-FeO-Fe electrochemical system is used as a simplified model of the steelmaking process. In this project two mathematical models of the system are developed: the classical sharp interface model and a diffuse interface model. In the diffuse interface model, the Cahn-Hilliard Equation is extended to include fluid flow and migration of ionized species due to an electric field. The voltage field is solved for using conservation of charge. Asymptotic solutions and scaling results are derived to explain phenomena surrounding the cathode. The diffuse interface model is discretized using the finite-difference method. The resulting system of nonlinear algebraic equations are solved using a Newton-Krylov solver.

The simplified 2D Fe-FeO-Fe system does not capture all phenomena of the physical slag-metal system, but does provide a foundation for a more comprehensive model to be developed in the future. The methodology developed here for coupling transport limited electrochemistry with transport equations is fundamental in that the extension to more complex systems is limited only by the development of a free energy model and the knowledge of system properties.

Acknowledgements

First I would like to thank my advisor, Professor Adam Powell. Thanks for always taking the time to answer my questions. When I was your only student and I didn't know where to start with mostly everything in the lab, you always made time for me. Thanks for being supportive and trusting my work. When the project took a turn for the worst, you supported my decision on how we could change things. Your flexibility as an advisor sometimes made things harder for me in the short term, but helped me to be a better researcher and how to solve long term problems. You were always more concerned about my well being than the status of the project. Perhaps the most important thing that I'll take from my time with you is not to lose sight of humanity when dealing with science.

To Professor McKelliget and Dr. Gerardo Trapaga, thank you for helping me in my transition into MIT. You introduced me to Professor Powell, and then backed off. Things could have been allot harder for me. You let me pretty much drop the project that we were working on, so I could focus on my studies at MIT. I probably couldn't have gotten through my first semester here without your help.

Raymundo, thanks for your help with thermodynamics. You're a good teacher. I think we complimented each other well. To my lab mates Robert and Bo, thanks for your help with Materials Science and your help with the computers. You guys were my best resources. Chris, we got through are classes together. The study sessions were great. Thanks for the talks too. Professor Sonin, thanks for agreeing to be my ME reader. Gloria, you could read me like a book. Thanks for helping me through some tough times.

To my family and friends, thanks for giving me space so I could focus at school. You let me slip into my own world at school for weeks at a time. I think that I had to do that to get through things here. Then I'd have some time off and everything would be cool again. I couldn't be around physically or mentally all the time, and you never held it against me. Thanks.

Last, I would like to thank the NIST Green's function working group for supporting part of this research.

Contents

List of Figures

Chapter 1

Introduction

1.1 Introductory Remarks

The objective of this thesis is to develop a mathematical model which describes two-phase fluid/fluid systems with transport limited electrochemical reactions. There are many applications for the model. The application described in this paper is a new method for low carbon steel refining known as the electric field enhanced smelting and refining of steel. In this section, relevant previous modeling methods are given, and the extension of the current modeling methods to the system of interest is outlined. Following that is a description of the physical system along with a brief background to steelmaking. Finally, an overview of the entire thesis is given.

1.2 Modeling and Simulation

The model developed in this thesis is for a two phase isothermal liquid/liquid system undergoing transport limited electrochemical reactions. In order to avoid interface tracking and interface boundary conditions, a diffuse interface phase-field model was used. In the phase-field method, a composition field variable $C(x, y, z)$ varies from 0 in one phase to 1 in the other phase. The interface spans a finite region and is represented by fractions of C.

The phase-field method is based on the Cahn-Hilliard equation which is a diffuse interface

diffusion equation originally applied to spinoidal decomposition [16]. The Cahn-Hilliard equation was extended to fluid/fluid systems by Jacqmin [9, 10] by using a modified stress tensor to account for surface tension. A general phase-field model for non-isothermal binary fluid/solid systems was developed by Sekerka and others in [18]. Papers on phase-field application and theory include [19, 20, 21, 22]. For a rigorous comparison of diffuse interface and sharp interface descriptions of fluid systems including heat transfer see Anderson and McFadden [15]. The Cahn-Hilliard free energy formulation was extended to general multi-component systems by Hoyt [17]. Multi-phase, multi-component systems are an area of active research.

In this thesis, the diffuse interface model developed by Jacqmin for two phase, two component, liquid/liquid, isothermal, flow is extended to include transport limited electrochemical reactions. To couple the transport of chemical species with electrochemistry, a migration term was added to the diffusion of chemical species equation. The Cahn-Hilliard free energy model allowed for inter-phase diffusion. Because the electrochemistry is in the transport limited region, the constitutive exponential current-voltage relations reduce to linear current-mass flux relations which reduces coupling in the governing equations. The voltage field is solved for using conservation of charge. Assuming rapid charge redistribution, the conservation of charge equation reduces to an equation for zero divergence of current flux and implicitly allows for nonuniform charge density.

1.3 Current Steelmaking Method

Steel is an iron alloy consisting of approximately 95 to 99 wt% iron, 0.01 to 2 wt% carbon, and traces of other elements such as magnesium, phosphorus, sulfur, silicon, nickel, and chromium. The amount of carbon has a direct influence on the mechanical properties of the steel such as yield strength and ductility. In general as the percentage of carbon decreases, yield strength decreases and ductility increases. For example, steel used for tools is 1.35 wt% carbon and steel used for construction is 0.25 wt% carbon. The process by which steel is derived from iron ore consists of primarily two steps: the blast furnace and the basic oxygen process. For low carbon

Figure 1.1: Slag/metal system

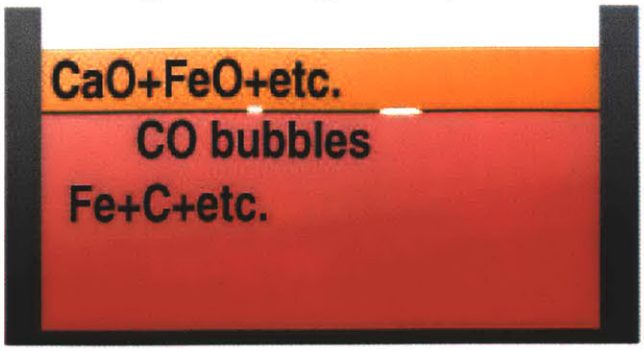

steel, the steel is further processed in what is called vacuum degassing.

In the blast furnace iron ore enters along with lime (CaO), coke (refined coal) and hot air. The products react over a range of 200 to 2000 degrees C. The exiting products include hot gases such as CO and CO_2, molten iron, and molten slag (a mixture of oxide impurities left over from the iron ores). The density of slag is on the order of $1/2$ that of steel. Thus, the slag and steel separate mechanically. The resulting slag is discarded, while the resulting iron, referred to as pig iron, is on the order of 5 wt% carbon.

The slag/melt system is shown in Figure 1.1. In the basic oxygen process a jet of oxygen is applied to the slag layer. The speed of the oxygen gas is such that the slag gets pushed aside and the gas reaches the iron melt where it combines with carbon to form carbon monoxide.

$$O_2(gas) + 2C(metal) \rightarrow 2CO(bubble) \tag{1.1}$$

However, the oxygen also reacts with the iron in the melt to form iron oxide.

$$O_2(gas) + 2Fe(metal) \rightarrow 2FeO(slag) \tag{1.2}$$

The loss of iron from the melt to the slag is an inefficiency inherent to this method. The presence of FeO in the slag leads to slag foaming and corrosion of cylinder walls, and the increase in slag mass leads to environmental issues. Discarded slag contains typically 20 to 25 wt% iron. The

Figure 1.2: Slag/metal system with electrodes

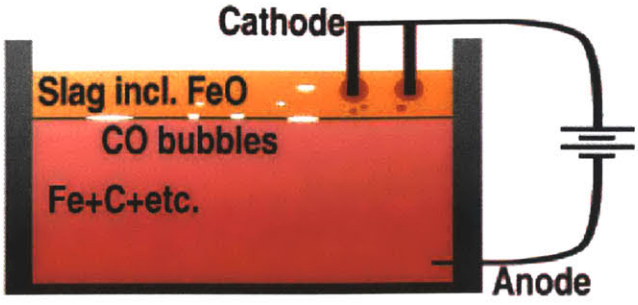

resulting steel is on the order of 0.1 wt% carbon.

In the vacuum degassing stage, the carbon content is reduced further. In this stage a vacuum is pulled over the slag-steel system. Because there is a low partial pressure of CO there is a thermodynamic driving force for CO bubbles to form and escape (along with traces of all other elements in the system). The system is not heated during the vacuum stage. Instead, the system temperature is elevated before the vacuum is applied such that the steel remains molten during the process. The resulting steel is on the order of 0.01 wt% carbon. The inefficiencies associated with this step are the energy associated with elevating the steel temperature, the energy associated with maintaining the vacuum, and the impurity of the CO removed . The carbon and oxygen must diffuse through a concentration boundary layer to reach the interface before forming CO. Thus, the process is limited by a diffusion time-scale.

1.4 Proposed Changes

A new process for refining steel known as 'Electric Field-Enhanced Refining of Steel' was developed by Professor Uday Pal of Boston University [13]. The idea behind this system is to generate CO from the oxygen already in the slag. The proposed system is shown in Figure 1.2. There is no external supply of oxygen. An external circuit is added to the system. The cathode lies in the slag phase, while the anode lies in the melt. Because iron is a good electrical conductor, the entire melt effectively becomes the anode. The FeO in the slag exists in ionic form, Fe^{2+} and O^{2-}. There are two interfaces where electrochemical reactions occur, the slag/cathode interface

and the slag/anode interface. With this configuration there is a thermodynamic driving force for electrochemical reactions to occur that are consistent with the current through the circuit. Electrons flow from the anode to the cathode. At the cathodic interface Fe is formed on the electrode.

$$Fe^{2+}(slag) + 2e^{-} \rightarrow Fe(melt) \tag{1.3}$$

At the anodic interface CO is formed.

$$O^{2-}(slag) + C(melt) \rightarrow CO(gas) + 2e^{-} \tag{1.4}$$

Thus, CO is formed without an external supply. The inefficiencies described above are not present in this process. The Fe that is formed on the cathode falls back into the melt (the mechanics are described in Chapter 2). Therefore, Fe is recovered from the slag instead of being lost to the slag, and there is a decrease in slag mass instead of an increase in slag mass.

The current savings associated with this process are as follows. The decrease of 20 wt% FeO in slag translates roughly into a savings of 179 MJ per metric ton of steel or \$2.33 per metric ton of steel. There are 800 million tons of steel produced per year. Therefore, the total savings would be $143 * 10^{15} J$ per year or \$1.8 billion per year.

1.5 Overview of Thesis

The physical electrochemical slag/metal system described above is represented throughout the thesis by a simplified Fe-FeO electrochemical system. Both systems are referred to throughout the thesis. However, the chapters intentionally display a great deal of independence. The model developed here builds on previous works, but still does not capture all phenomena associated with typical applications. The independence is designed to benefit to the development of future work.

Chapter 2 introduces the classical sharp interface model for general multicomponent fluid

electrochemical systems. The conservation equations are given without simplifications. Interface conditions are derived based on conservation principles. Assuming that the reader is familiar with thermodynamics, an introduction to electrochemisty is given. Constitutive current-voltage relations are derived and the transport limited case is shown as an asymptotic limit. Finally, for the physical slag/metal system, the governing equations are solved for a number of simplified asymptotic cases giving rise to system length, time, and velocity scales.

Chapter 3 introduces the diffuse interface model for a two component liquid/liquid system and applies it to the Fe-FeO system. The Cahn-Hilliard equation is derived, and the coefficients are related to system properties. The phase-field model is derived by scaling parameters in the Cahn-Hilliard equation while retaining the system's surface tension. The diffuse interface governing equations are first presented in general and then are applied to the Fe-FeO system. Voltage is solved using conservation of charge. Given that the system is transport limited and that there is rapid charge redistribution, a number of terms in the conservation of charge equation are neglected and the coupling of the equations is significantly reduced.

The resulting system of equations are solved numerically. Chapter 4 describes in detail the numerical methods used. The finite difference method was used for space and the Crank-Nicholson scheme was used for time. Shadow nodes were used for symmetry boundary conditions. Once discretized, the system of partial differential equations becomes a system of nonlinear algebraic equations. Newton's method was used for the nonlinear solver and the generalized conjugate residual algorithm was used for the linear solver. Together they are commonly referred to as a Newton-Krylov solver. The solver allows for a finite-difference approximation to the Jacobian matrix. PETSc (The Portable, Extensible Toolkit for Scientific Computing), a collection of C libraries, was used for managing data storage and for parallel processing.

Chapter 5 contains numerical simulations of case studies. Each case study is designed to capture a single phenomenon associated with physical system. The first simulation demonstrates interface diffusion and the effect that interface scaling has on the output. The second simulation demonstrates diffusion coupled with migration. Interface motion due to an electric field is

displayed along with the growth of interface perturbations. The third simulation demonstrates two phase surface tension driven convection by looking at an oscillating 2D drop. And the fourth simulation demonstrates two phase surface tension driven convection in the presence of a gravitational field. The same 2D drop is used, and the interface profile agrees with analytical calculations.

Chapter 6 and Chapter 7 are the discussion and conclusion respectively. The key assumptions are revisited. Limitations of the model are discussed. The application of the model to other physical systems is briefly described. Future development of the model to broaden the range of application is discussed. Simulation results are summarized.

Chapter 2

Sharp Interface Model

2.1 Introductory Remarks

The slag/steel system is represented here by a two-phase fluid continuum. There are two ways of modeling the system, the sharp interface model (given in this chapter) and the diffuse interface model (given in Chapter 4). In the sharp interface model the governing equations are applied to each separate phase, and boundary conditions are set at the internal interfaces. In the diffuse interface model the governing equations are applied to all phases at once, so boundary conditions are not needed at the internal interfaces. Of course, for both methods boundary conditions must be set on the outer surfaces.

This Chapter follows the sharp interface model. First, the governing equations are given for as general a case as possible. For this reason some modeling which is problem dependent is left out. Next, a number of instabilities associated with the slag/metal system are described and asymptotic solutions are derived.

2.2 Governing Equations

The equations that follow are for a two-dimensional, single-phase, compressible, multi-component, ionic fluid with variable properties. The field variables associated with this system are:

1. u, x-component of velocity
2. v, y-component of velocity
3. p, pressure
4. ω_i, mass fraction of species i
5. ϕ, voltage
6. ρ_f, free charge density (free charge per unit volume of fluid) (this parameter is introduced below)

Six governing equations are needed. The fluid has a density ρ, a viscosity η, and a velocity $\vec{V}$. In general there will be a gravitational field characterized by the gravitational acceleration $\vec{g}$. The first equation is conservation of x-direction momentum.

$$\begin{aligned} \frac{\partial}{\partial t}(\rho u) + \vec{\nabla} \bullet \left(\rho \vec{V} u\right) &= -\frac{\partial p}{\partial x} + \vec{\nabla} \bullet \left(\eta \vec{\nabla} u\right) + \rho g_x \\ &\quad + \vec{\nabla} \bullet \left(\eta \frac{\partial \vec{V}}{\partial x}\right) - \frac{2}{3}\frac{\partial}{\partial x}\left(\eta \vec{\nabla} \bullet \vec{V}\right) \end{aligned} \tag{2.1}$$

The second equation is conservation of y-direction momentum.

$$\begin{aligned} \frac{\partial}{\partial t}(\rho v) + \vec{\nabla} \bullet \left(\rho \vec{V} v\right) &= -\frac{\partial p}{\partial y} + \vec{\nabla} \bullet \left(\eta \vec{\nabla} v\right) + \rho g_y \\ &\quad + \vec{\nabla} \bullet \left(\eta \frac{\partial \vec{V}}{\partial y}\right) - \frac{2}{3}\frac{\partial}{\partial y}\left(\eta \vec{\nabla} \bullet \vec{V}\right) \end{aligned} \tag{2.2}$$

The first two viscous stress terms in the above two equations follow the familiar diffusion form and for a fluid with constant properties are the only remaining viscous terms. The other viscous stress terms are due to variable viscosity and incompressibility. The third equation is conservation of mass.

$$\frac{\partial \rho}{\partial t} + \vec{\nabla} \bullet \left(\rho \vec{V}\right) = 0 \tag{2.3}$$

The fourth equation is conservation of species.

$$\frac{\partial}{\partial t}\left(\rho \omega_i\right) + \vec{\nabla} \bullet \left(\rho \vec{V} \omega_i\right) = -\vec{\nabla} \bullet \left(\vec{j_i}\right) \tag{2.4}$$

There is no generation of species in this formulation. The reactions occur at the slag/metal interface and are introduced through boundary conditions. $\vec{j_i}$ is the mass flux of species i (units are $\frac{kg}{m^2 * s}$), where the flux is measured relative to the bulk velocity (diffusion flux). The molar flux of species i $\vec{J}$ (units are $\frac{moles}{m^2 * s}$) is given by [1]

$$\vec{J_i} = -D_i \vec{\nabla} c_i - \frac{z_i F}{RT} D_i c_i \vec{\nabla} \phi \tag{2.5}$$

The first term represents diffusion due to concentration gradients, and the second term represents diffusion due to the effect of an electric field on an ionic component. Here D_i is the diffusion coefficient of species i (units are $\frac{m^2}{s}$), z_i is the charge of species i (units are mole of excess protons per mole of species i, for example, $z_{Fe^{2+}} = 2$ and $z_{O^{2-}} = -2$), F is Faraday's constant ($F = 96485 \frac{C}{mole}$, where mole corresponds to mole of excess proton), R is the molar gas constant ($R = 8.314 \frac{J}{mol * K}$), and T is absolute temperature ($T = 1900K$). Mass flux is related to molar flux through the molar mass M_i (units are mass of i per mole of i).

$$\vec{j_i} = M_i \vec{J_i} \tag{2.6}$$

Therefore, the conservation of species equation becomes

$$\frac{\partial}{\partial t}\left(\rho \omega_i\right) + \vec{\nabla} \bullet \left(\rho \vec{V} \omega_i\right) = M_i \vec{\nabla} \bullet \left(D_i \vec{\nabla} c_i + \frac{z_i F}{RT} D_i c_i \vec{\nabla} \phi\right) \tag{2.7}$$

The fifth equation is Gauss's Law inside matter, which introduces ρ_f defined above.

$$\vec{\nabla} \bullet \vec{D} = \rho_f \tag{2.8}$$

$\vec{D}$ is called the electric displacement, and for a linear media it is related to the electric field $\vec{E}$ through

$$\vec{D} = \varepsilon \vec{E} \tag{2.9}$$

where ε is the permittivity of the media (units are $\frac{C^2}{N*m^2}$). Combining gives

$$\vec{\nabla} \bullet \varepsilon \vec{E} = \rho_f \tag{2.10}$$

The sixth and last governing equation is conservation of charge.

$$\frac{D\rho_f}{Dt} = -\vec{\nabla} \bullet \vec{J_c} \tag{2.11}$$

The substantial derivative is used to adjust for the transport of charge due to convection. $\vec{J_c}$ is the flux of charge (units are $\frac{C^2}{m^2*s}$). The charge flux $\vec{J_c}$ is related to the molar flux $\vec{J_i}$ through

$$\vec{J_c} = \sum \vec{J_i} z_i F \tag{2.12}$$

Combining gives

$$\frac{D\rho_f}{Dt} = -\vec{\nabla} \bullet \left(\sum \vec{J_i} z_i F \right) \tag{2.13}$$

where $\vec{j_i}$ is given by Equation 2.5.

2.3 Interface Conditions

First, the velocity interface condition is derived by a mass balance at the interface. Consider the slag/metal system shown in Figure 2.1. The interface moves with a velocity $\vec{V}_{int}$. The

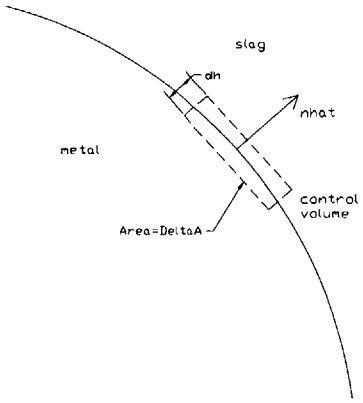

Figure 2.1: Slag/metal Interface

unit vector normal to the interface is given by $\vec{n}$, where $\vec{n}$ is positive when pointing in the slag direction. A infinitesimal cylindrical control volume of height dh and cross-sectional area ΔA encloses a small portion of the interface. The control volume moves with the interface, so mass enters on the slag side and mass leaves on the metal side (according to this positive sign convention). Applying conservation of mass gives

$$\rho_{slag}\left(\vec{V}_{int} - \vec{V}_{slag}\right) \bullet \vec{n} = \rho_{metal}\left(\vec{V}_{int} - \vec{V}_{metal}\right) \bullet \vec{n} \tag{2.14}$$

Or, in terms of the normal components of the vectors

$$\rho_{slag}\left(V_{int,n} - V_{slag,n}\right) = \rho_{metal}\left(V_{int,n} - V_{metal,n}\right) \tag{2.15}$$

The tangential velocity is given by the no-slip condition.

$$V_{metal,tangent} = V_{int,tangent} = V_{slag,tangent} \tag{2.16}$$

The normal component of the interface velocity is found by applying conservation of electrons at the interface. The interface moving through a distance dx during a time dt. A number of electrons N_{e^-} enter the control volume from the metal, and a number of Fe^{2+} atoms $N_{Fe^{2+}}$ enter the control volume from the slag. They are related by

$$N_{e^-} = 2N_{Fe^{2+}} = 2\frac{N_{Fe^{2+}}}{Vol}dx\Delta A \tag{2.17}$$

Dividing through by dt and rearranging gives

$$V_{int,n} = \frac{JV_s}{2F} \tag{2.18}$$

where V_s is the molar volume of slag (units are volume of slag per mole of Fe), and J is the current density (units are C / unit area / unit time). There will be a discontinuity in pressure across the interface due to surface tension. The relation is

$$\Delta p = \sigma\left(\frac{1}{R_1} + \frac{1}{R_2}\right) \tag{2.19}$$

Where σ is the surface tension and R_1 and R_2 are the principal radii of curvature. The last interface condition involves ρ_f and ϕ. Writing Gauss's law in integral form

$$\oint_S \vec{D} \bullet \vec{n}\, dA = Q_{f,enclosed} \tag{2.20}$$

where $Q_{f,enclosed}$ is the total charge enclosed in the control volume shown in FIGURE. Simplifying gives

$$D_{n,slag} - D_{n,metal} = \sigma_f \tag{2.21}$$

where σ_f is the surface free charge density on the interface (units are charge / unit area). Continuing, there will be a discontinuity in the D field and a corresponding discontinuity in the E field which would imply a discontinuous gradient on voltage. However the voltage is

continuous across the interface. That is,

$$\phi_{slag} = \phi_{metal} \tag{2.22}$$

2.4 Electrochemistry

Electrochemistry is the science of chemical reactions involving electron transfer at an interface. A general electrochemical reaction has the form

$$O + ne = R \tag{2.23}$$

where n is called the electron transfer number. The reaction occurs at an electrode/electrolyte interface. The electrode is an electrical conductor, and the electrolyte is an ionic conductor. The electrode at which reduction (reduction in oxidation number) takes place is called the cathode, and the electrode at which oxidation (increase in oxidation number) takes place is called the anode. Referring to the slag/metal system described in Section 1.4, Fe^{2+} is reduced to form Fe on the cathode

$$Fe^{2+}(slag) + 2e^- \rightarrow Fe(melt) \tag{2.24}$$

and O^{2-} is oxidized to form CO at the anode.

$$O^{2-}(slag) + C(melt) \rightarrow CO(gas) + 2e^- \tag{2.25}$$

The overall chemical reaction of the system is

$$O^{2-}(slag) + C(melt) \rightarrow CO(gas) + 2e^- \tag{2.26}$$

2.4.1 Thermodynamics

In this section energy principles are applied to electrochemical systems in equilibrium. The resulting equation known as the Nernst equation relates the cell voltage to the concentrations of each species.

Consider the general chemical reaction

$$aA + bB \rightarrow cC + dD \tag{2.27}$$

The free energy change associated with this reaction is

$$\Delta G = \Delta G^0 + RT \ln \left(\frac{a_C^c a_D^d}{a_A^a a_B^b} \right) \tag{2.28}$$

The free energy is also equal to the work done on the electrons as they pass through the circuit.

$$\Delta G = -W_{rev} = -nF\varepsilon \tag{2.29}$$

where F is Faraday's constant, and ε is the circuit voltage (cell emf). Inserting Equation 2.29 into Equation 2.28 gives Nernst Equation.

$$\varepsilon = \varepsilon^0 - \frac{RT}{nF} \ln \left(\frac{a_C^c a_D^d}{a_A^a a_B^b} \right) \tag{2.30}$$

where ε^0 is the standard potential of the reaction. Considering a non-ideal solution

$$\begin{aligned} \varepsilon &= \varepsilon^0 - \frac{RT}{nF} \ln \left(\frac{\gamma_C^c \gamma_D^d}{\gamma_A^a \gamma_B^b} \right) - \frac{RT}{nF} \ln \left(\frac{[C]^c [D]^d}{[A]^a [B]^b} \right) \\ &= \varepsilon^{0'} - \frac{RT}{nF} \ln \left(\frac{[C]^c [D]^d}{[A]^a [B]^b} \right) \end{aligned} \tag{2.31}$$

where $\varepsilon^{0'}$ is called the formal potential. For the general electrochemical reaction,

$$\varepsilon_{eq} = \varepsilon^{0'} - \frac{RT}{nF} \ln \left(\frac{C_R^{eq}}{C_O^{eq}} \right) \tag{2.32}$$

2.4.2 Kinetics

In this section constitutive equations are given which describe electrochemical systems that are not in equilibrium. The resulting equation relates the current through the circuit to the applied voltage and the concentrations of each species.

Consider the general electrochemical reaction

$$O + ne \rightleftharpoons R \tag{2.33}$$

The arrows are used to emphasize the idea that the system is not in equilibrium. Instead forward and backward reactions are considered to be happening simultaneously.

$$v_f = k_f C_O \tag{2.34}$$

$$v_b = k_b C_R \tag{2.35}$$

v_f and v_b are the reaction rates in the forward and backward direction (units are $\frac{mole}{m^2 * s}$), k_f and k_b are rate constants (units are $\frac{m}{s}$), and C_O and C_R are the the concentrations of each species at the interface. The net reaction rate is given by

$$v_{net} = v_f - v_b = k_f C_O - k_b C_R \tag{2.36}$$

If the system is in equilibrium, then $v_{net} = 0$

$$v_{net} = 0 = k_f C_O^{eq} - k_b C_R^{eq} \Rightarrow k_f C_O^{eq} = k_b C_R^{eq} \tag{2.37}$$

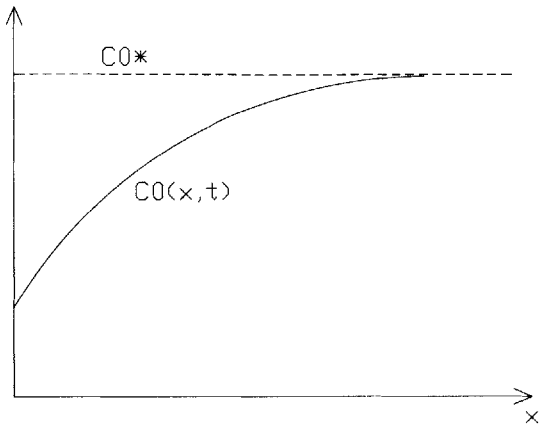

Figure 2.2: Concentration profile in slag

The reaction rate at equilibrium is called the exchange velocity v_0.

$$v_0 = k_f C_O^{eq} = k_b C_R^{eq} \tag{2.38}$$

The reaction rate is related to current by using Faraday's Law.

$$v = \frac{1}{A}\frac{dN}{dt} = \frac{1}{A}\frac{d}{dt}\left(\frac{Q}{nF}\right) = \frac{i}{nFA} \tag{2.39}$$

Consider the one dimensional profile shown in Figure 2.2. The rate of forward reaction is given by

$$v_f = k_f C_0\,(x = 0, t) = \frac{i_{cathodic}}{nFA} \tag{2.40}$$

and the rate of backward reaction is given by

$$v_f = k_b C_R\,(x = 0, t) = \frac{i_{anodic}}{nFA} \tag{2.41}$$

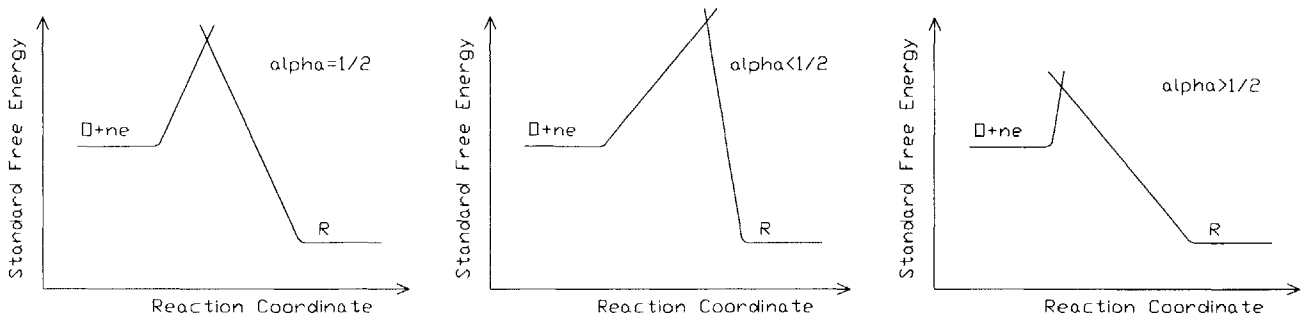

Figure 2.3: Transfer coefficient and free energy

The rate constants are related to the voltage by

$$k_f = k_f^0 \exp\left(-\frac{\alpha n F \varepsilon}{RT}\right) \tag{2.42}$$

$$k_b = k_b^0 \exp\left((1-\alpha)\frac{nF\varepsilon}{RT}\right) \tag{2.43}$$

where k_f^0 and k_b^0 are the rate constants at $\varepsilon = 0$ for the voltage scale in use, and α, the transfer coefficient, is a measure of asymmetry of the activation barrier of the free energy curve of the reaction. The effect of α is shown qualitatively in Figure 2.3. If the system is in equilibrium and the solution is such that $C_O^* = C_R^*$, then the Nernst Equation gives $\varepsilon = \varepsilon^{0'}$. Under these conditions 2.37 becomes

$$k_f C_O^{eq} = k_b C_R^{eq} \Rightarrow k_f = k_b \tag{2.44}$$

Using Equations 2.42 and 2.43

$$k_f^0 \exp\left(-\frac{\alpha n F \varepsilon^{0'}}{RT}\right) = k_b^0 \exp\left((1-\alpha)\frac{nF\varepsilon^{0'}}{RT}\right) = k^0 \tag{2.45}$$

where k^0 is called the standard rate constant. Therefore, $k^0 = k_f\left(\varepsilon^{0'}\right) = k_b\left(\varepsilon^{0'}\right)$. Inserting the above equation into Equations 2.42 and 2.43 gives

$$k_f = k^0 \exp\left(-\frac{\alpha n F}{RT}\left(\varepsilon - \varepsilon^{0'}\right)\right) \tag{2.46}$$

$$k_b = k^0 \exp\left((1-\alpha)\frac{nF}{RT}\left(\varepsilon - \varepsilon^{0'}\right)\right) \tag{2.47}$$

The positive sign convention for the net current is the cathodic direction.

$$i = i_{cathodic} - i_{anodic} \tag{2.48}$$

Using Equations 2.40 and 2.41

$$i = nFAk_f C_0\left(x=0,t\right) - nFAk_b C_R\left(x=0,t\right) \tag{2.49}$$

Using Equations 2.46 and 2.47 gives the complete current voltage characteristic of the electrode.

$$\begin{aligned} i = {} & nFAk^0 C_0\left(x=0,t\right)\exp\left(-\frac{\alpha nF}{RT}\left(\varepsilon - \varepsilon^{0'}\right)\right) \\ & -nFAk^0 C_R\left(x=0,t\right)\exp\left((1-\alpha)\frac{nF}{RT}\left(\varepsilon - \varepsilon^{0'}\right)\right) \end{aligned} \tag{2.50}$$

At equilibrium the current-voltage relation should reduce to the Nernst Equation. At equilibrium, $i = 0$, $C_R\left(0,t\right) = C_R^*$, and $C_O\left(0,t\right) = C_O^*$. The equation reduces to

$$C_0^* \exp\left(-\frac{\alpha nF}{RT}\left(\varepsilon_{eq} - \varepsilon^{0'}\right)\right) = C_R^* \exp\left((1-\alpha)\frac{nF}{RT}\left(\varepsilon_{eq} - \varepsilon^{0'}\right)\right) \tag{2.51}$$

$$\Rightarrow \exp\left(\frac{nF}{RT}\left(\varepsilon_{eq} - \varepsilon^{0'}\right)\right) = \frac{C_O^*}{C_R^*} \tag{2.52}$$

which is an exponential form of the Nernst Equation. Therefore, as the system approaches equilibrium the kinetic model agrees with the laws of thermodynamics.

Now, the current-voltage relation will be written in terms of exchange current and overpotential. The exchange current i_0 is defined as the magnitude of the cathodic or anodic current at equilibrium.

$$i_0 = nFAk^0 C_O^* \exp\left(-\frac{\alpha nF}{RT}\left(\varepsilon_{eq} - \varepsilon^{0'}\right)\right) \tag{2.53}$$

Raising equation 2.51 to the power $-\alpha$ and combining with the above equation gives the final equation for exchange current.

$$i_0 = nFAk^0 C_O^{*(1-\alpha)} C_R^{*\alpha} \tag{2.54}$$

Overpotential η is defined by

$$\eta \equiv \varepsilon - \varepsilon^{eq} \tag{2.55}$$

Dividing equation 2.51 by equation 2.54 gives

$$\begin{aligned} \frac{i}{i_0} = & \frac{C_0(x=0,t)}{C_O^*}\left(\frac{C_O^*}{C_O^*}\right)^{\alpha} \exp\left(-\frac{\alpha nF}{RT}\left(\varepsilon - \varepsilon^{0'}\right)\right) \\ & -\frac{C_R(x=0,t)}{C_R^*}\left(\frac{C_O^*}{C_O^*}\right)^{-(1-\alpha)} \exp\left((1-\alpha)\frac{nF}{RT}\left(\varepsilon - \varepsilon^{0'}\right)\right) \end{aligned} \tag{2.56}$$

Using equation 2.52 gives the final equation.

$$\frac{i}{i_0} = \frac{C_0(x=0,t)}{C_O^*}\exp\left(-\frac{\alpha nF}{RT}\eta\right) - \frac{C_R(x=0,t)}{C_R^*}\exp\left((1-\alpha)\frac{nF}{RT}\eta\right) \tag{2.57}$$

Now, the current-voltage relation will be written in terms of limiting current. Limiting current is the current associated with a mass transfer limited reaction. Here migration effects are excluded, and steady state is assumed. Referring to Figure 2.2, the flux of O to the interface in terms of the mass transfer coefficient m_O is

$$v_{mt} = m_O\left(C_O^* - C_O(x=0)\right) \tag{2.58}$$

Using equation 2.40

$$\frac{i}{nFA} = m_O\left(C_O^* - C_O(x=0)\right) \tag{2.59}$$

The largest flux or reaction rate allowed by mass transfer is when $C_O(x=0) = 0$. Therefore,

the cathodic current of a mass transfer limited reaction is given by

$$i_{limiting,cathodic} = i_{l,c} = nFAm_O C_O^* \tag{2.60}$$

Combining equations 2.59 and 2.60 gives an expression for for surface concentration

$$\frac{C_O(x=0)}{C_O^*} = 1 - \frac{i}{i_{l,c}} \tag{2.61}$$

Similarly, for the anodic current

$$\frac{i}{nFA} = -m_R\left(C_R^* - C_R(x=0)\right) \tag{2.62}$$

$$i_{limiting,anodic} = i_{l,a} = -nFAm_R C_R^* \tag{2.63}$$

$$\frac{C_R(x=0)}{C_R^*} = 1 - \frac{i}{i_{l,a}} \tag{2.64}$$

Using equations 2.60 and 2.64, the current-overpotential equation becomes

$$\frac{i}{i_0} = \left(1 - \frac{i}{i_{l,c}}\right)\exp\left(-\frac{\alpha nF}{RT}\eta\right) - \left(1 - \frac{i}{i_{l,a}}\right)\exp\left((1-\alpha)\frac{nF}{RT}\eta\right) \tag{2.65}$$

Solving for i

$$i = \frac{\exp\left(-\frac{\alpha nF}{RT}\eta\right) - \exp\left((1-\alpha)\frac{nF}{RT}\eta\right)}{\frac{1}{i_0} + \frac{1}{i_{l,c}}\exp\left(-\frac{\alpha nF}{RT}\eta\right) - \frac{1}{i_{l,a}}\exp\left((1-\alpha)\frac{nF}{RT}\eta\right)} \tag{2.66}$$

This equation is plotted in Figures 2.4 and 2.5.

In Figure 2.4 $\frac{i}{i_l}$, $\frac{i_c}{i_l}$, and $\frac{i_a}{i_l}$ are plotted vs η for $i_{l,c} = -i_{l,a} = i_l$, $\frac{i_0}{i_l} = 1$, $n = 1$, $T = 298K$, and $\alpha = 0.5$. The solid curve is the total current, the dashed curve is the cathodic current, and the dotted curve is the anodic current. At large positive overpotential the cathodic current is negligible, and at large negative overpotential the anodic current is negligible. Near equilibrium at $\eta = 0$, the cathodic and anodic contributions are the same order of magnitude. As $|\eta|$ increases the system is moved further from equilibrium, and the current increases until it is limited by

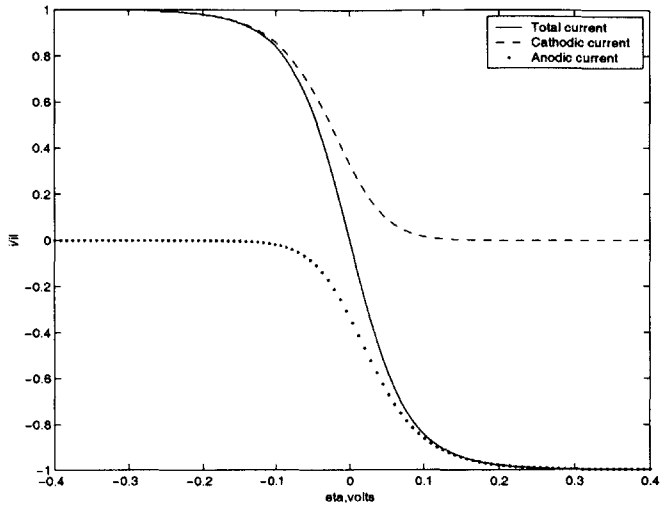

Figure 2.4: Current vs. overpotential

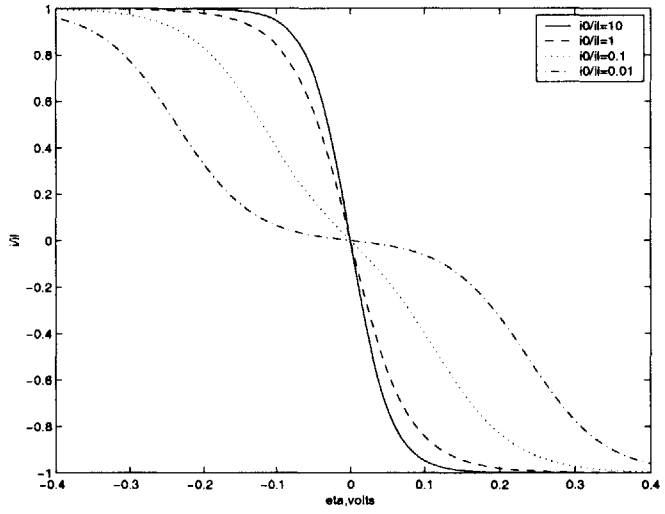

Figure 2.5: Current vs. overpotential for different exchange currents

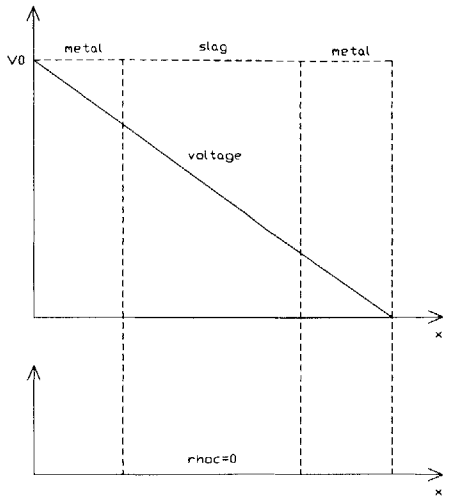

Figure 2.6: Initial voltage profile, 1D system

mass transfer. In Figure 2.5, $\frac{i}{i_l}$ is plotted vs. η for various values of $\frac{i_0}{i_l}$. As $\frac{i_0}{i_l}$ increases for a fixed η the current increases. Or, as $\frac{i_0}{i_l}$ decreases a larger η is required to reach the limiting current.

2.4.3 Charge Buildup Layer

During the initial stages of an experiment there is an inhomogeneous distribution of current and charge is seen to build up near the interface in a very thin region on the order of $10^{-10}m$. To explain the formation of net charge buildup at the interfaces, consider the metal-slag-metal electrochemical system shown in Figure 2.6. For simplicity, there is no flow, mass transfer is by migration only, and the system has a uniform permittivity ϵ. The governing equations are conservation of charge

$$\frac{\partial \rho_c}{\partial t} = \frac{\partial}{\partial x}\left(\sigma \frac{\partial \phi}{\partial x}\right) \tag{2.67}$$

and Gauss's Law

$$0 = \frac{\partial^2 \phi}{\partial x^2} + \frac{\rho_c}{\epsilon} \tag{2.68}$$

At $t = 0$, a voltage is applied to the system. The system initially has homogeneous charge neutrality. At small times $\rho_c = 0$, and according to equation 2.68 there will be a linear voltage

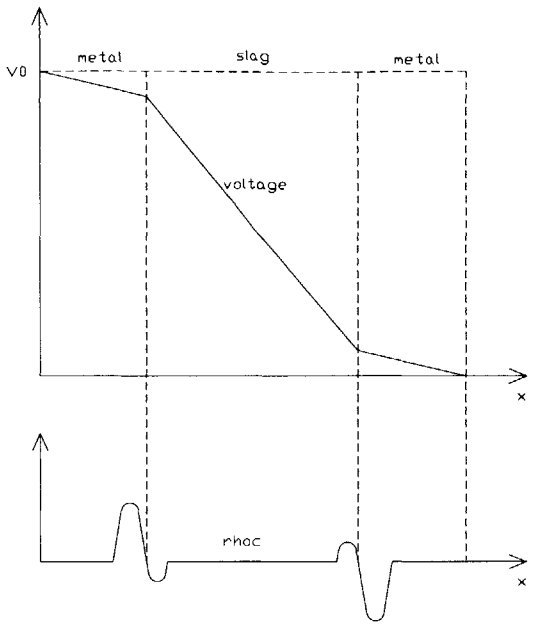

Figure 2.7: Final voltage profile, 1D system

profile. The flux of charge is given by

$$J_c(x) = \sigma(x) \frac{\partial \phi}{\partial x} \tag{2.69}$$

In general $\sigma_{metal} >> \sigma_{slag}$, so at small times $J_{c,metal} >> J_{c,slag}$. Charge (or a deficiency of electrons) will accumulate at the first interface, and there will be a net loss of charge at the second interface. The local charge densities will produce local electric fields which at the first interface lead to a decrease in the rate of incoming charge and an increase in the rate of the exiting charge and at the second electrode lead to an increase the rate of incoming charge and a decrease in the rate of exiting charge. A the same time, electrostatic forces act to bring negative charge to the slag side of the first interface and positive charge to the slag side of the second interface. At steady state $J_{c,metal} = J_{c,slag}$, so $\frac{\partial \phi}{\partial x}$ will be nonuniform. The final profiles are shown in Figure 2.7.

2.5 Scaling and Asymptotic Solutions

It has been experimentally shown that when iron is reduced on the cathode, it does not grow out in an orderly fashion. Instead it grows out and forms liquid dendrites or fingers. The fingers are approximately cylindrical with a length of 1-4 mm and a diameter of 1/4 mm. The iron fingers are then shown to break off and fall back into the melt. In this section simple analytical results are derived which explain this phenomena.

2.5.1 1D Electrochemical System

To first gain some insight into the cathode dynamics consider a 1D metal/slag electrochemical system with constant properties under a constant external electric field $-\frac{d\phi}{dx}$. Here, conservation of species is applied to Fe^{2+} only, so subscripts are excluded. Referring to Equation 2.5, the total molar flux (diffusion plus convection) of species is given by

$$\vec{J} = -D\vec{\nabla}c - \frac{zF}{RT}Dc\vec{\nabla}\phi + cu \tag{2.70}$$

There is no bulk fluid motion in the slag or the metal. The speed of the interface in the positive x-direction is given by U, see Figure2.8. Therefore, relative to a coordinate system moving with the interface, the total molar flux becomes

$$\vec{J} = -D\vec{\nabla}c - \frac{zF}{RT}Dc\vec{\nabla}\phi - cU \tag{2.71}$$

An additional simplification is that relative to the moving interface, the system is in a steady-state. Conservation of species gives

$$D\frac{d^2C}{dx^2} + \left(\frac{z_iF}{RT}D\frac{d\phi}{dx} + U\right)\frac{dc}{dx} = 0 \Rightarrow \frac{d^2c}{dx^2} + A\frac{dc}{dx} = 0 \tag{2.72}$$

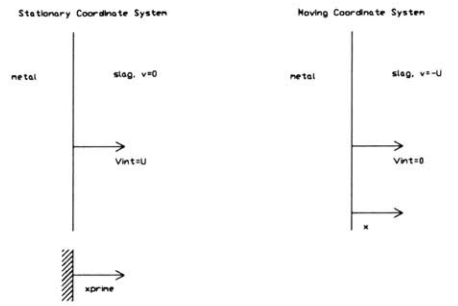

Figure 2.8:

where A is a constant. The boundary conditions are

$$\begin{aligned} c(x=0) &= 0 \\ c(x \to \infty) &\to c_{bulk} \end{aligned} \tag{2.73}$$

The solution is given by

$$\frac{c(x)}{c_{bulk}} = \left(1 - e^{-Ax}\right) \tag{2.74}$$

which gives a diffusion length scale of

$$L_{diff} \sim \frac{1}{A} \tag{2.75}$$

The interface velocity is given by Equation 2.18

$$U = \frac{JV_s}{2F} \sim \frac{\left(0.5\frac{A}{cm^2}\right)\left(15\frac{cm^3}{mol}\right)}{2\left(96485\frac{C}{mole}\right)} \sim 3.9 * 10^{-4}\frac{mm}{s} \tag{2.76}$$

A closer look at A shows that it can be decomposed into a term due to the electric field and a term due to the diffusion limited growth of the interface.

$$A = \frac{zF}{RT}\frac{d\phi}{dx} + \frac{U}{D} \tag{2.77}$$

$$A_{Efield} = \frac{zF}{RT}\frac{d\phi}{dx} \sim \frac{2\left(96485\frac{C}{mole}\right)\left(\frac{0.2V}{1mm}\right)}{\left(8.314\frac{J}{mol*K}\right)(1900K)} \sim 2.4mm^{-1} \tag{2.78}$$

$$A_{growth} = \frac{U}{D} \sim \frac{\left(3.9 * 10^{-4}\frac{mm}{s}\right)}{\left(10^{-6}\frac{cm^2}{s}\right)} \sim 3.9mm^{-1} \tag{2.79}$$

The effects are shown to be of the same order of magnitude. Finally, the diffusion length scale

$$L_{diff} \sim \frac{1}{A} \sim \frac{1}{3.9mm^{-1} + 2.4mm^{-1}} \sim 0.16mm \tag{2.80}$$

2.5.2 Charge Buildup Layer

In this section a somewhat quantitative explanation of the charge buildup layer is given using simplified governing equations and scaling arguments. For a more rigorous explanation see the Gouy-Chapman model [1].

For simplicity, consider a liquid Fe-FeO system with no flow, with mass transfer by migration only, and with a uniform permittivity ϵ. The governing equations are conservation of charge

$$\frac{\partial \rho_c}{\partial t} = \frac{\partial}{\partial x}\left(\sigma\frac{\partial \phi}{\partial x}\right) \tag{2.81}$$

and Gauss's Law

$$0 = \frac{\partial^2 \phi}{\partial x^2} + \frac{\rho_c}{\epsilon} \tag{2.82}$$

The charge buildup is characterized by a length scale L. In the charge buildup layer the two

terms in Gauss's law are the same order of magnitude.

$$\frac{\partial^2 \phi}{\partial x^2} \sim \frac{\rho_c}{\epsilon} \Rightarrow \frac{\Delta \phi}{L^2} \sim \frac{\rho_c}{\epsilon} \tag{2.83}$$

Solving for L gives

$$L \sim \sqrt{\frac{\Delta \phi \epsilon}{\rho_c}} \tag{2.84}$$

Using the bulk concentration of Fe in FeO, c^*_{Fe}, as an estimate for charge density, the open circuit voltage as an estimate for the voltage difference, and the $\epsilon \sim \epsilon_0$

$$L \sim \sqrt{\frac{\varepsilon \epsilon_0}{c^*_{Fe} z_{Fe^{2+}} F}} \sim \sqrt{\frac{(0.2V)\left(8.854 * 10^{-12} \frac{C^2}{N*m^2}\right)}{\left(4.983 * 10^4 \frac{mol}{m^3}\right)(2)\left(96485 \frac{C}{mole}\right)}} \sim 10^{-11} m \tag{2.85}$$

The time scale for the charge buildup layer to form is given by τ. As the charge buildup layer is forming the terms in equation 2.81 will be the same order of magnitude.

$$\frac{\partial \rho_c}{\partial t} \sim \frac{\partial}{\partial x}\left(\sigma \frac{\partial \phi}{\partial x}\right) \Rightarrow \frac{\rho_c}{\tau} \sim \frac{\sigma \Delta \phi}{L^2} \Rightarrow \tau \sim \frac{\rho_c L^2}{\sigma \Delta \phi} \tag{2.86}$$

Using equation 2.83 to eliminate ρ_c

$$\tau \sim \frac{\rho_c L^2}{\sigma \Delta \phi} \sim \left(\frac{\epsilon \Delta \phi}{L^2}\right) \frac{L^2}{\sigma \Delta \phi} \sim \frac{\epsilon}{\sigma} \tag{2.87}$$

Recall the molar flux is given by

$$\vec{J}_i = -D_i \vec{\nabla} c_i - \frac{z_i F}{RT} D_i c_i \vec{\nabla} \phi \tag{2.88}$$

Therefore, the conductivity of the slag is

$$\sigma_{FeO} \sim \frac{\left(z_{Fe^{2+}} F\right)^2}{RT} D_{Fe} c^*_{Fe} \tag{2.89}$$

Figure 2.9: Distorted slag/metal interface

$$\sim \frac{(2)^2 \left(96485 \frac{C}{mole}\right)^2 \left(10^{-10} \frac{m^2}{sec}\right) \left(4.983 * 10^4 \frac{mol}{m^3}\right)}{\left(8.314 * \frac{J}{mol*K}\right)(1900K)} \sim 11.7 \frac{1}{\Omega * m}$$

In contrast, $\sigma_{Fe} = 7 * 10^5 \frac{1}{\Omega * m}$. Continuing, using $\epsilon \sim \epsilon_0$ and the conductivity of the slag, the time-scale becomes

$$\tau \sim \frac{\epsilon_0}{\sigma_{FeO}} \sim \frac{8.854 * 10^{-12} \frac{C^2}{N*m^2}}{11.7 \frac{1}{\Omega * m}} \sim 10^{-12} s \tag{2.90}$$

The length scale and time scale calculated here are very rough estimates and could be off by a factor of 10 or so. However, if the values are so extreme that they are many orders of magnitude different than other length and time scales of interest (as is the case here and as will be displayed later), then the rough estimates are sufficient.

2.5.3 Diffusion Limited Growth

The initial distortion of the interface into fingers is characterized by a balance between surface tension and mass transfer. Consider the slag/metal system shown in Figure 2.9. Since the system is limited by the transport of Fe^{2+} to the cathode, a diffusion boundary layer will develop in the slag. Given an initial interface perturbation there will be a local change in the boundary layer thickness L_{diff}, and since the mass transfer to the interface in inversely proportional to L_{diff} ,

$$j \sim D \frac{(C_{bulk} - C_{interface})}{L_{diff}} \tag{2.91}$$

there will be a corresponding additional local change in interface distortion. For example, at a point where L_{diff} decreases due to a perturbation, j will increase which decreases L_{diff} and so on. Now, as the fingers start to grow surface tension forces act to smooth out the interface. The balance between the two forces was studied by Mullins and Sekerka [4, 5]. If the length of the system is larger than the length of the finger spacing as is the case here, then surface tension

Figure 2.10: Capillary instability

forces are not strong enough to eliminate the perturbation, and fingers will form.

2.5.4 Capillary Instability

As the fingers form on the cathode they have been shown to break up into droplets. This can be explained is by surface tension forces. A finger is modeled here as a cylinder of metal surrounded by an infinite supply of slag (see Figure 2.10). . There will be a higher pressure inside the cylinder due to surface tension. Given an initial perturbation on the cylinder walls there will be a corresponding pressure change given by Equation 2.19.

$$\Delta p = \gamma \left(\frac{1}{R_1} + \frac{1}{R_2} \right) \sim \frac{\gamma}{R_{local,cylinder}} \sim \frac{\left(1 \frac{N}{m}\right)}{\left(\frac{1}{8} mm\right)} \sim 8 * 10^3 \frac{N}{m^2} \tag{2.92}$$

Now, at regions where the local radius is smaller there will be a larger Δp, and in regions where the local radius is larger there will be a smaller Δp. Flow will be induced from regions of high pressure to regions of low pressure. As the cylinder changes shape due to induced flow the pressure changes are magnified ultimately leading to the breakup of fingers into droplets.

The capillary instability is more formally known as a Rayleigh instability. Rayleigh's analysis shows that non-axisymmetric modes decay and axisymmetric modes larger then the perimeter grow. Thus, the wavelength of oscillations is equal to the cross-sectional perimeter $2\pi R$.

2.5.5 Buoyancy Instability

Large drops of metal has been shown to fall from the bottom of the cathode. These drops are on the order of the finger lengths. They are not droplets from single fingers. Rather, they are groups of fingers that join and fall together. This can be explained by gravitational forces. The metal at the bottom of the cathode is modeled as a perfect hemisphere. A force balance between gravity forces, pressure forces, and surface tension forces gives an order of magnitude for the

droplet radius

$$\Delta\rho\frac{1}{2}\left(\frac{4}{3}\pi R^3\right)g = \gamma\left(2\pi R\right) \tag{2.93}$$

$$\Rightarrow R \sim \sqrt{\frac{3\gamma}{\Delta\rho g}} \sim \sqrt{\frac{3\left(1\frac{N}{m}\right)}{\left(\frac{7000}{2}\frac{kg}{m^3}\right)\left(9.81\frac{m}{s^2}\right)}} \sim 9.3mm \tag{2.94}$$

which lies within the expected range.

To find the speed at which a drop falls, the falling metal drop is modeled as a solid sphere falling in a stationary slag fluid under steady laminar conditions. A balance between gravity forces, pressure forces and drag forces gives

$$\left(\rho_{metal} - \rho_{slag}\right)g\left(\frac{4}{3}\pi R^3\right) = f_{drag}\left(\frac{1}{2}\rho_{slag}V^2\right)\left(\pi R^2\right) \tag{2.95}$$

where f_{drag} is the drag coefficient. For laminar flow

$$f_{drag} = \frac{24}{Re_D} = 24\left(\frac{\eta_{slag}}{\rho_{slag}V2R}\right) \tag{2.96}$$

Combining gives

$$\left(\rho_{metal} - \rho_{slag}\right)g\left(\frac{4}{3}\pi R^3\right) = 24\left(\frac{\eta_{slag}}{\rho_{slag}V2R}\right)\left(\frac{1}{2}\rho_{slag}V^2\right)\left(\pi R^2\right) \tag{2.97}$$

Solving for V

$$V = \frac{2\left(\rho_{metal} - \rho_{slag}\right)gR^2}{9\eta_{slag}} \sim \frac{2\left(\frac{7000}{2}\frac{kg}{m^3}\right)\left(9.81\frac{m}{s^2}\right)\left(\frac{1}{8}mm\right)^2}{9\left(0.012\frac{kg}{m*s}\right)} \sim 1\frac{cm}{s} \tag{2.98}$$

Chapter 3

Diffuse Interface Model

3.1 Cahn-Hilliard

The free energy of a typical phase-separating solution is shown in Figure 3.1 where f is the free energy density (free energy per unit volume of solution) and C is a dimensionless intensive measure of concentration (C will be normalized such that it is a dimensionless parameter which is 0 in phase 1 and 1 in phase2). The two equilibrium phases are c_1 and c_2. The Free energy of an inhomogeneous system (a system with concentration gradients) is assumed to be close to that of a homogeneous system. Therefore, the free energy of an inhomogeneous system is found by using a Taylor series expansion of the free energy about the homogeneous state [23].

$$f_{inh}\left(C, \vec{\nabla} C\right) = f\left(C, 0\right) + \vec{L} \bullet \vec{\nabla} C + \frac{1}{2} \vec{\nabla} C \left[K\right] \vec{\nabla} C + \cdots \tag{3.1}$$

where

$$L_i = \frac{\partial f}{\partial \left(\frac{\partial C}{\partial x_i}\right)} \tag{3.2}$$

and

$$K_{i,j} = \frac{\partial^2 f}{\partial \left(\frac{\partial C}{\partial x_i}\right) \partial \left(\frac{\partial C}{\partial x_j}\right)} \tag{3.3}$$

Figure 3.1: Free energy density vs. concentration

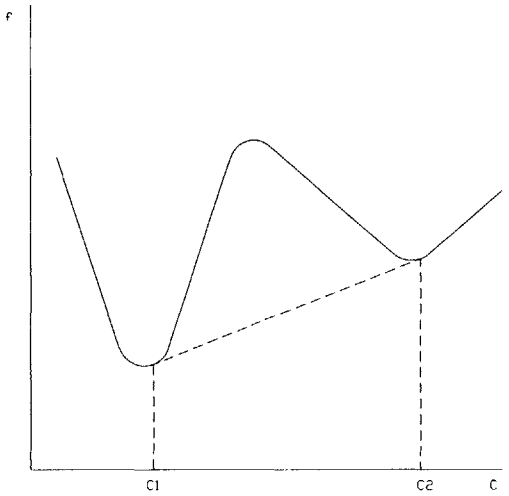

If the homogeneous material has a center of symmetry and if the homogeneous material is isotropic, then the expansion to second order reduces to

$$f_{inhomogeneous}\left(C, \vec{\nabla}C\right) = f\left(C, 0\right) + \frac{\alpha}{2}\left(\vec{\nabla}C\right) \bullet \left(\vec{\nabla}C\right) \tag{3.4}$$

where α is called the gradient penalty coefficient. An inhomogeneous system with a planar interface is shown in Figure 3.2. The system is an infinite medium (length is 2L where $L \rightarrow \infty$) with a planar interface at the y-z plane. The width of the interface is ϵ. The total free energy of this system is

$$F = \int_{\Omega}\left(f + \frac{\alpha}{2}\vec{\nabla}C \bullet \vec{\nabla}C\right)d\Omega = \int_{\Omega}\left(f + \frac{\alpha}{2}\frac{dC}{dx}\frac{dC}{dx}\right)Adx \tag{3.5}$$

where Ω is the volume of the system and A is the cross sectional area. Expanding the integral

$$\frac{F}{A} \cong \int_{-L}^{-\frac{\epsilon}{2}} f\left(C_1\right)dx + \int_{-\frac{\epsilon}{2}}^{+\frac{\epsilon}{2}} f dx + \int_{-\frac{\epsilon}{2}}^{+\frac{\epsilon}{2}} \frac{\alpha}{2}\frac{dC}{dx}\frac{dC}{dx}dx + \int_{-\frac{\epsilon}{2}}^{+L} f\left(C_2\right)dx \tag{3.6}$$

Simplifying

$$\frac{F}{A} = f\left(C_1\right)\left(L - \frac{\epsilon}{2}\right) + \frac{f\left(C_1\right) + f\left(C_2\right)}{2}\left(\epsilon\right) + \int_{-\frac{\epsilon}{2}}^{+\frac{\epsilon}{2}} f_{hump}dx \tag{3.7}$$

Figure 3.2: Inhomogeneous system

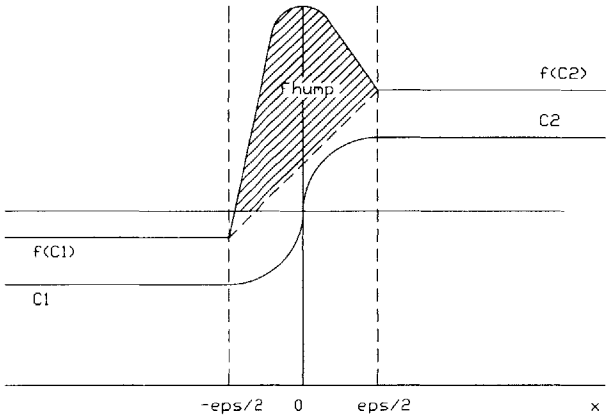

$$+\int_{-\frac{\epsilon}{2}}^{+\frac{\epsilon}{2}} \frac{\alpha}{2}\frac{dC}{dx}\frac{dC}{dx}dx + f(C_2)\left(L-\frac{\epsilon}{2}\right)$$

$$\frac{F}{A} = f(C_1)(L) + \int_{-\frac{\epsilon}{2}}^{+\frac{\epsilon}{2}} f_{hump}dx + \int_{-\frac{\epsilon}{2}}^{+\frac{\epsilon}{2}} \frac{\alpha}{2}\frac{dC}{dx}\frac{dC}{dx}dx + f(C_2)(L) \tag{3.8}$$

where referring to Figure 3.2

$$\frac{F_{hump}}{A} = \int_{-\frac{\epsilon}{2}}^{+\frac{\epsilon}{2}} f_{hump}dx \tag{3.9}$$

To simplify the analysis let C be a dimensionless parameter which has a value of 0 in phase 1 and 1 in phase 2.

$$C \equiv \frac{c-c_1}{c_2-c_1} \tag{3.10}$$

The free energy density associated with the hump is modeled with the polynomial $\Psi(C)$ as shown in Figure 3.3.

$$f_{hump} = \beta\Psi(C) = \beta C^2(1-C)^2 \tag{3.11}$$

β is a scaling coefficient related to the peak of the free energy curve.

$$f_{peak} = \beta\Psi_{max} = \beta\Psi\left(\frac{1}{2}\right) = \frac{\beta}{16} \Rightarrow \beta = 16f_{peak} \tag{3.12}$$

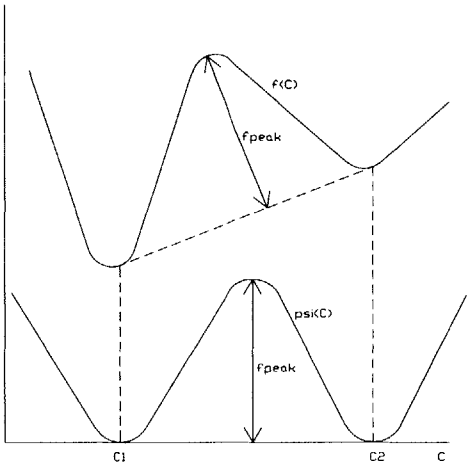

Figure 3.3: Free energy hump

Now, consider a reference system with no interfacial energy. Letting $\epsilon \rightarrow 0$

$$\frac{F_{ref}}{A} = f(C_1)(L) + f(C_2)(L) \tag{3.13}$$

The energy of the system relative to the reference system is the energy of the interface, and it is quantified macroscopically by the surface tension (or surface energy) σ.

$$\gamma = \frac{F}{A} - \frac{F_{ref}}{A} \tag{3.14}$$

$$\gamma = \int_{-\frac{\epsilon}{2}}^{+\frac{\epsilon}{2}} \left(\beta\Psi(C) + \frac{\alpha}{2}\left(\frac{dC}{dx}\right)^2 \right) dx \tag{3.15}$$

The composition profile $C(x)$ will be such that the interface energy is minimized. The calculus of variations is used to find the profile. Rewriting the above equation

$$\gamma = \int_{-\frac{\epsilon}{2}}^{+\frac{\epsilon}{2}} \left(f_{inh}\left(x, C, \frac{dC}{dx}\right)\right) dx \tag{3.16}$$

According to Euler's Equation, the function that minimizes the above integral obeys

$$\frac{d}{dx}\left(\frac{\partial f_{inh}}{\partial\left(\frac{dC}{dx}\right)}\right)-\frac{\partial f_{inh}}{\partial C}=0 \tag{3.17}$$

Simplifying gives

$$\frac{d}{dx}\left(\alpha\frac{dC}{dx}\right)-\beta\frac{d\Psi}{dC}=0 \tag{3.18}$$

The left hand side physically represents the local increase of free energy density due to a local addition in composition $\delta C(x)$. Multiplying through by $\frac{dC}{dx}$ and integrating

$$\frac{dC}{dx}\frac{d}{dx}\left(\alpha\frac{dC}{dx}\right)-\beta\frac{d\Psi}{dC}\frac{dC}{dx}=0 \tag{3.19}$$

$$\frac{d}{dx}\left(\frac{\alpha}{2}\left(\frac{dC}{dx}\right)^2\right)-\beta\frac{d\Psi}{dx}=0 \tag{3.20}$$

$$\frac{\alpha}{2}\left(\frac{dC}{dx}\right)^2=\beta\Psi+const \tag{3.21}$$

At $C=C_1$, $\frac{dC}{dx}=0$ and $\Psi=0$, so $const=0$.

$$\frac{\alpha}{2}\left(\frac{dC}{dx}\right)^2=\beta\Psi\Rightarrow\frac{dC}{dx}=\sqrt{\frac{2\beta\Psi}{\alpha}} \tag{3.22}$$

The analytical solution is

$$C(x)=\frac{1}{2}+\frac{1}{2}\tanh\left(\frac{x}{2}\sqrt{\frac{2\beta}{\alpha}}\right) \tag{3.23}$$

Combining Equations 3.22 and 3.15, the surface tension becomes

$$\gamma=\int_{-\frac{\epsilon}{2}}^{+\frac{\epsilon}{2}}\left(2\beta\Psi(C)\right)dx=\int_{C_1}^{C_2}\left(2\beta\Psi(C)\right)\frac{1}{\frac{dC}{dx}}dC \tag{3.24}$$

$$\Rightarrow\gamma=\int_{C_1}^{C_2}\sqrt{2\alpha\beta\Psi}dC=\sqrt{2\alpha\beta}\int_{C_1}^{C_2}\sqrt{\Psi}dC \tag{3.25}$$

Solving for alpha

$$\alpha = \frac{\gamma^2}{2\beta\left(\int_{C_1}^{C_2}\sqrt{\Psi}dC\right)^2} = \frac{\gamma^2}{2\beta\left(\frac{1}{6}\right)^2} = \frac{18\gamma^2}{\beta} \tag{3.26}$$

The analytical solution gives $C(x \to \infty) \to 1$. The interface width can be approximated with

$$C\left(\pm\frac{\epsilon}{2}\right) \cong 0.9 \tag{3.27}$$

$$\frac{1}{2} + \frac{1}{2}\tanh\left(\frac{\epsilon}{4}\sqrt{\frac{2\beta}{\alpha}}\right) = 0.9 \tag{3.28}$$

$$\epsilon = 4\sqrt{\frac{\alpha}{2\beta}}\tanh^{-1}\left(2\left(0.9 - \frac{1}{2}\right)\right) \cong 3.1\sqrt{\frac{\alpha}{\beta}} \tag{3.29}$$

In general the flux of species is proportional to the gradient in chemical potential μ.

$$\vec{J_i} = -\kappa_i \vec{\nabla}\mu_i \tag{3.30}$$

where κ is the mobility (similar to the diffusion coefficient). For a homogeneous system

$$\mu_i \equiv \left(\frac{\partial G}{\partial n_i}\right)_{T,p,n_j \neq n_i} \tag{3.31}$$

Consistent with the above analysis the chemical potential for an inhomogeneous system is defined by

$$\mu_i \equiv \beta\frac{d\Psi}{dC} - \alpha\nabla^2 C \tag{3.32}$$

Note that the units of μ_i are joules per unit volume as opposed to the tradition units of joules per mole. Therefore, to give molar flux κ_i has units of $\frac{mol*m}{J*s}$.

κ_i in general is a function of composition. At the homogeneous equilibrium compositions, C_1 and C_2 the flux reduces to the traditional constitutive equation. For example using the concentration at phase 1,

$$J_i = -D_i\frac{\partial c_i}{\partial x} = -\kappa_i\frac{\partial}{\partial x}\left(\beta\frac{d\Psi}{dC}\right) \tag{3.33}$$

$$\Rightarrow D_i \frac{\partial c_i}{\partial x} = \kappa_i \beta \frac{d}{dC}\left(\frac{d\Psi}{dC}\right)\frac{\partial C}{\partial x} \tag{3.34}$$

Recalling the definition of C

$$C \equiv \frac{c_i - c_1}{c_2 - c_1} \Rightarrow \frac{\partial C}{\partial x} = \frac{1}{c_2 - c_1}\frac{\partial c_i}{\partial x} \tag{3.35}$$

Combining gives

$$\kappa_i\,(C=0) = \frac{D_i\,(c_2 - c_1)}{\beta\left(\frac{d^2\Psi}{dC^2}\right)_{C=0}} \tag{3.36}$$

where D_i is the diffusion coefficient of species component i in phase 1.

In summary, the parameters of the Cahn-Hilliard equation are

$$\beta = 16 f_{peak} \tag{3.37}$$

$$\alpha = \frac{18\gamma^2}{\beta} \tag{3.38}$$

$$\epsilon \cong 3.1\sqrt{\frac{\alpha}{\beta}} \tag{3.39}$$

$$\kappa_i\,(C=0) = \frac{D_i\,(c_2 - c_1)}{\beta\left(\frac{d^2\Psi}{dC^2}\right)_{C=0}} \tag{3.40}$$

3.2 Fe-FeO System

In this section a mathematical diffuse interface model of the slag-metal system is presented. The metal phase is modeled as pure Fe, and the slag phase is modeled as pure FeO. The system is at 1900 K.

3.2.1 Cahn-Hilliard

A free energy function for the Fe-FeO system was developed using the sublattice ionic liquid model from CALPHAD [11]. Gibb's free energy is plotted as a function of X_{Fe} in Figure 3.4. Since the free energy hump is all that is needed for the Cahn-Hilliard equation, the reference free

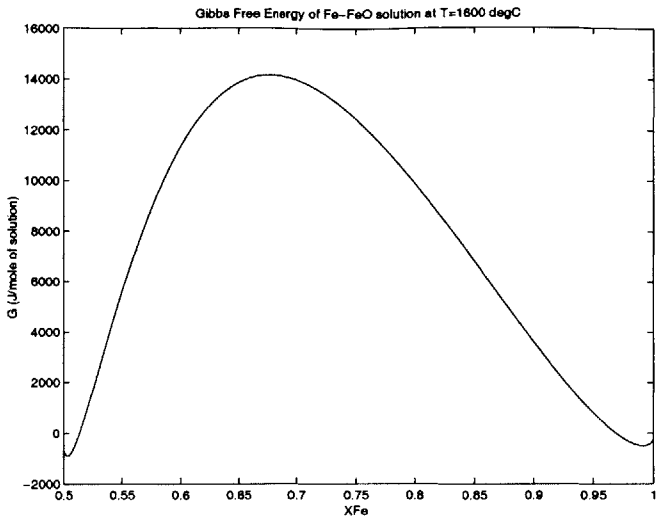

Figure 3.4: Free energy of Fe-FeO system using sublattice ionic liquid model

energies were set to zero. The figure shows a peak free energy of approximately $\underline{G} \cong 14,000 \frac{J}{mole}$ at $X_{Fe} \cong 0.68$. The peak in free energy in terms of free energy density is

$$f_{peak} = \underline{G}c = \underline{G}\frac{\rho}{M} \cong 1.7 * 10^9 \frac{J}{m^3} \tag{3.41}$$

α and β become

$$\beta = 16 f_{peak} = 2.72 * 10^{10} \frac{J}{m^3} \tag{3.42}$$

$$\alpha = \frac{18\gamma^2}{\beta} = 6.6 * 10^{-10} N \tag{3.43}$$

which gives an interface width of

$$\epsilon \cong 3.1\sqrt{\frac{\alpha}{\beta}} = 4.8 * 10^{-10} m \tag{3.44}$$

To track a one dimensional interface of this thickness on a solution domain on the order of 1cm would require on the order of 10^7 grid points. With such extreme length scales, modifications must be made to the diffuse interface model for practical use.

The interface width is a function of f_{peak} and γ. To scale the interface, one of these physical parameters must be altered. In this project f_{peak} was altered. ϵ was set according to the grid,

and β was found as a function of ϵ. In terms of ϵ, α and β become

$$\alpha = \left(\sqrt{\frac{18}{3.1}}\right)\gamma\epsilon \tag{3.45}$$

$$\beta = \left(\sqrt{(18)\,(3.1)}\right)\frac{\gamma}{\epsilon} \tag{3.46}$$

This type of scaling is commonly called the phase field method.

3.2.2 Governing Equations

The equations given in this section are similar to the equations given for the sharp interface formulation. See Section 2.2 for a more detailed description of variables and terms. The Navier-Stokes equations were extended to the phase field model (see Jacqmin [10]) by adding an extra surface tension term. Conservation of x-direction momentum reads

$$\begin{aligned}\frac{\partial}{\partial t}(\rho u) + \vec{\nabla}\bullet\left(\rho\vec{V}u\right) &= -\frac{\partial p}{\partial x} + \vec{\nabla}\bullet\left(\eta\vec{\nabla}u\right) + \rho g_x \\ &\quad + \vec{\nabla}\bullet\left(\eta\frac{\partial\vec{V}}{\partial x}\right) \\ &\quad - \frac{2}{3}\frac{\partial}{\partial x}\left(\eta\vec{\nabla}\bullet\vec{V}\right) - C\frac{\partial\mu}{\partial x}\end{aligned} \tag{3.47}$$

and conservation of y-direction momentum reads

$$\begin{aligned}\frac{\partial}{\partial t}(\rho v) + \vec{\nabla}\bullet\left(\rho\vec{V}v\right) &= -\frac{\partial p}{\partial y} + \vec{\nabla}\bullet\left(\eta\vec{\nabla}u\right) + \rho g_y \\ &\quad + \vec{\nabla}\bullet\left(\eta\frac{\partial\vec{V}}{\partial y}\right) \\ &\quad - \frac{2}{3}\frac{\partial}{\partial y}\left(\eta\vec{\nabla}\bullet\vec{V}\right) - C\frac{\partial\mu}{\partial y}\end{aligned} \tag{3.48}$$

Conservation of mass is given by

$$\frac{\partial \rho}{\partial t} + \vec{\nabla} \bullet \left(\rho \vec{V}\right) = 0 \tag{3.49}$$

The transport equation for conservation of iron is

$$\frac{\partial}{\partial t}\left(\rho \omega_{Fe}\right) + \vec{\nabla} \bullet \left(\rho \vec{V} \omega_{Fe}\right) = -M_{Fe} \vec{\nabla} \bullet \left(\vec{J}_{Fe}\right) \tag{3.50}$$

where the molar flux is given by

$$\overrightarrow{J_{Fe}} = -\kappa_{Fe} \vec{\nabla} \mu_{Fe} - \frac{z_{Fe} F}{RT} D_{Fe} \frac{\rho \omega_{Fe}}{M_{Fe}} \vec{\nabla} \phi \tag{3.51}$$

The conductivity of ferrous ions σ_{Fe} (not to be confused with the electrical conductivity of iron) is defined by

$$\vec{J}_{charge,Fe} = \sigma_{Fe} \vec{E} = -\sigma_{Fe} \vec{\nabla} \phi \tag{3.52}$$

and is related to molar flux by

$$\vec{J}_{charge,Fe} = z_{Fe} F \vec{J}_{Fe} \Rightarrow \vec{J}_{Fe} = -\left(\frac{\sigma_{Fe}}{z_{Fe} F}\right) \vec{\nabla} \phi \tag{3.53}$$

Comparing this result to equation 3.51 gives an expression for the conductivity of ferrous ions

$$\frac{\sigma_{Fe}}{z_{Fe} F} = \frac{z_{Fe} F}{RT} D_{Fe} \frac{\rho \omega_{Fe}}{M_{Fe}} \Rightarrow \sigma_{Fe} = \frac{z_{Fe}^2 F^2}{RT} D_{Fe,slag} \frac{\rho \omega_{Fe}}{M_{Fe}} \tag{3.54}$$

Combining gives

$$\frac{\partial}{\partial t}\left(\rho \omega_{Fe}\right) + \vec{\nabla} \bullet \left(\rho \vec{V} \omega_{Fe}\right) = M_{Fe} \vec{\nabla} \bullet \left(\kappa_{Fe} \vec{\nabla} \mu_{Fe} + \frac{\sigma_{Fe}}{z_{Fe} F} \vec{\nabla} \phi\right) \tag{3.55}$$

Recall the chemical potential was given by 3.32

$$\mu_i \equiv \beta \frac{d\Psi}{dC} - \alpha \nabla^2 C \tag{3.56}$$

C is defined here as

$$C \equiv \frac{\omega_{Fe} - \omega_{Fe,slag}}{\omega_{Fe,metal} - \omega_{Fe,slag}} \tag{3.57}$$

$$\Rightarrow \omega_{Fe} = \left(\omega_{Fe,metal} - \omega_{Fe,slag}\right) C + \omega_{Fe,slag} = \Delta\omega_{Fe} C + \omega_{Fe,slag} \tag{3.58}$$

In terms of C the left hand side of equation 3.55 is

$$\begin{aligned} \frac{\partial}{\partial t}\left(\rho\omega_{Fe}\right) + \vec{\nabla} \bullet \left(\rho \vec{V} \omega_{Fe}\right) &= \frac{\partial}{\partial t}\left[\rho\left(\Delta\omega_{Fe} C + \omega_{Fe,slag}\right)\right] \\ &\quad + \vec{\nabla} \bullet \left[\rho \vec{V}\left(\Delta\omega_{Fe} C + \omega_{Fe,slag}\right)\right] \end{aligned} \tag{3.59}$$

$$\begin{aligned} \Rightarrow \frac{\partial}{\partial t}\left(\rho\omega_{Fe}\right) + \vec{\nabla} \bullet \left(\rho \vec{V} \omega_{Fe}\right) &= \Delta\omega_{Fe}\left[\frac{\partial}{\partial t}\left(\rho C\right) + \vec{\nabla} \bullet \left(\rho \vec{V} C\right)\right] \\ &\quad + \omega_{Fe,slag}\left[\frac{\partial}{\partial t}\left(\rho\right) + \vec{\nabla} \bullet \left(\rho \vec{V}\right)\right] \end{aligned} \tag{3.60}$$

The second term is zero by the continuity equation. Writing equation 3.55 explicitly in terms of C gives the final form of the conservation of iron equation.

$$\begin{aligned} \frac{\partial}{\partial t}\left(\rho C\right) + \vec{\nabla} \bullet \left(\rho \vec{V} C\right) &= \frac{M_{Fe}}{\Delta\omega_{Fe}} \vec{\nabla} \bullet \left[\kappa_{Fe} \vec{\nabla}\left(\beta \frac{d\Psi}{dC} - \alpha \nabla^2 C\right)\right] \\ &\quad + \frac{M_{Fe}}{\Delta\omega_{Fe}} \vec{\nabla} \bullet \left(\frac{\sigma_{Fe}\left(C\right)}{z_{Fe}\left(C\right) F} \vec{\nabla}\phi\right) \end{aligned} \tag{3.61}$$

where the functional dependence of σ_{Fe} and z_{Fe} on C has been indicated. Note that σ_{Fe} depends on C through z_{Fe} and ω_{Fe}. The mobility is assumed to be constant and given by equation 3.36

$$\kappa_{Fe} = \kappa_{Fe}\left(C = 0\right) = \frac{D_{Fe,slag}\left(c_{Fe,metal} - c_{Fe,slag}\right)}{\beta\left(\frac{d^2\Psi}{dC^2}\right)_{C=0}} \tag{3.62}$$

Note that since $C = 1$ is pure Fe, kappa is irrelevant at $C = 1$. $z_{Fe}\left(C\right)$ is the charge of Fe

atoms (and ions) per mole of Fe atoms (and ions).

$$z_{Fe}(C) \equiv \frac{z_{Fe^{2+}} N_{Fe^{2+}}}{N_{Fe^{2+}} + N_{Fe^0}} = \frac{2X_{Fe^{2+}}}{X_{Fe^{2+}} + X_{Fe^0}} = \frac{2X_{Fe^{2+}}}{X_{Fe}} \tag{3.63}$$

where $N_{Fe^{2+}}$ is the number of Fe^{2+} ions, N_{Fe^0} is the number of neutral Fe atoms. Note that $z_{Fe^{2+}} = 2$, but z_{Fe} varies from 0 in metal to 2 in slag. Assuming charge neutrality

$$2X_{Fe^{2+}} - 2X_{O^{2-}} = 0 \Rightarrow X_O = X_{Fe^{2+}} \tag{3.64}$$

and using the mole fraction relation

$$X_O + X_{Fe} = 1 \tag{3.65}$$

gives

$$z_{Fe}(C) = \frac{2(1 - X_{Fe}(C))}{X_{Fe}(C)} \tag{3.66}$$

Conservation of charge was given by equation 2.13

$$\frac{D\rho_f}{Dt} = -\vec{\nabla} \bullet \left(\sum \vec{J}_i z_i F \right) \tag{3.67}$$

Expanding the right hand side,

$$\frac{D\rho_f}{Dt} = -\vec{\nabla} \bullet \left(\vec{J}_{Fe} F z_{Fe}(C) + \vec{J}_O F z_O + \vec{J}_{charge,e} \right) \tag{3.68}$$

For a multi-component system where the velocity is defined by the mass average velocity, the sum of the diffusion mass fluxes is zero.

$$M_{Fe} \vec{J}_{Fe} + M_O \vec{J}_O = 0 \Rightarrow \vec{J}_O = -\frac{M_{Fe}}{M_O} \vec{J}_{Fe} \tag{3.69}$$

Eliminating $\vec{J}_O$ from the above two equations gives

$$\begin{aligned}\frac{D\rho_f}{Dt} &= -\vec{\nabla}\bullet\left(\vec{J}_{Fe}Fz_{Fe}(C)+\left(-\frac{M_{Fe}}{M_O}\vec{J}_{Fe}\right)Fz_O+\vec{J}_{charge,e}\right) \\ &= -\vec{\nabla}\bullet\left(\vec{J}_{Fe}F\left[z_{Fe}(C)-\frac{M_{Fe}}{M_O}z_O\right]+\vec{J}_{charge,e}\right)\end{aligned} \tag{3.70}$$

For convenience let $\tilde{z}(C)$ be defined by

$$\tilde{z}(C)\equiv z_{Fe}(C)-\frac{M_{Fe}}{M_O}z_O \tag{3.71}$$

Note that because $z_{Fe}\geq 0$ and $z_O=-2$, $\tilde{z}(C)>0$. The flux of charge due to electrons is given by

$$\vec{J}_{charge,e}=\sigma_e(C)\vec{E}=-\sigma_e(C)\vec{\nabla}\phi \tag{3.72}$$

where σ_e reduces to zero in the slag. Conservation of charge becomes

$$\frac{D\rho_f}{Dt}=-\vec{\nabla}\bullet\left(\tilde{z}(C)F\vec{J}_{Fe}-\sigma_e(C)\vec{\nabla}\phi\right) \tag{3.73}$$

The molar flux of iron is given by

$$\vec{J}_{Fe}=-\kappa_{Fe}\vec{\nabla}\mu_{Fe}-\frac{\sigma_{Fe}(C)}{z_{Fe}(C)F}\vec{\nabla}\phi \tag{3.74}$$

Combining gives

$$\frac{D\rho_f}{Dt}=-\vec{\nabla}\bullet\left(\tilde{z}(C)F\left(-\kappa_{Fe}\vec{\nabla}\mu_{Fe}-\frac{\sigma_{Fe}(C)}{z_{Fe}(C)F}\vec{\nabla}\phi\right)-\sigma_e(C)\vec{\nabla}\phi\right) \tag{3.75}$$

Simplifying,

$$\begin{aligned}\frac{D\rho_f}{Dt} &= \vec{\nabla}\bullet\left(\tilde{z}(C)F\kappa_{Fe}\vec{\nabla}\mu_{Fe}\right)+\vec{\nabla}\bullet\left(\frac{\tilde{z}(C)}{z_{Fe}(C)}\sigma_{Fe}(C)\vec{\nabla}\phi\right) \\ &\quad +\vec{\nabla}\bullet\left(\sigma_e(C)\vec{\nabla}\phi\right)\end{aligned} \tag{3.76}$$

Charge density exists only at the interfaces, or more generally where the conductivity changes. Recall from equation 2.90 that the timescale for charge accumulation at the interfaces is on the order of $\tau_{DL} \sim 10^{-12}s$. The timescale of interest here is that of bulk fluid motion and diffusion of species. A physical timescale of interest for the macroscopic system can be obtained from scale of the interface velocity (equation 2.76) and the diffusion boundary layer (equation 2.80).

$$\tau_{macro,interest} \sim \frac{L_{bl}}{U_{int}} \sim \frac{0.16mm}{4 * 10^{-4} \frac{mm}{s}} = 400s \tag{3.77}$$

A timescale for a mesoscopic system would be that associated with the oscillating of a small droplet due to surface tension forces. Consider the following simplified model. A hemisphere of radius R initially at rest is pulled through a distance R, by a surface tension force. the equation of motion is

$$F = ma \Rightarrow \gamma 2\pi R = \left(\rho \frac{4}{3}\pi R^3\right)\left(\frac{2R}{t^2}\right) \tag{3.78}$$

Using properties of liquid iron and $R = 1mm$,

$$\tau_{meso,interest} = \sqrt{\frac{\rho \frac{4}{3} R^3}{\gamma}} \sim \sqrt{\frac{\left(7160 \frac{kg}{m^3}\right) \frac{4}{3} (1mm)^3}{\left(1 \frac{N}{m}\right)}} \sim 3 * 10^{-3}s \tag{3.79}$$

The analytical result for an oscillating drop with $\gamma = 0.03 \frac{N}{m}$, $\rho = 1000 \frac{kg}{m^3}$ and $R \cong \frac{3}{16} cm$ is a frequency of $f \cong 50Hz$, so the above order of magnitude for an small oscillating iron drop seems reasonable. The main point is that the timescale of the electrical effects in the charge buildup layer are microscopic with respect to the system. Therefore, the conservation of charge equation is effectively at steady state and the unsteady term is neglected.

$$\begin{aligned} \vec{V} \bullet \vec{\nabla} \rho_f &= \vec{\nabla} \bullet \left(\tilde{z}(C) F \kappa_{Fe} \vec{\nabla} \mu_{Fe}\right) + \vec{\nabla} \bullet \left(\frac{\tilde{z}(C)}{z_{Fe}(C)} \sigma_{Fe}(C) \vec{\nabla} \phi\right) \\ &\quad + \vec{\nabla} \bullet \left(\sigma_e(C) \vec{\nabla} \phi\right) \end{aligned} \tag{3.80}$$

The dimensionless parameter N_1 is defined to measure the ratio of the order of magnitude of a

convection term to an electric field term.

$$N_1 \sim \frac{\vec{V} \bullet \vec{\nabla} \rho_f}{\vec{\nabla} \bullet \left(\sigma \vec{\nabla} \phi\right)} \sim \frac{\frac{U \rho_f}{L}}{\frac{\sigma \phi}{L^2}} \sim \frac{U \rho_f L}{\sigma \phi} \tag{3.81}$$

From equation 2.83 Gauss's law gives

$$\frac{\phi}{L^2} \sim \frac{\rho_f}{\epsilon} \Rightarrow \rho_f \sim \frac{\epsilon \phi}{L^2} \tag{3.82}$$

Combining,

$$N_1 \sim \frac{U \epsilon}{\sigma L} \tag{3.83}$$

Using $\epsilon \sim \epsilon_0$, U from the falling sphere of equation 2.98, σ_{slag} from equation 2.90, and the diffusion length scale as a representative macroscopic length scale,

$$N_1 \sim \frac{\left(1 \frac{cm}{s}\right)\left(8.84 * 10^{-12} \frac{C^2}{N * m^2}\right)}{\left(11.7 \frac{1}{\Omega * m}\right)(0.15 mm)} \sim 10^{-14} \tag{3.84}$$

So, the transport of charge by convection can be neglected. Note that because $N_1 << 1$, convection can be safely neglected even for the case of forced convection. Equation 3.81 becomes

$$\begin{aligned} 0 \;=\; & \vec{\nabla} \bullet \left(\tilde{z}(C) F \kappa_{Fe} \vec{\nabla} \mu_{Fe}\right) + \vec{\nabla} \bullet \left(\frac{\tilde{z}(C)}{z_{Fe}(C)} \sigma_{Fe}(C) \vec{\nabla} \phi\right) \\ & + \vec{\nabla} \bullet \left(\sigma_e(C) \vec{\nabla} \phi\right) \end{aligned} \tag{3.85}$$

The dimensionless parameter N_2 is defined to measure the ratio of the order of magnitude of the the diffusion term to the electric field terms.

$$N_2 \sim \frac{\tilde{z}(C) F \vec{\nabla} \bullet \left(\kappa \vec{\nabla} \mu\right)}{\vec{\nabla} \bullet \left(\sigma \vec{\nabla} \phi\right)} \sim \frac{\tilde{z}(C) F \vec{\nabla} \bullet \left(D \vec{\nabla} c\right)}{\vec{\nabla} \bullet \left(\sigma \vec{\nabla} \phi\right)} \sim \frac{F D_{slag} \Delta c}{\sigma \Delta \phi} \tag{3.86}$$

Here it has been assumed that the length scales of diffusion and voltage are similar. This assumption may break down for systems with small concentration boundary layers (such as

ternary systems). Using estimated operating conditions,

$$N_2 \sim \frac{\left(96,485\frac{C}{mole}\right)\left(10^{-10}\frac{m^2}{s}\right)\left(10^4\frac{mol}{m^3}\right)}{\left(11.7\frac{1}{\Omega * m}\right)(1V)} \sim 8 * 10^{-3} \tag{3.87}$$

So, the transport of charge due to diffusion can also be neglected. Note that as the applied potential increases and as the conductivity increases, N_2 decreases.

$$0 = \vec{\nabla} \bullet \left(\frac{\tilde{z}(C)}{z_{Fe}(C)}\sigma_{Fe}(C)\vec{\nabla}\phi\right) + \vec{\nabla} \bullet \left(\sigma_e(C)\vec{\nabla}\phi\right) \tag{3.88}$$

The first term vanishes in the metal, and the second term vanishes in the slag. Further simplifications can be made in terms of notation. Defining an effective electrical conductivity, the final form of conservation of charge is

$$0 = \vec{\nabla} \bullet \left(\sigma_{eff}(C)\vec{\nabla}\phi\right) \tag{3.89}$$

where

$$\sigma_{eff}(C) \equiv \frac{\tilde{z}(C)}{z_{Fe}(C)}\sigma_{Fe}(C) + \sigma_e(C) \tag{3.90}$$

$$\tilde{z}(C) \equiv z_{Fe}(C) - \frac{M_{Fe}}{M_O}z_O \tag{3.91}$$

$$\sigma_{Fe}(C) = \frac{z_{Fe}^2(C)F^2}{RT}D_{Fe,slag}\frac{\rho(C)\omega_{Fe}(C)}{M_{Fe}} \tag{3.92}$$

The conditions necessary for the simplifications to the conservation of charge equation described above are summarized in words as rapid charge redistribution. Note that charge redistribution in an aqueous electrolyte is a diffusive process. Since charge redistribution in aqueous electrolytes is fundamentally different than that of slags and molten salts, the simplifications derived here may not hold for aqueous systems.

Chapter 4

Numerical Methods

4.1 Introductory Remarks

In general, the governing equations for a system with fluid flow are a system of coupled non-linear partial differential equations (PDEs). To solve the system of equations numerically the system must first be discretized. The common methods for discretizing PDEs are finite difference methods, finite volume methods, finite element methods, and boundary element methods. Whichever method is chosen, the final result is the same, a system of nonlinear algebraic equations which can be solved with principles of linear algebra and numerical analysis.

This section describes a procedure for discretizing a system of conservation equations and numerically solving the corresponding system of algebraic equations. The methods described here are given for as general a case as possible. The case of 2D flow with an indefinite number of field variable is considered. First, the equations are discretized using the finite difference method. Then, a solution procedure for the resulting nonlinear algebraic equations known as a Newton-Krylov solver is described.

The methods described in this section were taken from Numerical Simulation classes at MIT [24, 25].

Figure 4.1: Finite difference grid

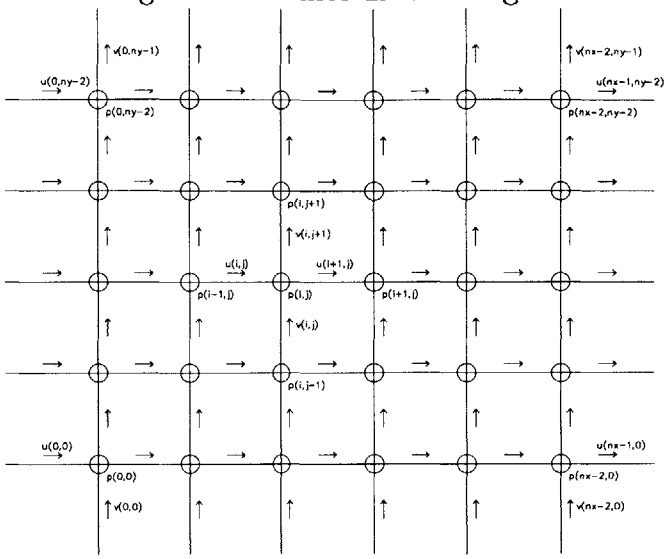

4.2 Discretization of Governing Equations, Finite Difference Method

The uniform mesh for this system is shown in Figure 4.1. The pressure nodes are represented by circles at the main grid points, and the velocity nodes are represented by arrows. nx and ny are the numbers of grid points in the x and y directions respectively. In general all field variables except for the velocity components (for example: temperature, voltage, etc.) are stored at the main grid points. The u and v nodes are stored on staggered grids so as to avoid the familiar pressure checkerboard spurrious mode [6]. Note that due the staggered grids, there will be extra u nodes in the x-direction and extra v nodes in the y-direction. The x-direction grid spacing is Δx, and the y-direction grid spacing is Δy. Notice that the velocity boundaries do not coincide with the pressure boundaries. This is convenient for symmetry boundary conditions or periodic boundary conditions. For the case of fixed velocity boundary conditions this mesh may result in unacceptable errors, so the mesh shown in Figure 4.2 may be used. The disadvantage to this mesh is that the grid spacing is not uniform, and the equations near the boundaries must be adjusted.

Figure 4.2: Finite difference grid

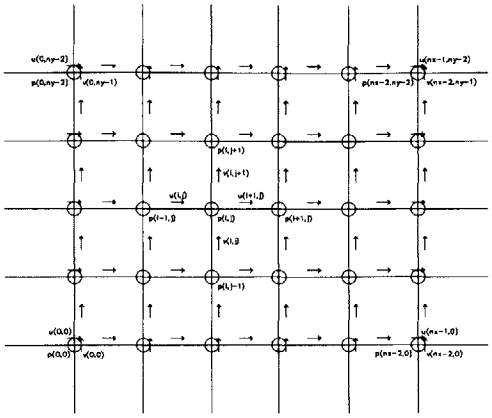

The following general conservation equation will now be discretized

$$\frac{\partial \psi}{\partial t} + \vec{\nabla} \bullet \left(\vec{V} \psi \right) = \nabla^2 \psi + S \tag{4.1}$$

where ψ represents any field. The terms are referred to from left to right as unsteady, convection, diffusion, and source. Accepting a loss of generality, ψ is limited to be a field variable stored on the main grid point (for u and v the procedure is only slightly different, and so it is not given here). In 2D the vector notation expand to

$$\frac{\partial \psi}{\partial t} + \frac{\partial}{\partial x}(u\psi) + \frac{\partial}{\partial y}(v\psi) = \frac{\partial^2 \psi}{\partial x^2} + \frac{\partial^2 \psi}{\partial y^2} + S \tag{4.2}$$

Using central differences in space this equation becomes

$$\begin{aligned} \frac{d\psi(i,j)}{dt} &= \left(\frac{\psi(i+1,j) - \psi(i,j) + \psi(i-1,j)}{\Delta x^2} \right) && (4.3) \\ &+ \left(\frac{\psi(i,j+1) - \psi(i,j) + \psi(i,j-1)}{\Delta y^2} \right) && (4.4) \\ &+ S(i,j) && (4.5) \\ &- \left(\frac{u(i+1,j)\,\psi\left(i+\frac{1}{2},j\right) - u(i,j)\,\psi\left(i-\frac{1}{2},j\right)}{\Delta x} \right) \end{aligned}$$

$$-\left(\frac{v\left(i,j+1\right)\psi\left(i,j+\frac{1}{2}\right)-v\left(i,j\right)\psi\left(i,j-\frac{1}{2}\right)}{\Delta y}\right) \tag{4.6}$$

where the convection term has been brought over to the right hand side. Note that because we have discretized in space only, the unsteady term has become a total derivative. Interpolations must be used to calculate ψ in between grid points. There are many methods for interpolating the field variable in the convection term [6]; linear interpolation was used in project. Let $f_{\psi(i,j)}$ represent the right hand side corresponding to the equation for $\psi\left(i,j\right)$.

$$\frac{d\psi\left(i,j\right)}{dt}=f_{\psi(i,j)} \tag{4.7}$$

To correspond to linear algebra notation, the unknowns are stored as vectors. The following function is used to map a field variable into a single vector.

$$\psi\left(i,j\right)\Rightarrow\psi_{j*nx+i} \tag{4.8}$$

Expanding, the vector reads

$$\vec{\psi}=\begin{bmatrix}\psi\left(0,0\right)\\ \psi\left(1,0\right)\\ \vdots\\ \psi\left(i,j\right)\\ \vdots\\ \psi\left(nx-2,ny-1\right)\\ \psi\left(nx-1,ny-1\right)\end{bmatrix}=\begin{bmatrix}\psi_0\\ \psi_1\\ \vdots\\ \psi_{j*nx+i}\\ \vdots\\ \psi_{nodes-2}\\ \psi_{nodes-1}\end{bmatrix} \tag{4.9}$$

Here subscript notation has been introduced to represent a vector index. For multi-field variables situations all field variables can be mapped into a single unknown vector $\vec{x}$ with the following

function.

$$\psi(i,j) \Rightarrow x_{(j*nx+i)nvars+nvar} \tag{4.10}$$

where $nvars$ is the total number of field variables and $nvar$ is an integer representing the field variable. For example: $nvar_u = 0$, $nvar_v = 1$, $nvar_p = 2$, $nvar_\phi = 3$, $nvars = 4$. Expanding $\vec{x}$ for this case,

$$\vec{x} = \begin{bmatrix} u(0,0) \\ v(0,0) \\ p(0,0) \\ \phi(0,0) \\ u(1,0) \\ \vdots \\ u(i,j) \\ v(i,j) \\ p(i,j) \\ \phi(i,j) \\ \vdots \\ u(nx-1, ny-1) \\ v(nx-1, ny-1) \\ p(nx-1, ny-1) \\ \phi(nx-1, ny-1) \end{bmatrix} \tag{4.11}$$

Equation 4.7 can now be written

$$\frac{dx_i}{dt} = f_i(\vec{x}) \tag{4.12}$$

where $f_i(\vec{x})$ is used to denote a function of all the elements of $\vec{x}$ (f_i in general will not be a function of all the elements. This is written for the sake compact notation.) The three basic time differencing schemes commonly used (other schemes can be found in the literature) are the

forward Euler scheme,

$$\frac{x_i^{t+1} - x_i^t}{\Delta t} = f_i^t\left(\vec{x}\right) \tag{4.13}$$

the backward Euler scheme,

$$\frac{x_i^{t+1} - x_i^t}{\Delta t} = f_i^{t+1}\left(\vec{x}\right) \tag{4.14}$$

and the trapezoidal rule,

$$\frac{x_i^{t+1} - x_i^t}{\Delta t} = \frac{1}{2}\left(f_i^{t+1}\left(\vec{x}\right) + f_i^t\left(\vec{x}\right)\right) \tag{4.15}$$

The forward Euler scheme is an explicit scheme in that $\vec{x}^{t+1}$ depends only on $\vec{x}^t$. The backward Euler scheme and the Crank-Nicholson scheme are implicit schemes in that $\vec{x}^{t+1}$ depends on $\vec{x}^{t+1}$ leading to a system of coupled equations. Numerical analysis results for linear systems are well established. For this reason, a theorem on time differencing for linear systems is given here. For the case where $\vec{f}$ is a linear function it may be written as $\vec{f} = [A]\,\vec{x}$. The theorem reads:

> A finite difference method for solving initial value problems on [0,T] is said to be order p convergent if given any $[A]$ and any initial condition
>
> $$\max_{l\epsilon\left[0,\frac{T}{\Delta t}\right]} \left\| x^l - x_{analytical}\left(l\Delta t\right)\right\| \leq C\left(\Delta t\right)^p \tag{4.16}$$
>
> for all Δt less than a given Δt_0. Forward and backward Euler are order 1 convergent and the Crank-Nicholson scheme of order 2 convergent.

Thus, because the Crank-Nicholson scheme displays better convergence for linear systems, although unjustified, this idea is extended to nonlinear systems. The Crank-Nicholson scheme was used in this project for all field variables.

The resulting system of equations will be solved using Newton's method. Therefore, before leaving this section the equations are cast into a form consistent with a Newton solver. In general, Newton's method solves for $\vec{x}$ such that $\vec{F}\left(x_0, x_1, \cdots, x_N\right) = \vec{F}\left(\vec{x}\right) = 0$. Similar to $\vec{x}$, $\vec{F}$ expands to

$$\vec{F} = \begin{bmatrix} F_{xmom}(0,0) \\ F_{ymom}(0,0) \\ F_{cont}(0,0) \\ F_{\phi}(0,0) \\ F_{xmom}(1,0) \\ \vdots \\ F_{xmom}(i,j) \\ F_{ymom}(i,j) \\ F_{cont}(i,j) \\ F_{\phi}(i,j) \\ \vdots \\ F_{xmom}(nx-1,ny-1) \\ F_{ymom}(nx-1,ny-1) \\ F_{cont}(nx-1,ny-1) \\ F_{\phi}(nx-1,ny-1) \end{bmatrix} \tag{4.17}$$

Special consideration must be taken with the continuity equation because pressure does not appear as a time derivative. In fact, the continuity equation, which is needed to solve for pressure, does not contain a pressure term. The vector $\vec{f}$ is used to represent the right hand side of a conservation equation and includes the convection term. Similar to $\vec{F}_{equation}$, $\vec{f}_{equation}$ is used to represent the right hand side of an individual equation. Using the Crank-Nicholson scheme , the elements of $\vec{F}$ are

$$F_{xmom}(i,j) = u^{t+1}(i,j) - u^{t}(i,j) - \frac{\Delta t}{2}\left(f^{t+1}_{xmom}(\vec{x}) + f^{t}_{xmom}(\vec{x})\right) \tag{4.18}$$

$$F_{ymom}(i,j) = v^{t+1}(i,j) - v^{t}(i,j) - \frac{\Delta t}{2}\left(f^{t+1}_{ymom}(\vec{x}) + f^{t}_{ymom}(\vec{x})\right) \tag{4.19}$$

$$F_{cont}(i,j) = \rho^{t+1}(i,j) - \rho^{t}(i,j) - \frac{\Delta t}{2}\left(f^{t+1}_{cont}(\vec{x}) + f^{t}_{cont}(\vec{x})\right) \tag{4.20}$$

$$F_\phi(i,j) = \phi^{t+1}(i,j) - \phi^t(i,j) - \frac{\Delta t}{2}\left(f_\phi^{t+1}(\vec{x}) + f_\phi^t(\vec{x})\right) \tag{4.21}$$

The discretized equations can easily be modified to solve for simplified flow conditions. For example, for the case of incompressible flow, the continuity equation reduces is

$$0 = \vec{\nabla} \bullet \vec{V} \tag{4.22}$$

Thus, there is no unsteady term, and the discretized form reduces to

$$F_{cont}(i,j) = f_{cont}^{t+1}(\vec{x}) \tag{4.23}$$

Note that f_{cont} for incompressible flow is not equal to f_{cont} for compressible flow.

4.3 Symmetry Boundary Conditions, Shadow Nodes

When discretizing a differential equation with finite differences the resulting difference equations in general must be altered at the boundary to satisfy the boundary conditions. For fixed boundary conditions the difference equations govern all inner nodes and the boundary conditions can be set by

$$F(i,j) = value - \psi(i,j) \tag{4.24}$$

where *value* is the fixed boundary condition. For symmetry boundary conditions however the boundary node value is unknown, so the function F must be formed at the boundary. The problem here is that central differences, which have been used for the inner nodes, cannot be used on the boundary because there are only nodes on one side of the boundary. One way around this problem is to use forward differencing instead of central differencing at the boundaries. A more elegant way around this problem (and this is the method used in this project) is to use imaginary nodes called shadow nodes. A grid with shadow nodes is shown in Figure 4.3. The grid indexing starts at $(0,0)$. The variables u, v, and C are shown near the $i = 0$ boundary and

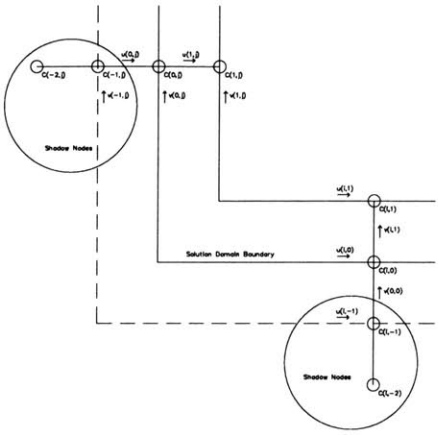

Figure 4.3: Shadow nodes

the $j = 0$ boundary. C is the dimensionless phase parameter used in the diffuse interface model. C is governed by the Cahn-Hilliard equation which is a fourth order PDE. Thus two boundary conditions for C are needed at each boundary. The shadow nodes are labeled with negative indices and are enclosed in circles. Two shadow nodes are needed for C because the governing equation contains 4th order derivatives. The symmetry conditions at $i = 0$ are

$$C(-1, j) = C(1, j) \tag{4.25}$$

$$C(-2, j) = C(2, j)$$

$$u(0, j) = -u(1, j)$$

$$v(-1, j) = v(1, j)$$

and the symmetry conditions at $j = 0$ are

$$C(i, -1) = C(i, 1) \tag{4.26}$$

$$C(i, -2) = C(i, 2)$$

$$u(i,-1) = u(i,1)$$

$$v(i,0) = -v(i,1)$$

Note that because of the staggered grid, $u(0,j)$ and $v(i,0)$ naturally act as shadow nodes.

The vector of unknowns $\vec{x}$ does not store the shadow nodes. The negative indices above are used for clarity. The code developed for this project implemented shadow nodes using the following method.

```
For i = 0 to nx-1
  For j = 0 to ny-1

    im1 = i - 1
    ip1 = i + 1
    jm1 = j - 1
    jp1 = j + 1
    if( i = 0 ); im1 = i + 1
    if( i = nx-1 ); ip1 = i - 1
    if( j = 0 ); jm1 = j + 1
    if( j = ny-1 ); jp1 = j - 1

    (d2C/dx2) = (C(ip1,j)-2C(i,j)+C(im1,j)) / (Δx)^2
    (d2C/dy2) = (C(i,jp1)-2C(i,j)+C(i,jm1)) / (Δy)^2

  end
end
```

The if statements inside the for loops may be inefficient, but as is the case for the code as a whole code clarity is chosen over code efficiency.

Figure 4.4: 1D Newton's method

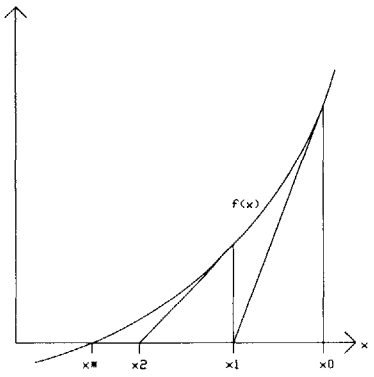

4.4 Nonlinear Solver, Multidimensional Newton's Method

Before introducing the multidimensional Newton's method, the one dimensional case is revisited to illustrate the concepts behind Newton's method. The procedure is as follows.

Problem statement: Find x^* such that $f(x^*) = 0$.

Solution: The solution procedure is shown graphically in Figure 4.4. x^* is the exact solution. Newton's method finds a numerical solution with an iterative procedure. The method begins with an initial guess value x^0 whose choice is critical to convergence, as can be seen from the picture. The equation is linearized at the guess value x^{iter}, and the new value x^{iter+1} is found by setting the linear system to zero.

$$f\left(x^{iter+1}\right) = f\left(x^{iter}\right) + \frac{df\left(x^{iter}\right)}{dx}\left(x^{iter+1} - x^{iter}\right) \tag{4.27}$$

$$\Rightarrow \frac{df\left(x^{iter}\right)}{dx}\left(x^{iter+1} - x^{iter}\right) = -f\left(x^{iter}\right) \tag{4.28}$$

$$\Rightarrow \frac{df\left(x^{iter}\right)}{dx}\Delta x^{iter} = -f\left(x^{iter}\right) \tag{4.29}$$

The computer implementation of the algorithm is:

$x^0 =$ Initial Guess, $iter = 0$

`Repeat{`

solve $\frac{df\left(x^{iter}\right)}{dx}\left(x^{iter+1}-x^{iter}\right)=-f\left(x^{iter}\right)$ for x^{iter+1}

$iter = iter + 1$

}Until $\|x^{iter+1}-x^{iter}\| < tolerance$ and $\|f\left(x^{iter+1}\right)\| < tolerance$

In the multidimensional case x is a vector of unknowns $\vec{x}$, and f is a system of nonlinear equations $\vec{F}$. Again the method begins with an initial guess $\vec{x}^0$. The system is linearized by using the calculus of several variables [8].

$$\vec{F}\left(\vec{x}^{iter+1}\right)=\vec{F}\left(\vec{x}^{iter}\right)+J\left(\vec{x}^{iter}\right)\left(\vec{x}^{iter+1}-\vec{x}^{iter}\right) \tag{4.30}$$

$$\Rightarrow J\left(\vec{x}^{iter}\right)\left(\vec{x}^{iter+1}-\vec{x}^{iter}\right)=-\vec{F}\left(\vec{x}^{iter}\right) \tag{4.31}$$

$$\Rightarrow J\left(\vec{x}^{iter}\right)\Delta\vec{x}^{iter}=-\vec{F}\left(\vec{x}^{iter}\right) \tag{4.32}$$

J is a matrix called the Jacobian. It is given by

$$J=\begin{bmatrix} \frac{\partial F_1}{\partial x_1} & \cdots & \frac{\partial F_N}{\partial x_N} \\ \vdots & \ddots & \vdots \\ \frac{\partial F_N}{\partial x_1} & \cdots & \frac{\partial F_N}{\partial x_N} \end{bmatrix} \tag{4.33}$$

J can be interpreted physically as the sensitivity of $\vec{F}$ to changes in $\vec{x}$. The computer implementation of the algorithm is given below. For completeness a relaxation parameter *relax* has been introduced which depending on $\vec{x}^0$ may be necessary for convergence. *relax* is a scalar parameter with a range [0,1]. In general, *relax* varies with each iteration and is chosen such that $\left\|\vec{F}\left(\vec{x}^{iter}+relax^{iter}*\Delta\vec{x}^{iter}\right)\right\|$ is minimized. In practice, *relax* is a constant, usually 1/4, 1/2 or 1. Newton's method with a relaxation parameter is called a damped Newton's method.

$\vec{x}^0$ = Initial Guess, $iter = 0$

Repeat{

solve $J\left(\vec{x}^{iter}\right)\Delta\vec{x}^{iter}=-\vec{F}\left(\vec{x}^{iter}\right)$ for $\Delta\vec{x}^{iter}$

$\vec{x}^{iter+1} = \vec{x}^{iter} + relax^{iter} * \Delta\vec{x}^{iter}$

$iter = iter + 1$

}Until $\|x^{iter+1} - x^{iter}\| < tolerance$ and $\|f(x^{iter+1})\| < tolerance$

Numerical analysis shows that Newton's method converges quadratically

$$\left\|F\left(\vec{x}^{iter+1}\right)\right\| \leq \text{(Bounded constant)} \left\|F\left(\vec{x}^{iter}\right)\right\|^2 \tag{4.34}$$

given that the Jacobian inverse is bounded and is Lipschitz continuous (continuous derivatives).

A final note on Newton's method is that the linear system can be represented by the common notation,

$$[M]\,\vec{x} = \vec{b} \tag{4.35}$$

where

$$[J] \rightarrow [M] \tag{4.36}$$

$$\vec{\Delta x} \rightarrow \vec{x} \tag{4.37}$$

$$-\vec{F} \rightarrow \vec{b} \tag{4.38}$$

The method for solving the linear system is described in the next section.

4.5 Krylov Subspace Linear Solver

4.5.1 QR Factorization, Gram-Schmidt Algorithm

An overview of the QR factorization is presented first. Given the system of linear equations

$$[M]\,\vec{x} = \vec{b} \tag{4.39}$$

The matrix M is decomposed into two matrices Q and R

$$[Q][R]\,\vec{x} = \vec{b} \tag{4.40}$$

where Q is orthonormal and R is upper triangular. Since Q is orthonormal, $Q^{-1} = Q^T$.

$$[R]\,\vec{x} = [Q]^T\,\vec{b} = \vec{\tilde{b}} \tag{4.41}$$

Since R is uppertriangular, $\vec{x}$ is found using a simple backsolve.

The details of the decomposition are now discussed. Consider viewing M as a collection of column vectors.

$$\begin{bmatrix} \uparrow & \cdots & \uparrow \\ \vec{M}_1 & \cdots & \vec{M}_N \\ \downarrow & \cdots & \downarrow \end{bmatrix} \begin{bmatrix} x_1 \\ \vdots \\ x_N \end{bmatrix} = \vec{b} \tag{4.42}$$

The system can be written

$$x_1\vec{M}_1 + x_2\vec{M}_2 + \cdots x_N\vec{M}_N = \vec{b} \tag{4.43}$$

$\vec{b}$ is said to be in the span of the columns of M if a solution exists. The corresponding QR system is

$$\begin{bmatrix} \uparrow & \cdots & \uparrow \\ \vec{Q}_1 & \cdots & \vec{Q}_N \\ \downarrow & \cdots & \downarrow \end{bmatrix} \begin{bmatrix} r_{11} & \cdots & r_{1N} \\ 0 & \ddots & \vdots \\ 0 & 0 & r_{NN} \end{bmatrix} \begin{bmatrix} x_1 \\ \vdots \\ x_N \end{bmatrix} = \vec{b} \tag{4.44}$$

To form $\vec{Q}_1$, $\vec{M}_1$ is normalized.

$$\vec{Q}_1 = \frac{\vec{M}_1}{\sqrt{\vec{M}_1 \bullet \vec{M}_1}} \tag{4.45}$$

$\vec{Q}_2$ is made orthogonal to $\vec{Q}_1$ by subtracting off part of $\vec{M}_1$ from $\vec{M}_2$. ($\vec{\tilde{Q}}_i$ represents orthogonal vectors that are not necessarily normal)

$$\vec{\tilde{Q}}_2 = \vec{M}_2 - r_{21}\vec{Q}_1 \tag{4.46}$$

$$\vec{Q}_1 \bullet \vec{\widetilde{Q}}_2 = \vec{Q}_1 \bullet \left(\vec{M}_2 - r_{21}\vec{Q}_1\right) = 0 \tag{4.47}$$

Since $\vec{Q}_1 \bullet \vec{Q}_1 = 1$,

$$r_{21} = \vec{Q}_1 \bullet \vec{M}_2 \tag{4.48}$$

Now, $\vec{\widetilde{Q}}_2$ is normalized

$$\vec{Q}_2 = \frac{\vec{\widetilde{Q}}_2}{\sqrt{\vec{\widetilde{Q}}_2 \bullet \vec{\widetilde{Q}}_2}} \tag{4.49}$$

The procedure is now extending to the general column $\vec{M}_i$. $\vec{\widetilde{Q}}_i$ is defined by

$$\vec{\widetilde{Q}}_i = \vec{M}_i - r_{i1}\vec{Q}_1 - r_{i2}\vec{Q}_2 - \cdots - r_{i,i-1}\vec{Q}_{i-1} \tag{4.50}$$

To make $\vec{M}_i$ orthogonal to the columns to the left of it,

$$\vec{Q}_1 \bullet \left(\vec{M}_i - r_{i1}\vec{Q}_1 - \cdots - r_{i,i-1}\vec{Q}_{i-1}\right) = 0 \Rightarrow r_{i1} = \vec{Q}_1 \bullet \vec{M}_i \tag{4.51}$$

$$\vec{Q}_2 \bullet \left(\vec{M}_i - r_{i1}\vec{Q}_1 - \cdots - r_{i,i-1}\vec{Q}_{i-1}\right) = 0 \Rightarrow r_{i2} = \vec{Q}_2 \bullet \vec{M}_i \tag{4.52}$$

$$\vdots$$

$$\vec{Q}_{i-1} \bullet \left(\vec{M}_i - r_{i1}\vec{Q}_1 - \cdots - r_{i,i-1}\vec{Q}_{i-1}\right) = 0 \Rightarrow r_{i,i-1} = \vec{Q}_{i-1} \bullet \vec{M}_i \tag{4.53}$$

Normalizing gives

$$\vec{Q}_i = \frac{\vec{\widetilde{Q}}_i}{\sqrt{\vec{\widetilde{Q}}_i \bullet \vec{\widetilde{Q}}_i}} \tag{4.54}$$

The computer implementation of this algorithm is the Gram-Schmidt Algorithm shown below:

```
For i = 1 to N (for each target column)
  M_i = M e_i (matrix vector product)
  For j = 1 to i-1 (orthogonalize to columns to left of target)
    r_ij = Q_j • M_i
```

$\vec{M}_i = \vec{M}_i - r_{ij} Q_j$

End

$r_{ii} = \sqrt{\vec{M}_i \bullet \vec{M}_i}$

$\vec{Q}_i = \frac{1}{r_{ii}} \vec{M}_i$ (normalize target column)

End

4.5.2 General Minimization Algorithm

A more general approach to solving the linear system

$$[M]\,\vec{x} = \vec{b} \tag{4.55}$$

is to minimize the residual product $\vec{r} \bullet \vec{r}$ where

$$\vec{r} \equiv \vec{b} - [M]\,\vec{x} \tag{4.56}$$

First, consider a 1D minimization. Here $\vec{x} = x\vec{e}_1$ and $[M]\,\vec{x} = x_1\,[M]\,\vec{e}_1 = x_1\vec{M}_1$. The residual norm is

$$\begin{aligned} \vec{r} \bullet \vec{r} &= \left(\vec{b} - x_1\vec{M}_1\right) \bullet \left(\vec{b} - x_1\vec{M}_1\right) && (4.57) \\ &= \vec{b} \bullet \vec{b} - 2\vec{b} \bullet \left(x_1\vec{M}_1\right) + \left(x_1\vec{M}_1\right) \bullet \left(x_1\vec{M}_1\right) && (4.58) \end{aligned}$$

The residual product will be minimized when the derivative is zero.

$$\frac{d}{dx_1}\left(\vec{r} \bullet \vec{r}\right) = -2\vec{b} \bullet \left(\vec{M}_1\right) + 2x_1 \left(\vec{M}_1\right) \bullet \left(\vec{M}_1\right) = 0 \tag{4.59}$$

Solving for x_1 gives

$$x_1 = \frac{\vec{b} \bullet \vec{M}_1}{\vec{M}_1 \bullet \vec{M}_1} = \vec{b} \bullet \widehat{M}_1 \tag{4.60}$$

where $\widehat{M}_1$ is a unit vector in the $\vec{M}_1$ direction. The 1D minimization is shown graphically in

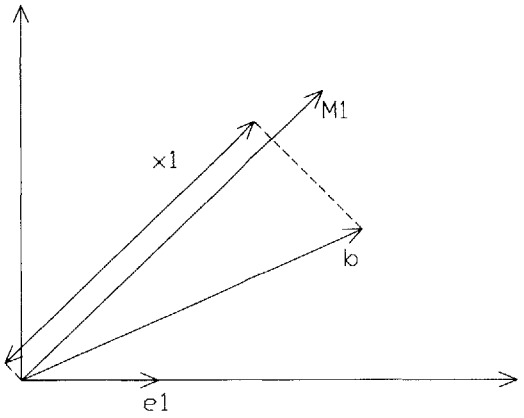

Figure 4.5: 1D minimization

Figure 4.5. Minimizing the residual is equivalent to forming the projection of $\vec{b}$ onto $\vec{M}_1$.

Now, consider a 2D minimization. Here $\vec{x} = x\vec{e}_1 + x\vec{e}_2$ and $M\vec{x} = x_1 M\vec{e}_1 + x_2 M\vec{e}_2$. The residual product is

$$\begin{aligned} \vec{r} \bullet \vec{r} &= \left(\vec{b} - x_1 M\vec{e}_1 - x_2 M\vec{e}_2\right) \bullet \left(\vec{b} - x_1 M\vec{e}_1 - x_2 M\vec{e}_2\right) \\ &= \vec{b} \bullet \vec{b} - 2x_1 \vec{b} \bullet (M\vec{e}_1) - 2x_2 \vec{b} \bullet (M\vec{e}_2) + x_1^2 (M\vec{e}_1) \bullet (M\vec{e}_1) \\ &\quad + x_2^2 (M\vec{e}_2) \bullet (M\vec{e}_2) + 2x_1 x_2 (M\vec{e}_1) \bullet (M\vec{e}_2) \end{aligned} \tag{4.61}$$

Note that the last term contains both x_1 and x_2. Taking derivatives gives

$$\begin{aligned} \frac{\partial}{\partial x_1}(\vec{r} \bullet \vec{r}) &= -2\vec{b} \bullet (M\vec{e}_1) + 2x_1 (M\vec{e}_1) \bullet (M\vec{e}_1) \\ &\quad + 2x_2 (M\vec{e}_1) \bullet (M\vec{e}_2) = 0 \end{aligned} \tag{4.62}$$

and

$$\begin{aligned} \frac{\partial}{\partial x_2}(\vec{r} \bullet \vec{r}) &= -2\vec{b} \bullet (M\vec{e}_2) + 2x_2 (M\vec{e}_2) \bullet (M\vec{e}_2) \\ &\quad + 2x_1 (M\vec{e}_1) \bullet (M\vec{e}_2) = 0 \end{aligned} \tag{4.63}$$

Solving for $\vec{x}$ would require solving a system of coupled equations. To avoid the coupling, general search directions are introduced. Referring to Figure 4.5, x_1 was limited to the $(M\vec{e}_1)$ direction. For 2D, the new search directions are $(M\vec{p}_1)$ and $(M\vec{p}_2)$. $\vec{x}$ becomes

$$\vec{x} = x\vec{e}_1 + x\vec{e}_2 = \nu_1\vec{p}_1 + \nu_2\vec{p}_2 \tag{4.64}$$

and $M\vec{x}$ becomes

$$M\vec{x} = \nu_1 (M\vec{p}_1) + \nu_2 (M\vec{p}_2) \tag{4.65}$$

The residual product becomes

$$\begin{aligned} \vec{r} \bullet \vec{r} &= \left(\vec{b} - \nu_1 M\vec{p}_1 - \nu_2 M\vec{p}_2\right) \bullet \left(\vec{b} - \nu_1 M\vec{p}_1 - \nu_2 M\vec{p}_2\right) \qquad (4.66) \\ &= \vec{b} \bullet \vec{b} - 2\nu_1 \vec{b} \bullet (M\vec{p}_1) - 2\nu_2 \vec{b} \bullet (M\vec{p}_2) + \nu_1^2 (M\vec{p}_1) \bullet (M\vec{p}_1) \\ &\quad + \nu_2^2 (M\vec{p}_2) \bullet (M\vec{p}_2) + 2\nu_1\nu_2 (M\vec{p}_1) \bullet (M\vec{p}_2) \end{aligned}$$

The coupling term is eliminated by applying the Gram-Schmidt Algorithm to the $M\vec{p}_i$ vectors instead of the $M\vec{e}_i$ vectors. . Therefore, the $M\vec{p}_i$ vectors will be orthonormal.

In general the residual product is

$$\begin{aligned} \vec{r} \bullet \vec{r} &= \left(\vec{b} - \nu_1 M\vec{p}_1 - \cdots - \nu_k M\vec{p}_k\right) \qquad (4.67) \\ &\quad \bullet \left(\vec{b} - \nu_1 M\vec{p}_1 - \cdots - \nu_k M\vec{p}_k\right) \qquad (4.68) \end{aligned}$$

Taking the derivative, all coupling terms are zero, and the only terms remaining are

$$\frac{\partial}{\partial x_i} (\vec{r} \bullet \vec{r}) = -2\vec{b} \bullet (M\vec{p}_i) + 2x_i (M\vec{p}_i) \bullet (M\vec{p}_i) = 0 \tag{4.69}$$

Solving for x_i,

$$x_i = \frac{\vec{b} \bullet (M\vec{p}_i)}{(M\vec{p}_i) \bullet (M\vec{p}_i)} \tag{4.70}$$

Thus, using the notation $\overrightarrow{Mp}_i = M\vec{p}_i$, the general minimization algorithm is:

```
For i = 1 to N (for each target column)
```
$\vec{p}_i = \vec{e}_i$

$\overrightarrow{Mp}_i = M\vec{e}_i$ (matrix vector product)

```
For j = 1 to i-1 (orthogonalize to columns to left of target)
```
$r_{ij} = \left(\overrightarrow{Mp}_j\right) \bullet \left(\overrightarrow{Mp}_i\right)$

$\left(\overrightarrow{Mp}_i\right) = \left(\overrightarrow{Mp}_i\right) - r_{ij}\left(\overrightarrow{Mp}_j\right)$

$\vec{p}_i = \vec{p}_i - r_{ij}\vec{p}_j$

End

$r_{ii} = \sqrt{\left(\overrightarrow{Mp}_i\right) \bullet \left(\overrightarrow{Mp}_i\right)}$

$\left(\overrightarrow{Mp}_i\right) = \frac{1}{r_{ii}}\left(\overrightarrow{Mp}_i\right)$ (normalize target column)

$\vec{x} = \vec{x} + \nu_i \vec{p}_i$

End

4.5.3 Krylov Subspace Generation

First, concept of a vector space is introduced. The unit vectors $\hat{i}$ and $\hat{j}$ are the unit vectors in the x any y directions respectively of the xy plane. With respect to the three dimensional xyz space, $\hat{i}$ and $\hat{j}$ span a 2D subspace, the xy plane. In general, the vector $\vec{x}$ with N components resides in an N dimensional space. The vectors that span the space are the $\vec{e}_i$ vectors.

$$\vec{x} = \begin{bmatrix} x_1 \\ \vdots \\ x_N \end{bmatrix} = x_1 \begin{bmatrix} 1 \\ 0 \\ \vdots \\ 0 \end{bmatrix} + \cdots + x_N \begin{bmatrix} 0 \\ \vdots \\ 0 \\ N \end{bmatrix} = x_1\vec{e}_1 + \cdots + x_N\vec{e}_N \tag{4.71}$$

The notation for the space associated with the $\vec{e}_i$ unit vectors is

$$\text{space} = \text{span}\left\{\vec{e}_1, \ldots, \vec{e}_k, \ldots, \vec{e}_N\right\} \tag{4.72}$$

A new subspace called the Krylov subspace is formed by using M and b.

$$\text{Krylov subspace } = \text{span}\left\{\vec{b}, M\vec{b}, MM\vec{b}, \ldots, M^k\vec{b}\right\} \tag{4.73}$$

Here matrix exponents have been introduced. For example, $MM = M^2$.

The general idea of the residual minimization was obtain the best approximation to $\vec{x}$ using a trial vector $\vec{x}^k$ which was composed of unit vectors that did not span the total space of the $\vec{e}_i$ vectors. The total solution is

$$\vec{x} = x_1\vec{e}_1 + \cdots + x_N\vec{e}_N \tag{4.74}$$

Using a subspace of k of the $\vec{e}_i$ unit vectors , an approximate solution can be obtained from

$$\vec{x}^k = x_1\vec{e}_1 + \cdots + x_k\vec{e}_k \tag{4.75}$$

Using an arbitrary k^{th} dimensional subspace,

$$\vec{x}^k = \alpha_1\vec{w}_1 + \cdots + \alpha_k\vec{w}_k \tag{4.76}$$

Using the Krylov subspace, $\vec{x}^k$ becomes

$$\vec{x}^k = \alpha_1\vec{b} + \alpha_2 M\vec{b} + \alpha_3 MM\vec{b} \cdots + \alpha_k M^{k-1}\vec{b} = \sum_{i=1}^{k}\alpha_i M^{i-1}\vec{b} \tag{4.77}$$

and the residual is

$$\vec{r}^k = \vec{b} - M\vec{x}^k = \left(1 - \sum_{i=1}^{k}\alpha_i M^i\right)\vec{b} \tag{4.78}$$

4.5.4 The Generalized Conjugate Residual Algorithm

Equation 4.78 shows the relation between the residual and the Krylov subspace vectors. For example, consider $\vec{r}_1$,

$$\vec{r}^1 = \vec{b} - M\vec{x}^1 = \vec{b} - M\left(\alpha_1 \vec{b}\right) \tag{4.79}$$

which implies

$$\text{span}\left\{\vec{b}, M\vec{b}\right\} = \text{span}\left\{\vec{b}, \vec{r}^1\right\}$$

For convenience $\vec{r}^0$ is defined

$$\vec{r}^0 \equiv \vec{b} \tag{4.80}$$

Generalizing equation 4.79, the residual vectors are shown to span the Krylov subspace.

$$\begin{aligned} \text{Krylov subspace} &= \text{span}\left\{\vec{b}, M\vec{b}, MM\vec{b}, \ldots, M^k\vec{b}\right\} \\ &= \text{span}\left\{\vec{r}^0, \ldots, \vec{r}^k\right\} \end{aligned} \tag{4.81}$$

In the Generalized Conjugate Residual Algorithm (GCR), the residual vectors are used as the initial search directions instead of the $\vec{e}_i$ vectors. The final Generalized Conjugate Residual Algorithm is shown below:

$\vec{r} = \vec{b}$

```
For i = 1 to N (for each target column)
```

$\vec{p}_i = \vec{r}$

$\vec{Mp}_i = M\vec{e}_i$ `(matrix vector product)`

```
For j = 1 to i-1 (orthogonalize to columns to left of target)
```

$r_{ij} = \left(\vec{Mp}_j\right) \bullet \left(\vec{Mp}_i\right)$

$\left(\vec{Mp}_i\right) = \left(\vec{Mp}_i\right) - r_{ij}\left(\vec{Mp}_j\right)$

$\vec{p}_i = \vec{p}_i - r_{ij}\vec{p}_j$

```
End
```

$r_{ii} = \sqrt{\left(\overrightarrow{Mp_i}\right) \bullet \left(\overrightarrow{Mp_i}\right)}$

$\left(\overrightarrow{Mp_i}\right) = \frac{1}{r_{ii}} \left(\overrightarrow{Mp_i}\right)$ (normalize target column)

$\overrightarrow{x} = \overrightarrow{x} + \nu_i \overrightarrow{p}_i$ (update solution)

$\overrightarrow{r} = \overrightarrow{r} - \nu_i \left(\overrightarrow{Mp_i}\right)$ (update residual)

if($\overrightarrow{r} \bullet \overrightarrow{r}$) < tolerance); then break loop;

End

If a solution exists then GCR converges to the exact solution in at most N steps (of the outer loop). In fact numerical analysis shows that if M has only q distinct eigenvalues, then GCR converges in at most q steps.

In closing this section, a qualitative description of the algorithm is discussed. The main for loop represents adding new terms to the trial solution

$$\overrightarrow{x}^{iter} = \nu_1 \overrightarrow{p}_1 + \cdots + \nu_{iter} \overrightarrow{p}_{iter} \tag{4.82}$$

The corresponding new search direction is

$$\overrightarrow{Mx}^{iter} = \nu_1 \overrightarrow{Mp}_1 + \cdots + \nu_{iter} \overrightarrow{Mp}_{iter} \tag{4.83}$$

The new term for the search vector $\left(\overrightarrow{Mp}_{iter}\right)$ is chosen such that it is orthonormal to the other search vectors, and the new component ν_{iter} is chosen such that the residual product is minimized. The main for loop ends when the residual product is acceptably small, or when the current search direction is close enough to $\overrightarrow{b}$. In general GCR converges with $i < N$.

4.6 Newton-Krylov Matrix Free Approximation

One of the key features of the Gram-Schmidt Algorithm is that only matrix vector products are needed. Recall the first step in the algorithm was $\overrightarrow{M}_i = M\overrightarrow{e}_i$ (matrix vector product). The

linear system in Newton's method at Newton iteration k is

$$J\left(\vec{x}^k\right)\Delta\vec{x}^{k+1} = -F\left(\vec{x}^k\right) \tag{4.84}$$

The corresponding search direction at GCR iteration *iter* is the matrix vector product

$$J\left(\vec{x}^k\right)\vec{p}^{iter} \tag{4.85}$$

In the matrix free approximation, a finite difference is used to approximate the matrix vector product.

$$J\left(\vec{x}^k\right)\vec{p}^{iter} \approx \frac{1}{\varepsilon}\left(F\left(\vec{x}^k + \varepsilon\vec{p}^{iter}\right) - F\left(\vec{x}^k\right)\right) \tag{4.86}$$

ε is a problem dependent constant usually on the order of 10^{-4}. Methods for choosing ε to optimize convergence can be found in numerical analysis literature. The combination of Newton's method with GCR enables solutions without calculating the Jacobian matrix.

4.7 PETSc

PETSc (The Portable, Extensible Toolkit for Scientific Computing) is a collection of C programming libraries used for the numerical solutions of PDEs on parallel and serial computers. PETSc includes functions for managing data storage for 1D, 2D, and 3D grids, Newton-Krylov solvers, and time integration schemes. PETSc uses the MPI standard for all message-passing communication for parallel processing. The official documentation can be found at http://www.mcs.anl.gov/petsc/docs/.

One limitation of PETSc is the time integration schemes constrain each field variable to use the same discretization scheme which conflicts with the continuity equation. To ensure complete flexibility, control and understanding, the code for forming the vectors and the numerical solution routines were written as part of this project. PETSc was used in this project only for managing field variable storage and for parallel processing. PETSc functions were used for linear algebra

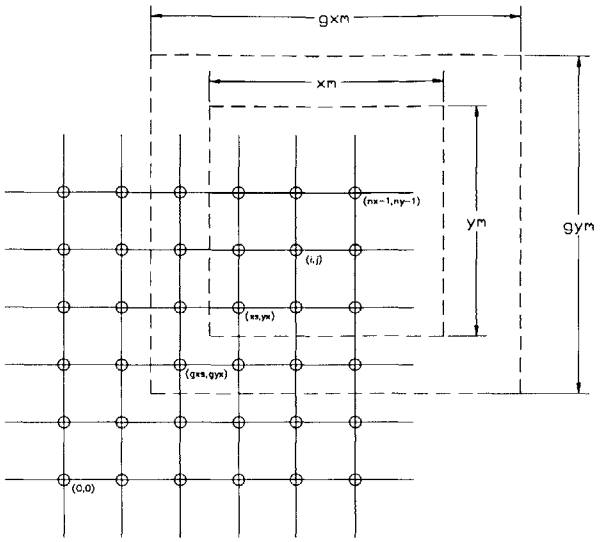

Figure 4.6: PETSc distributed array

operations such as vector addition, vector-scalar multiplication, vector norms, etc. This section explains parallel computer data storage with PETSc for a 2D grid with an arbitrary number of field variables.

A typical 2D grid is shown in Figure 4.6. The vector $\vec{x}$ contains the value of each field variable at every grid point. The mapping from grid to vector was given in equation 4.10

$$\phi(i,j) \Rightarrow x_{(j*nx+i)nvars+nvar} \tag{4.87}$$

and the vector was expanded in equation 4.11. When running a program in parallel, the program runs simultaneously on each processor. Each processor stores only a fraction of the grid points with a local vector $\overrightarrow{localx}$. Since $\vec{x}$ contains the values for every grid point it is called a global vector. The global vector $\vec{F}$, contains the discretized equation values. The local processor will store a corresponding local vector $\overrightarrow{localF}$. When a spatial derivative is discretized at an arbitrary grid point (i,j), the values at adjacent nodes are needed. For example, to discretize $\nabla^2\phi$ at point (i,j), $\phi(i,j)$, $\phi(i-1,j)$, $\phi(i+1,j)$, $\phi(i,j-1)$, and $\phi(i,j+1)$ are needed. Therefore, referring to the figure, the local processor needs the nodes in the outer box of $\overrightarrow{localx}$ to form the nodes in

the inner box of $\overrightarrow{localF}$. The same data storage is used for all local vectors, so the local processor stores the grid points in the outer box. Note that there will be some overlap of data storage across processors. The extra nodes between the inner and outer boxes stored on the local vector needed for discretization are called ghost nodes. The number of adjacent nodes needed per point (i, j) is called the stencil width. The grid shown here has a stencil width of 1, which corresponds to discretizing $\nabla^2\phi$. In this project, in order to discretize the (fourth order) Cahn-Hilliard equation, a stencil width of 2 was used.

The point (xs, ys) denotes the starting position of the inner box of the local grid, and xm and ym denote the number of grid points in the x-direction and y-direction respectively. For the grid shown $xm = 3$ and $ym = 3$. The point (gxs, gys) denotes the starting position of the outer box of the local grid, and gxm and gym denote the number of grids points in the x-direction and y-direction respectively. For the grid shown $gxm = 4$ and $gym = 4$. To map from a field variable to a local vector the following function is used.

$$\phi(i,j) \Rightarrow localx_{((j-gys)*gxm+(i-gxs))nvars+nvar} \tag{4.88}$$

To calculate local vectors the program loops over the local grid only. For example, to form $\overrightarrow{localF}$ the following loop is used.

```
for( i = xs ; i < xs + xm ; i++ ){
  for( j = ys ; j < ys + ym ; j++ ){
```

$$localF_{((j-gys)*gxm+(i-gxs))nvars+nvar} =$$

$$f(\phi(i,j), \phi(i+1,j), \phi(i-1,j), \phi(i,j+1), \phi(i,j-1), \cdots)$$

```
  }
}
```

Here the functional dependence of $\overrightarrow{localF}$ on neighboring grid points is expressed implicitly with f.

In closing, it is noted that the code for parallel processing is also valid for single processing. If the code is run on a single processor, then $gxs = gys = xs = ys = 0$, $gxm = xm$, and $gym = ym$. In this case, there is no distinction between local and global vectors.

Chapter 5

Numerical Simulation Case Studies

5.1 Introductory Remarks

In this section, the results from a series of simulations are presented. The simulations were chosen such that each case illustrates a single phenomenon associated with the physical system. The results are validated with asymptotic solutions.

For convenience, some details of the simulations, which are the same for all cases, are given here. The finite-difference method was used for spacial discretization, and the Crank-Nicholson sheme was used for temporal discretization. Symmetry (or zero flux) boundary conditions were used for the phase variable C using shadow nodes. All 2D plots do not have axes labeled. The x-axis positive direction is east, the y-axis positive direction is north, and the bottom left corner is point (0,0). Recall that, because of the staggered grids, the C grid is nx-1 by ny-1, the u grid is nx by ny-1, and the v grid is nx-1 by ny. The extra nodes for C were assigned the value of their adjacent nodes are included in the plots. Thus, for coarse grid cases the plots may appear slightly distorted.

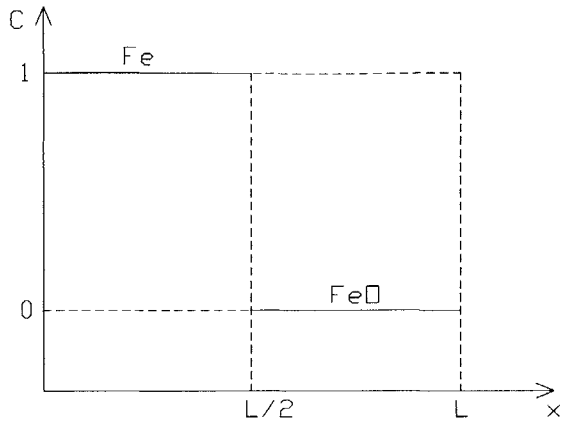

Figure 5.1: Initial concentration profile

5.2 Diffusion

In this section, two cases of inter-phase diffusion are presented. The first case is a single interface system, and the second case is a multi-interface system.

For the single interface case, consider the 1D Fe-FeO system shown in Figure . The figure shows the initial conditions of the phase variable C. $C = 0$ represents FeO, and $C = 1$ represents Fe. The governing equation is simply

$$\frac{\partial}{\partial t}(\rho C) = \frac{M_{Fe}}{\Delta\omega_{Fe}} \vec{\nabla} \bullet \left(\kappa \vec{\nabla} \mu\right) \tag{5.1}$$

where

$$\epsilon = N * dx \text{ integer number of grid spacing} \tag{5.2}$$

$$\alpha = \left(\sqrt{18}\right)\gamma\epsilon \tag{5.3}$$

$$\beta = \frac{\left(\sqrt{18}\right)\gamma}{\epsilon} \tag{5.4}$$

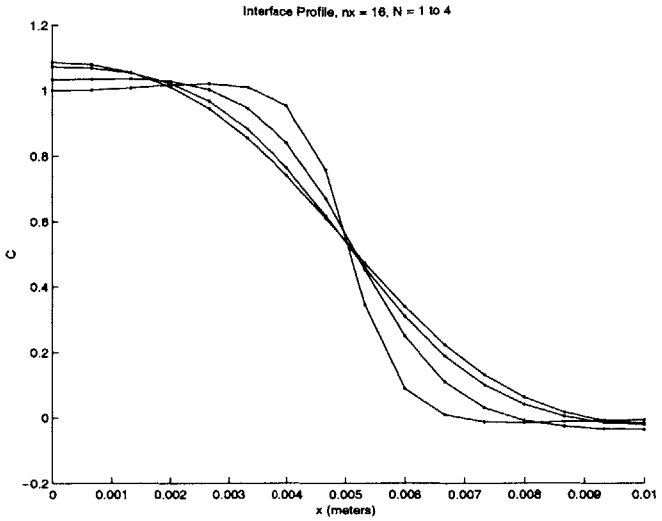

Figure 5.2: C at steady state, 1D system, 16 nodes

$$\kappa = \frac{D_{Fe,slag}\left(c_{Fe,metal} - c_{Fe,slag}\right)}{\beta\left(\frac{d^2\Psi}{dC^2}\right)_{C=0}} \tag{5.5}$$

Symmetry boundary conditions were used on all boundaries.

First, steady-state results are given for various grids and interface thicknesses, $\epsilon = N * dx$. Figures 5.2, 5.3, 5.4, and 5.5 show steady state concentration profiles across a diffuse interface using 16, 32, 64, and 128 grid points respectively.

Each figure contains 4 plots of various interface thicknesses, $N = 1, 2, 3, 4$. The length of the solution domain is $1cm$. Because an increasing interface thickness corresponds to an increasing N, the curves are not labeled. For $N = 1$, the diffuse interface spans approximately 6 nodes. This result is best seen from the 16 node case. The interface thickness is shown to increase linearly with N as is expected. For larger interface thicknesses, C is shown to exceed the expected limits of $[0, 1]$. This is a natural result of the initial conditions and the zero flux symmetry boundary conditions. As the interface diffuses, overall mass in conserved.

Next, unsteady effects are presented. Figure shows the interface evolution for the 32 node, $N = 2$ case. A time increment of $dt = 10s$ was used. The figure contains plots of four different timesteps $T = 0, 10, 100, steady$ which corresponds to elapsed times of $t = 0s, 10^2s, 10^4s, \infty$. At $100s$, the first significant effects of diffusion are shown. At 10^4s, the interface is approximately

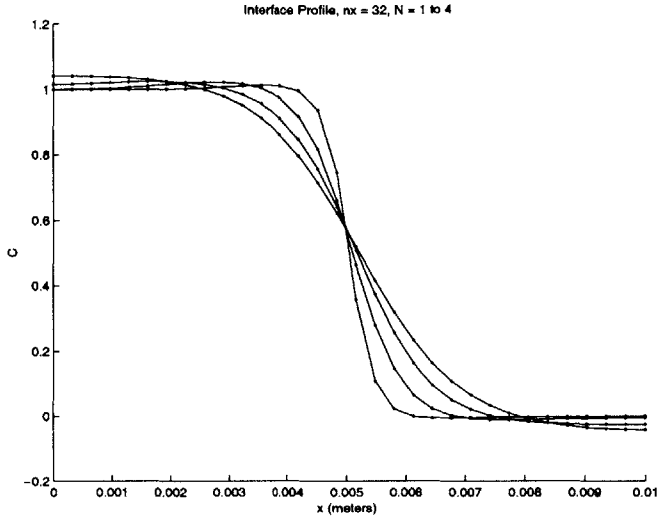

Figure 5.3: C at steady state, 1D system, 32 nodes

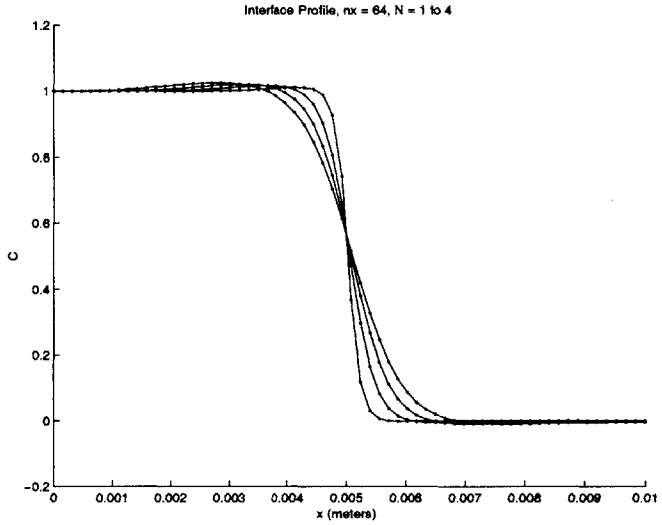

Figure 5.4: C at steady state, 1D system, 64 nodes

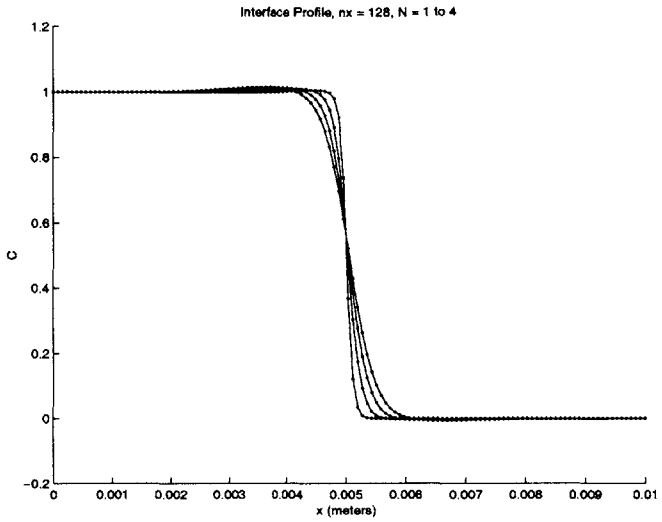

Figure 5.5: C at steady state, 1D system, 128 nodes

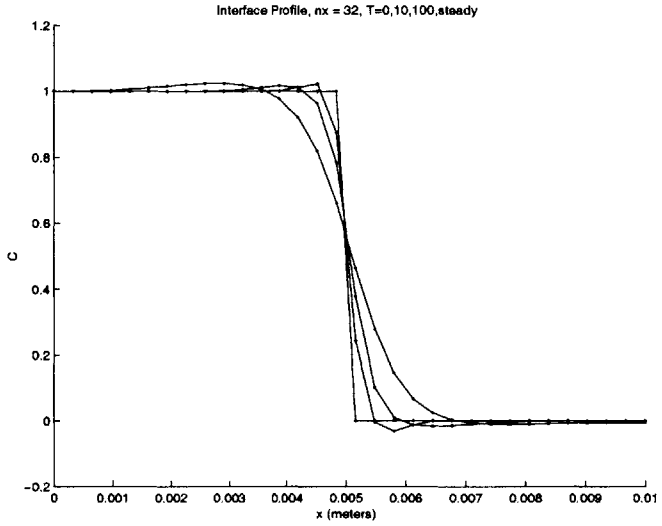

Figure 5.6: Evolution of concentration profile, 1D system, 32 nodes

halfway diffused to the steady state profile. These results support the macroscopic timescale $\tau_{macro} \sim 400s$ given in equation 3.77.

For the multi-interface system, consider the 2D Fe-FeO-Fe system shown in Figure 5.7. The figure shows the phase variable C at $t = 0$. $C = 0$ represents FeO, and $C = 1$ represents pure Fe. There are three main layers in the y-direction, Fe-FeO-Fe, and the FeO phase contains a small drop of Fe. The solution domain is $L_x = L_y = 1cm$. The grid is 64x64 nodes. Symmetry boundary conditions are used on all boundaries. Unsteady effects are similar to those shown in Figure 5.6; the interface smoothes out over a number of nodes corresponding to the interface thickness. (Numerical) Steady-state results are shown in Figures 5.8, 5.9, and 5.10 for $N = 1, 2, 3$ respectively.

For $N = 1$, the interface is relatively sharp, and the Fe drop does not influence the outer Fe layers. For $N = 2$ however, the interface is approximately twice as thick, and the Fe drop does influence the outer Fe layer. The drop and layer interfaces almost overlap pushing the outer Fe layer slightly away from the Fe drop. For $N = 3$, the drop completely disappears because the interfaces do overlap. Because the interfaces overlap, the drop forms a bridge between the outer Fe layers. Then the drop is consumed by the outer Fe layers minimizing the overall free energy of the system. The conclusion drawn from these three simulations is that the choice of interface thickness is a critical modeling factor. For example, to predict a stable interface the $N = 1$ case gave the best results, but to predict merging interfaces the $N = 2$ case gave the best results. Therefore, depending on the desired phenomenon to be predicted, the interface thickness can be set accordingly.

5.3 Diffusion, Migration

In this section, a voltage is applied to the Fe-FeO system. A migration term is added to the conservation of species equation. The electric field induces flux across the interface, leading to interface motion. Because the two phases have different densities, according to the continuity

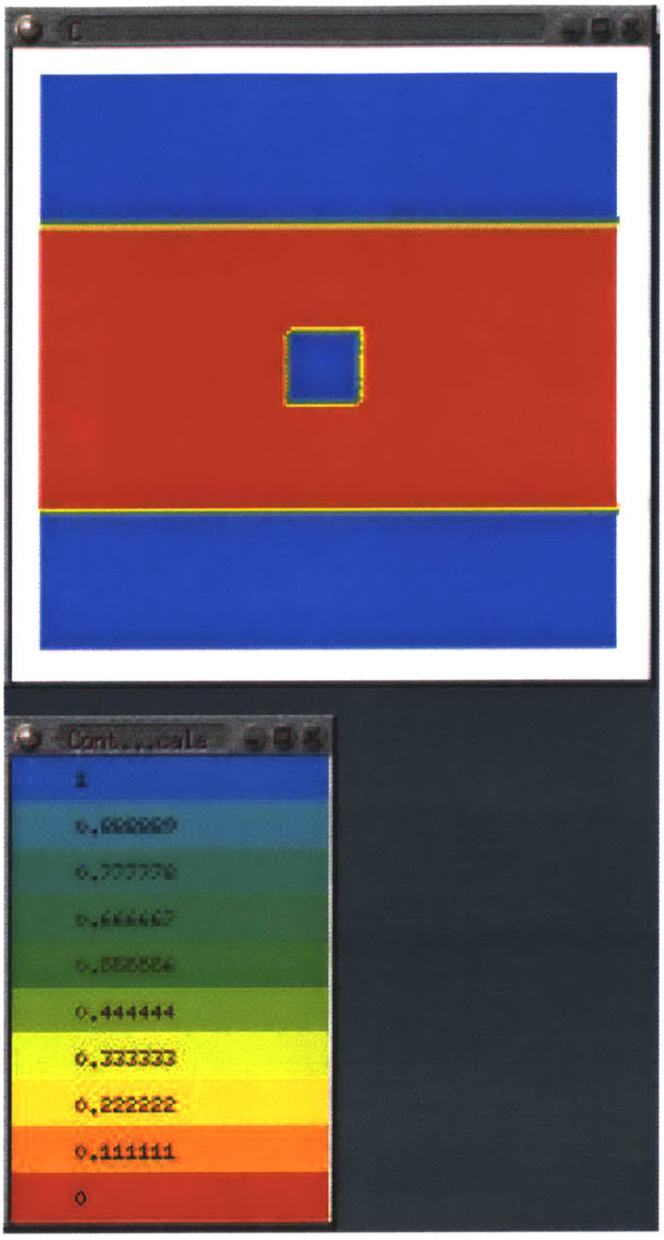

Figure 5.7: C at t=0, multi-interface system

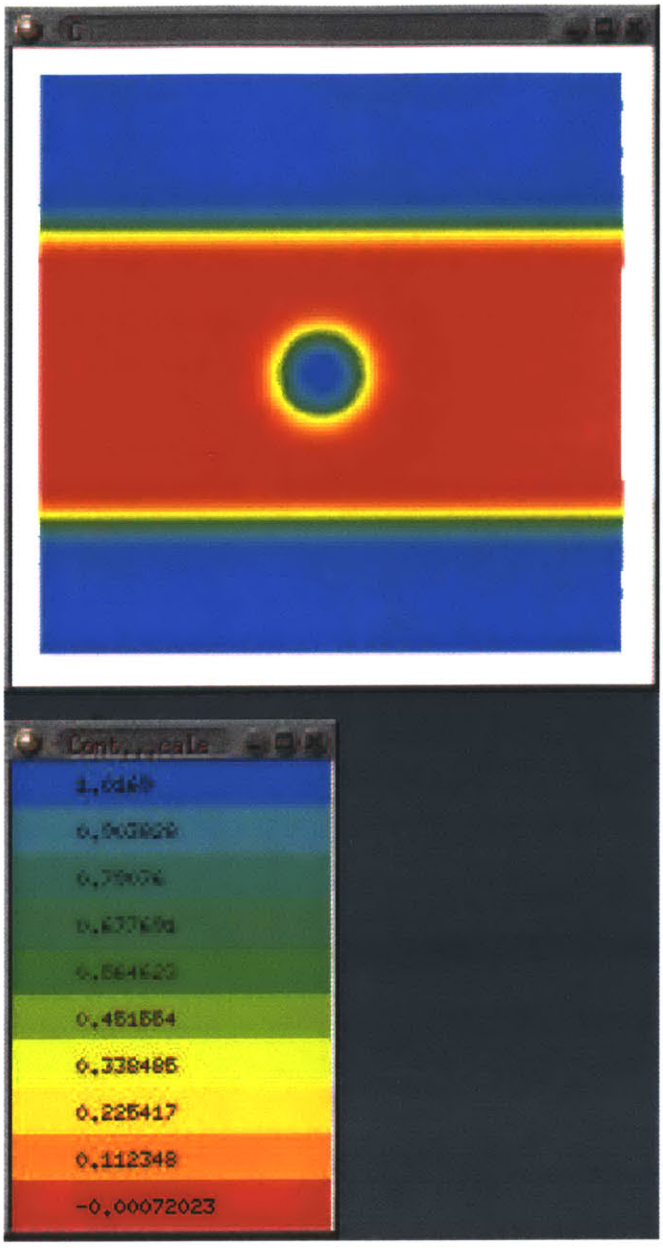

Figure 5.8: C at steady state, multi-interface system, N=1

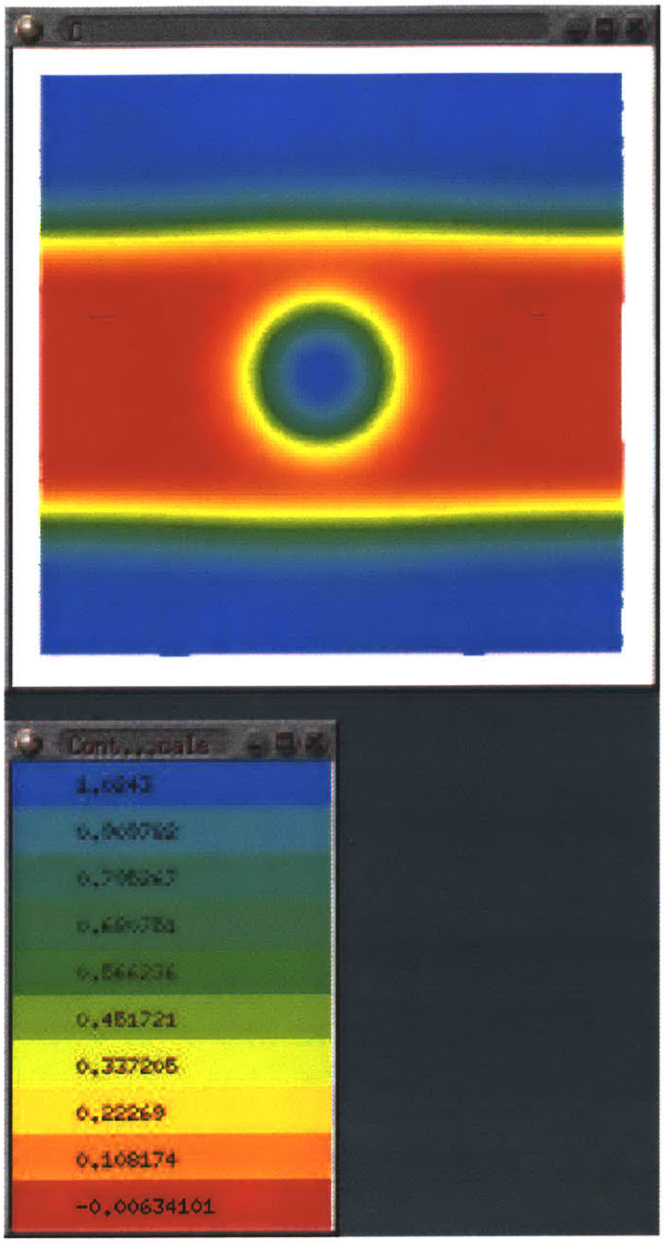

Figure 5.9: C at steady state, multi-interface system, N=2

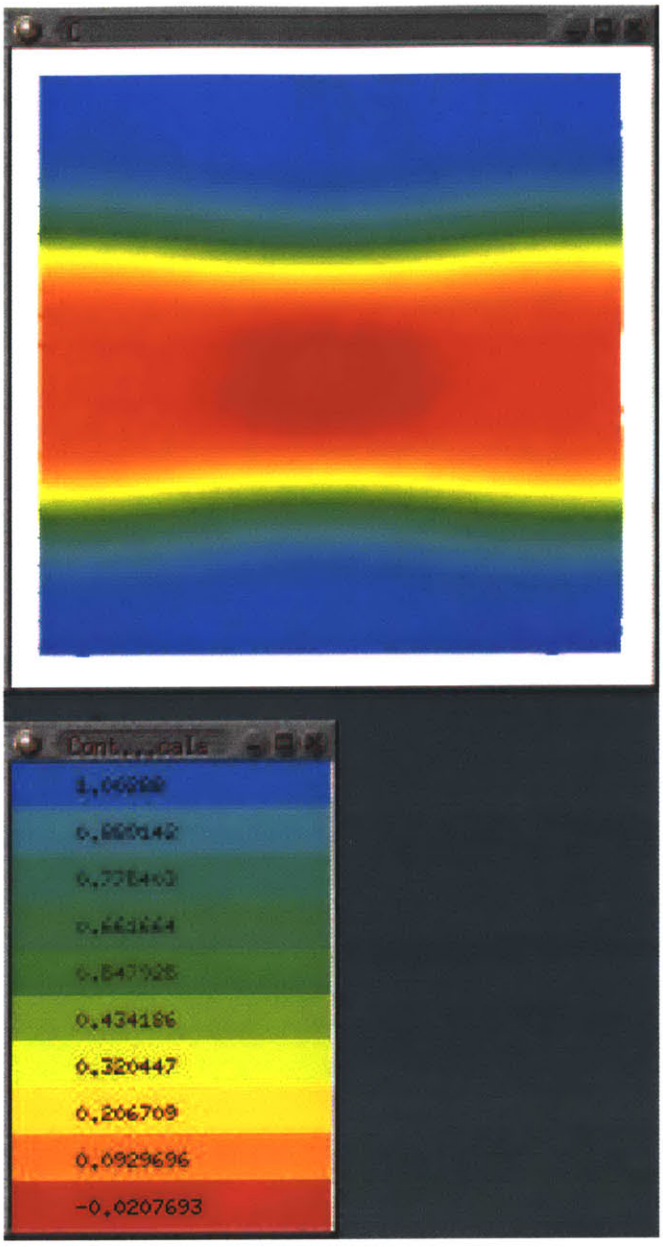

Figure 5.10: C at steady state, multi-interface system, N=3

equation, interface motion would induce bulk fluid motion. The purpose of this section is to simulate interface motion due to an electric field. Therefore, to simplify the equations, the system has uniform density $\rho = \rho_{Fe}$, and surface tension forces are not considered. Thus, there is no fluid velocity and the equations of motion do not need to be solved.

The governing equations are conservation of chemical species

$$\frac{\partial}{\partial t}(\rho C) = \frac{M_{Fe}}{\Delta\omega_{Fe}}\vec{\nabla} \bullet \left[\kappa_{Fe}\vec{\nabla}\mu_{Fe}\right] + \frac{M_{Fe}}{F\Delta\omega_{Fe}}\vec{\nabla} \bullet \left(\frac{\sigma_{Fe}(C)}{z_{Fe}(C)}\vec{\nabla}\phi\right) \tag{5.6}$$

and conservation of charge

$$0 = \vec{\nabla} \bullet \left(\sigma_{eff}(C)\,\vec{\nabla}\phi\right) \tag{5.7}$$

Symmetry boundary are used for C. For voltage,

$$@x = 0, \text{ symmetry} \tag{5.8}$$

$$@x = L_x, \text{ symmetry} \tag{5.9}$$

$$\phi(y = 0) = 0 \tag{5.10}$$

$$\phi(y = L_y) = 1volt \tag{5.11}$$

One constraint associated with this formulation is that if FeO exists at a fixed voltage boundary, then there will be a non-zero species flux at the boundary. The migration flux term is proportional to $\sigma_{Fe}(C)\,\vec{\nabla}\phi$. At a symmetry voltage boundary, $\left(\vec{\nabla}\phi\right) \bullet \hat{n} = 0$. However at a fixed voltage boundary $\left(\vec{\nabla}\phi\right) \bullet \hat{n} \neq 0$. In Fe, $\sigma_{Fe}(C) = 0$, but in FeO, $\sigma_{Fe}(C) \neq 0$. Therefore, to conserve species, boundaries with fixed voltage need to coincide with Fe.

The initial conditions for the first simulation are shown in Figure 5.11. There are three layers in the y-direction, $Fe(1/4cm)$-$FeO(1/2cm)$-$Fe(1/4cm)$. The domain is $1cm$ by $1cm$. The grid

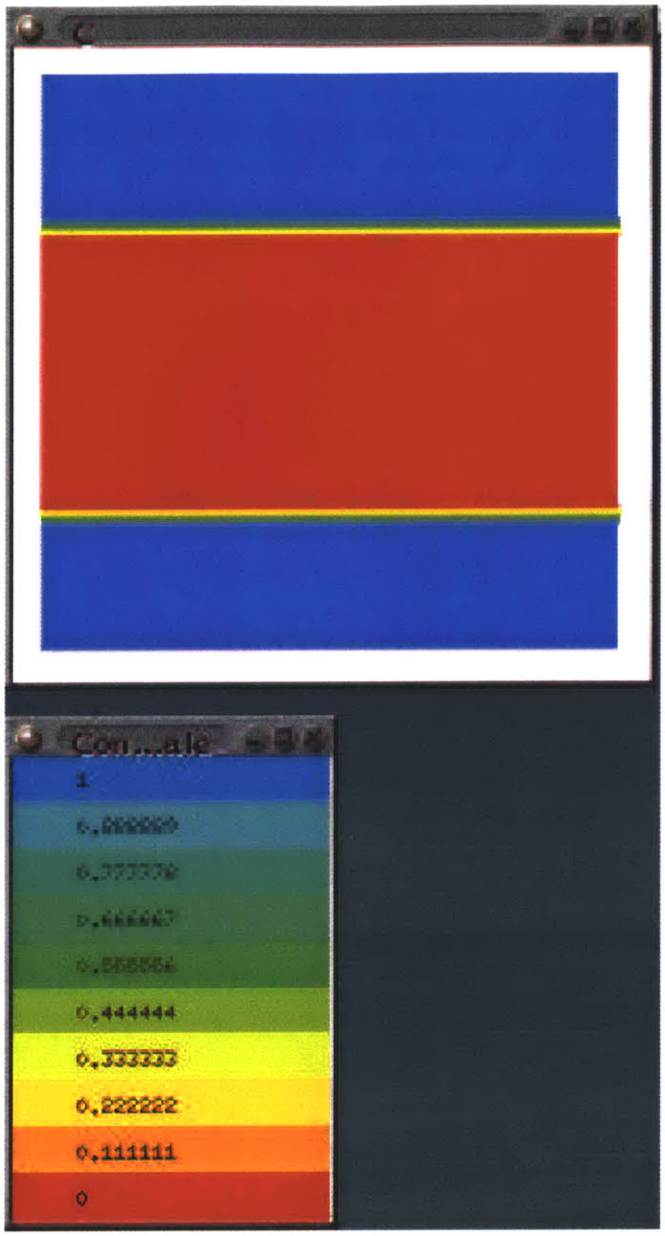

Figure 5.11: C at t=0, applied voltage

is 32x32, and $\epsilon = dx = dy$. Polynomial interpolation was used for $\sigma_e(C)$.

$$\sigma_e(C) = \sigma_{e,slag} + 3(\sigma_{e,metal} - \sigma_{e,slag})C^2 - 2(\sigma_{e,metal} - \sigma_{e,slag})C^3 \tag{5.12}$$

where $\sigma_{e,slag} = 0\frac{1}{\Omega * m}$. The electrical conductivity of Fe in the physical system is $7 * 10^5\frac{1}{\Omega * m}$. However for numerical stability, $\sigma_{e,metal}$ was set to $\sigma_{e,metal} = 10^3\frac{1}{\Omega * m}$. Recall that $\sigma_{Fe,slag} \cong 12\frac{1}{\Omega * m}$, so $\sigma_{e,metal} >> \sigma_{Fe,slag}$ is still satisfied. κ was scaled by 100 so that the timescale of diffusion is less than that of migration. The κ scaling was necessary to maintain a stable interface.

A positive voltage at $y = L_y$ creates an electric field in the negative y-direction. In the FeO, the electric field forces the Fe^{2+} downward and the O^{2-} upward. Because the electrochemical reactions at the interface are modeled as transport limited, the migration flux of species to the interface leads directly to interface motion. Results for $t = 1300s$ are shown in Figures 5.12 and 5.13.

The FeO phase moved a distance in the y-direction of approximately $1/8cm$. Because $\sigma_{e,metal} >> \sigma_{Fe,slag}$, there are very small gradients of ϕ in Fe.

Is this result reasonable? Here a more quantitative explanation is given. The interface velocity is given by equation 2.18.

$$V_{int} = \frac{J_{current}V_{slag}}{2F} = \frac{J_{current}}{2F}\left(\frac{M_{slag}}{\rho_{slag}}\right) \tag{5.13}$$

The flux of charge in the slag is given by

$$J_{current} = \frac{\tilde{z}}{z_{Fe}}\sigma_{Fe}\frac{d\phi}{dy} \tag{5.14}$$

Recall,

$$\tilde{z} = z_{Fe} - \frac{M_{Fe}}{M_O}z_O = 2 - \left(\frac{56}{16}\right)(-2) = 9 \tag{5.15}$$

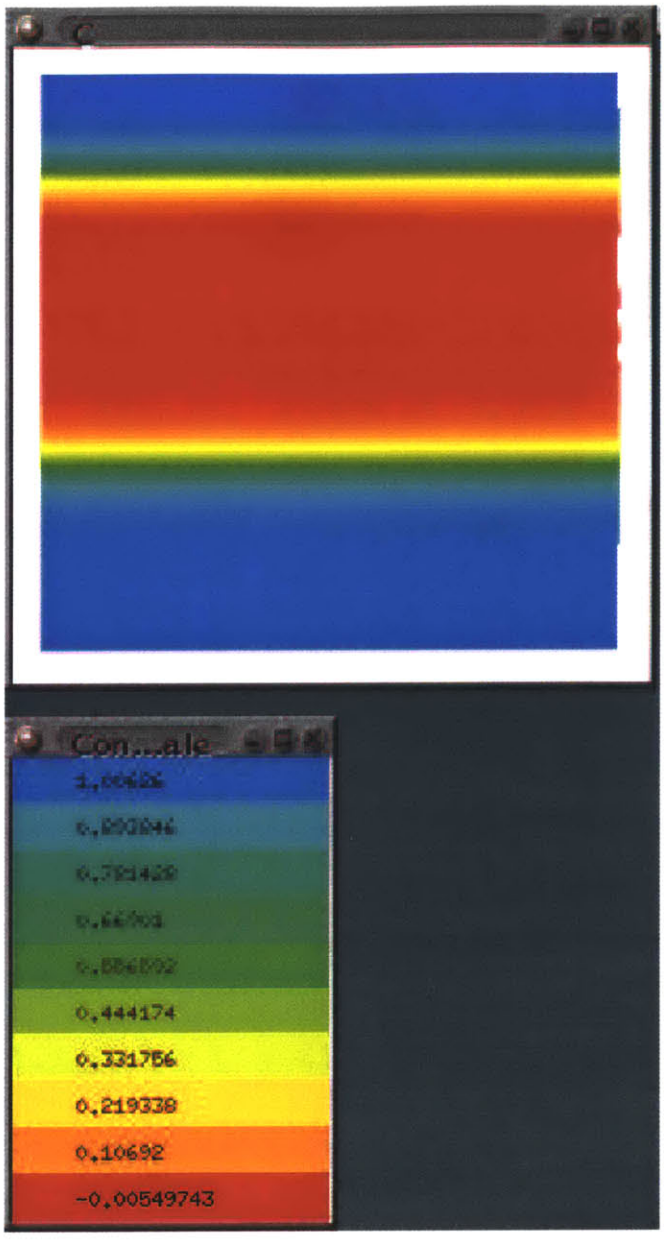

Figure 5.12: C at t=1300s, applied voltage

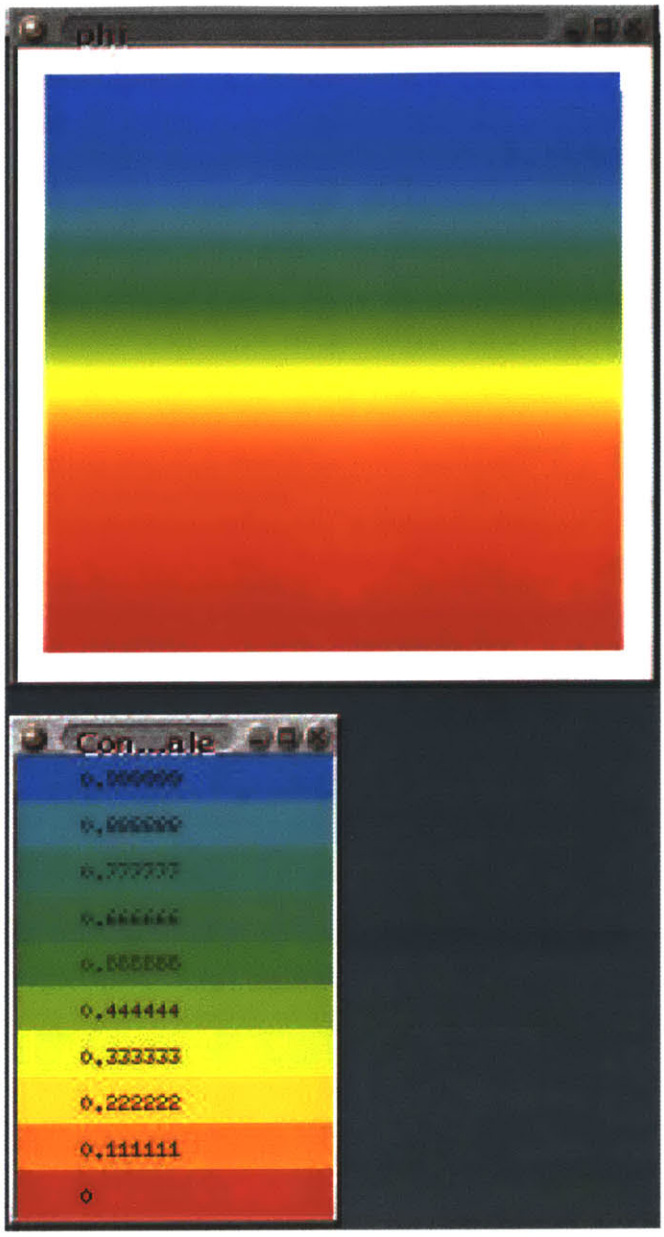

Figure 5.13: Voltage at t=1300s, applied voltage

so (adjusting for constant density)

$$J_{current} = \frac{9}{2}\left(12 * 2\frac{1}{\Omega * m}\right)\frac{1V}{0.5cm} = 2.16\frac{A}{cm^2} \tag{5.16}$$

Combining gives the interface velocity

$$V_{int} = \frac{\left(21,600\frac{C}{m^2 * s}\right)\left(36 * 10^{-3}\frac{kg}{mole}\right)}{2\left(96,485\frac{C}{mol}\right)\left(7000\frac{kg}{m^3}\right)} = 5.76 * 10^{-7}\frac{m}{s} \tag{5.17}$$

An expected time interval for an interface movement of $1/8cm$ is

$$V_{int} = \frac{L}{\tau} \Rightarrow \tau \sim \frac{\left(\frac{1}{8}cm\right)}{\left(5.76 * 10^{-7}\frac{m}{s}\right)} \sim 2000s \tag{5.18}$$

which agrees with the numerical simulation.

The next series of simulations deal with streamer growth due to an electric field. Two cases are considered: (1) a perturbed cathodic interface, (2) a perturbed anodic interface. The initial conditions are shown in Figures 5.14 and 5.15.

(The plots are symmetrical with respect to $x = \frac{L_x}{2}$.) Recall that the voltage boundary conditions are $\phi(y = 0) = 0V$ and $\phi(y = L_y) = 1V$. Therefore, the bottom face is the cathodic interface (Figure 5.14), and the top face is the anodic interface (Figure 5.15). Results at $t = 1660sec$ for cathodic growth and anodic growth are shown in Figures 5.16and 5.17 respectively.

It was found in section 5.2, that it is possible to predict interface merging with diffusion alone with the diffuse interface model depending on the choice of interface thickness. Therefore, for reference, results for the two systems at $t = 1660sec$ are also given for pure diffusion (no electric field). Figure 5.18 shows diffusion results for the perturbed cathodic interface, and Figure 5.19 shows results for the perturbed anodic interface.

Also for reference, Figure 5.20 shows the steady state profile for both the cathodic and anodic perturbed cases. The steady state result for the pure diffusion case shows that there is no artificial interface interaction due to interface scaling. The equilibrium configuration of the systems with

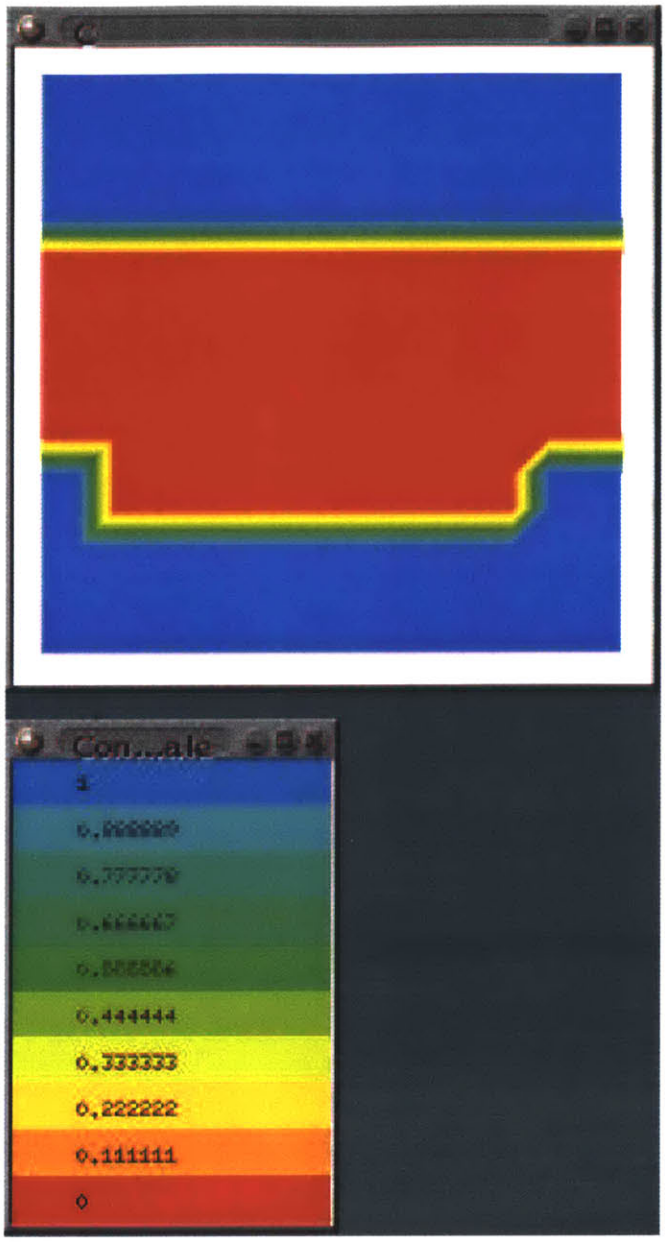

Figure 5.14: C at t=0, perturbed cathodic interface

Figure 5.15: C at t=0, perturbed anodic interface

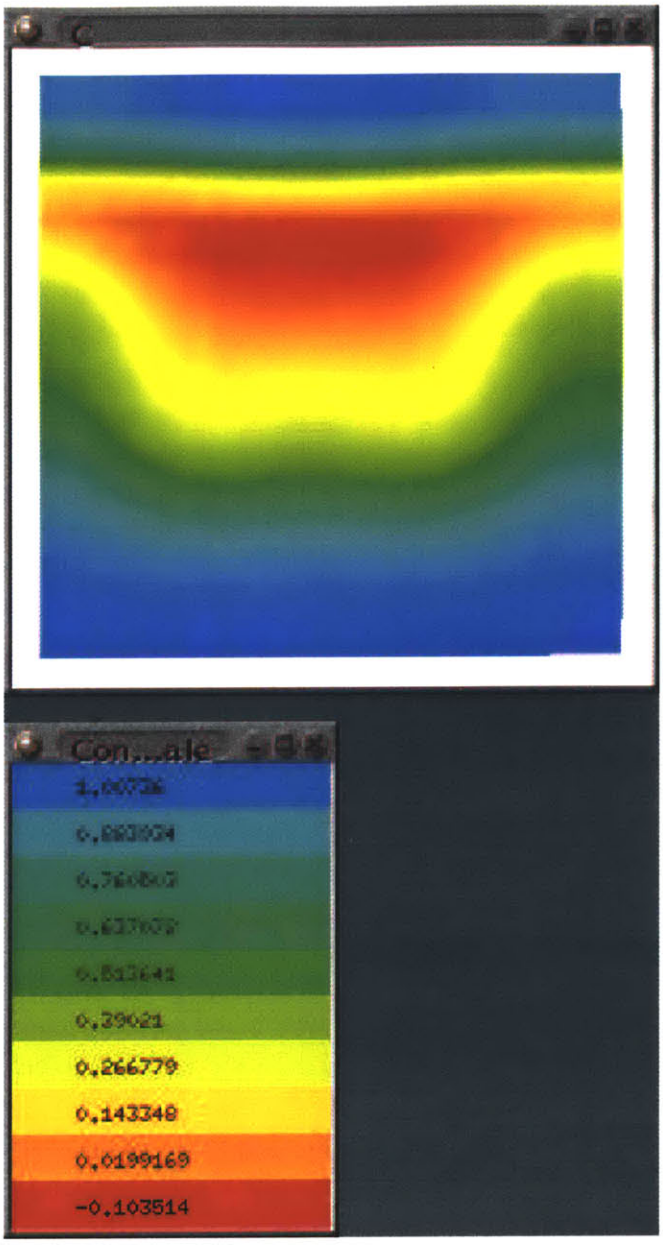

Figure 5.16: C at t=1660s, perturbed cathodic interface

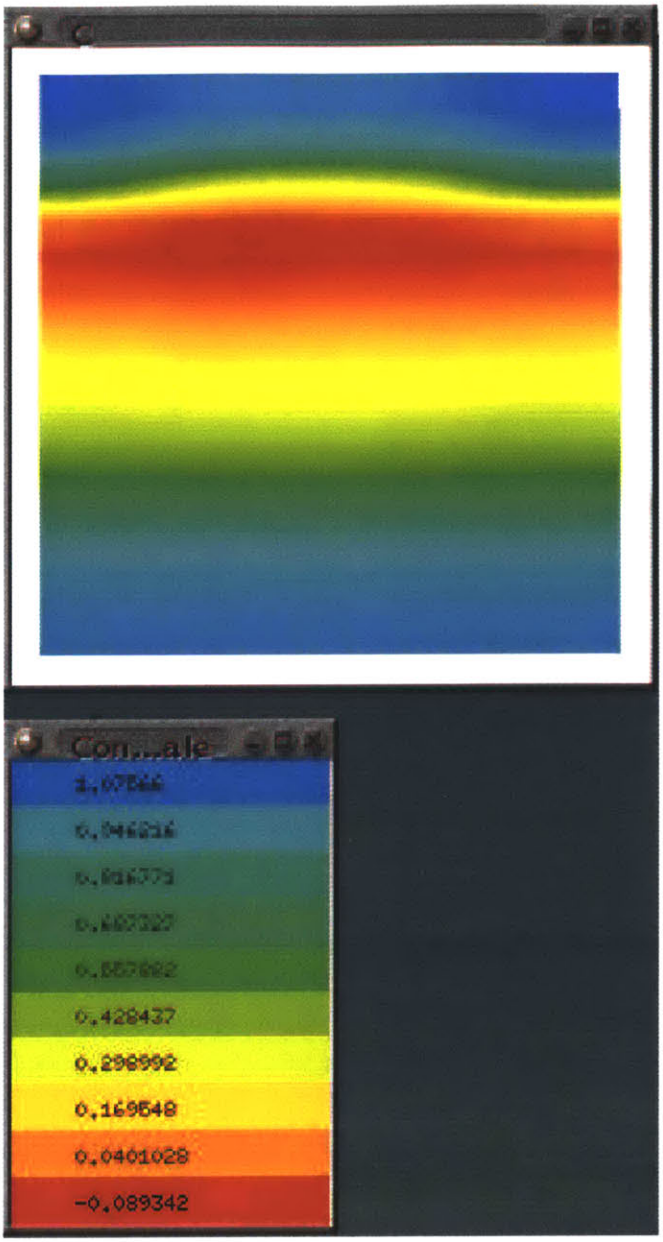

Figure 5.17: C at t=1660s, perturbed anodic interface

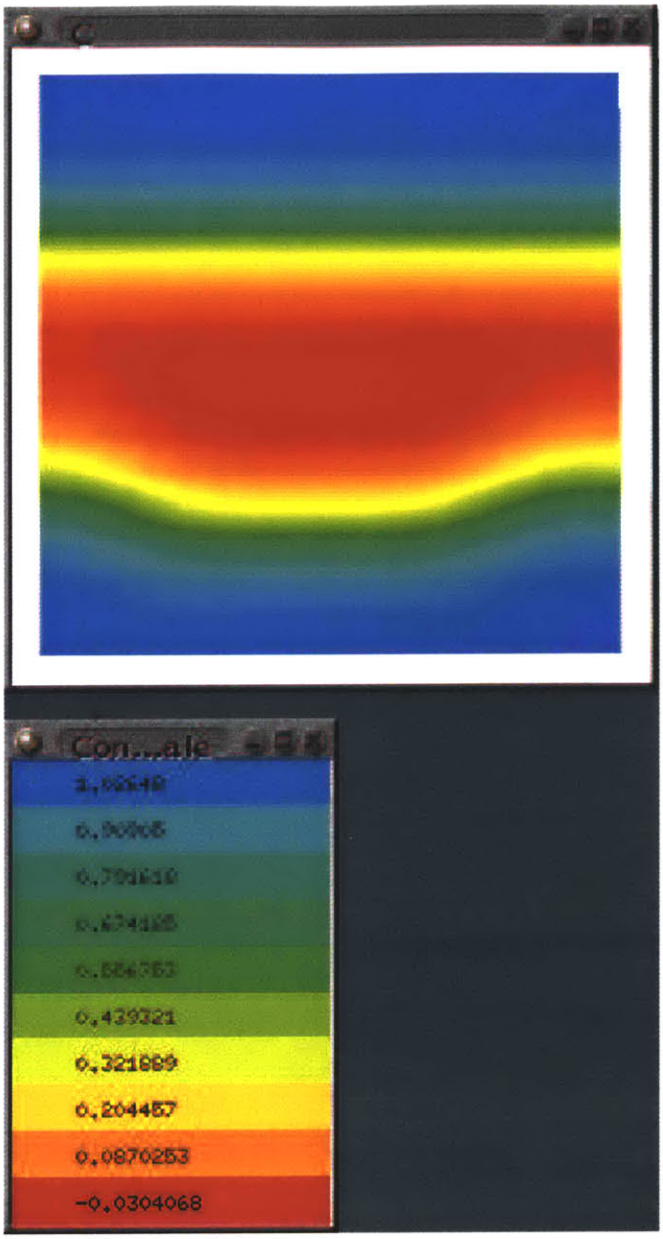

Figure 5.18: C at t=1660s, perturbed cathodic interface, no applied voltage

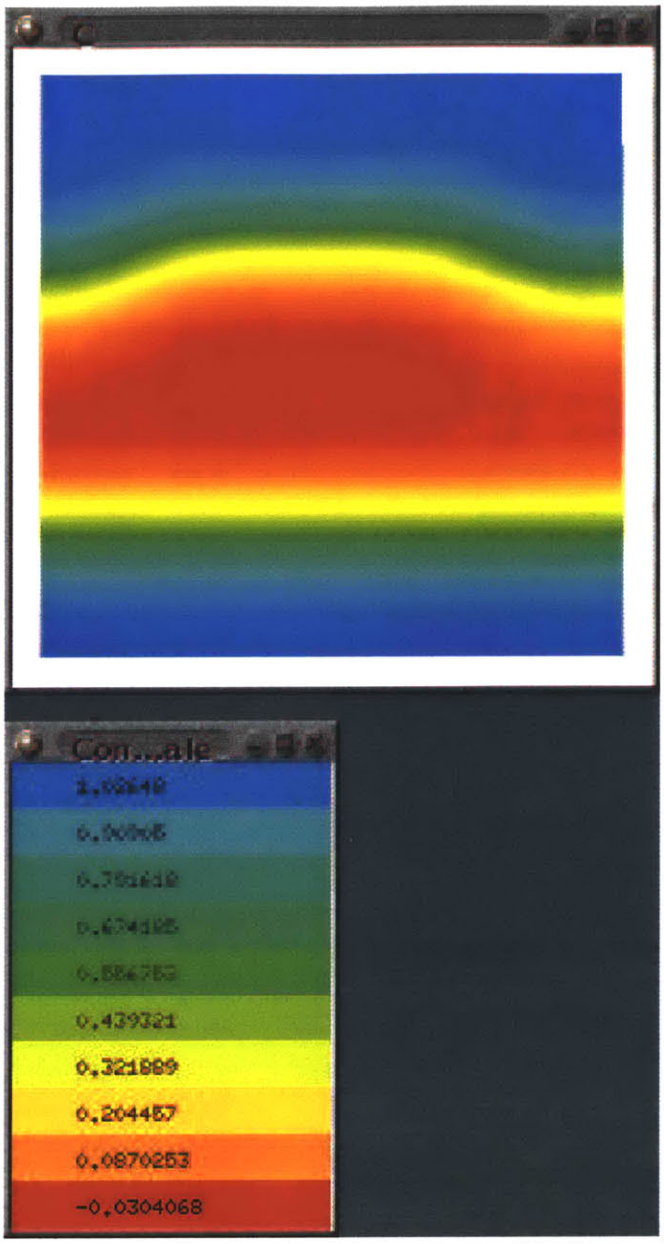

Figure 5.19: C at t=1660s, perturbed anodic interface, no applied voltage

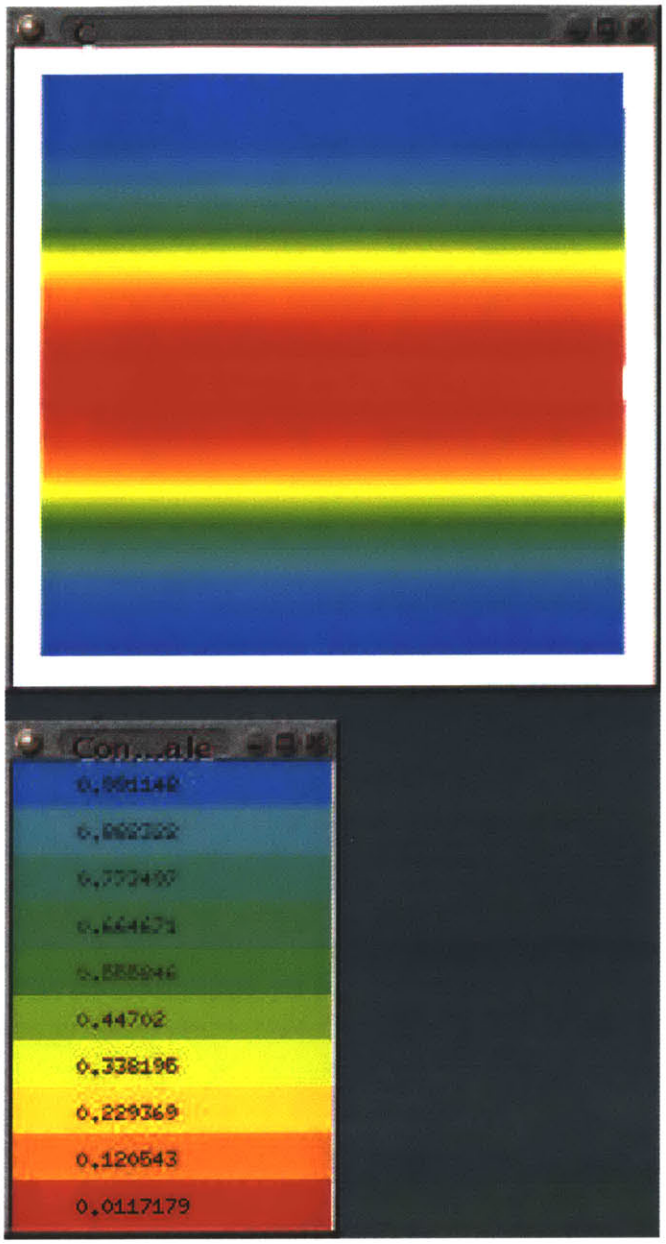

Figure 5.20: C at steady state, perturbed cathodic or anodic interface, no applied voltage

zero electric field is three layers vertically with interfacial area minimized. For the perturbed cathodic interface, the perturbation grows with an applied voltage and decays without an applied voltage. For the perturbed anodic interface, the perturbation decays with and without an applied voltage. Note that the rate of decay is greater with the applied voltage than without the applied voltage.

The interface growth can be explained by looking at the migration flux of chemical species. The flux is proportional to the electric field.

$$j \propto E \propto \frac{\Delta\phi}{L} \propto \frac{1V}{L_{FeO}} \tag{5.19}$$

At the perturbed regions the length of FeO is smaller than in the unperturbed region.

$$L_{FeO,perturbed} < L_{FeO,unperturbed} \tag{5.20}$$

So, the flux will be greater at the perturbed site.

$$j_{perturbed} > j_{unperturbed} \tag{5.21}$$

For the cathodic case, the increases flux leads to a decreased FeO length, and a growth instability occurs leading to the formation of streamers. For the anodic case, the increased flux leads to a decreased FeO length, and the interface stabilizes.

5.4 Diffusion, Surface Tension Driven Convection

Jacqmin [9] simulated a 2D oscillating drop with the phase field method. The calculations were performed using four grids: 16x16, 32x32, 64x64, 128x128; and the calculated frequencies were shown to approach the analytical result with increasing grid density. The simulation was repeated in this project to validate the surface tension forces in the diffuse interface model. The

drop simulation for this project is described below.

Initially the drop is a square $\frac{3}{8}cm$ by $\frac{3}{8}cm$. Due to symmetry, one quarter of the drop was simulated. The drop is surrounded by a fluid of different phase. $C = 1$ for the drop, and $C = 0$ for the surrounding fluid. The drop and surrounding fluid have the same properties.

$$\rho = 1000\frac{kg}{m^3} \tag{5.22}$$

$$\eta = 4 * 10^{-4}\frac{kg}{m * s} \tag{5.23}$$

$$\gamma_{interface} = 0.03\frac{N}{m} \tag{5.24}$$

The analytical frequency is $f = 47.89Hz$. The governing equations are: conservation of x-momentum

$$\begin{aligned}\frac{\partial}{\partial t}(\rho u) + \vec{\nabla} \bullet \left(\rho \vec{V} u\right) &= -\frac{\partial p}{\partial x} + \vec{\nabla} \bullet \left(\eta \vec{\nabla} u\right) + \rho g_x \\ &\quad + \vec{\nabla} \bullet \left(\eta \frac{\partial \vec{V}}{\partial x}\right) - C\frac{\partial \mu}{\partial x}\end{aligned} \tag{5.25}$$

conservation of y-momentum

$$\begin{aligned}\frac{\partial}{\partial t}(\rho v) + \vec{\nabla} \bullet \left(\rho \vec{V} v\right) &= -\frac{\partial p}{\partial y} + \vec{\nabla} \bullet \left(\eta \vec{\nabla} v\right) + \rho g_y \\ &\quad + \vec{\nabla} \bullet \left(\eta \frac{\partial \vec{V}}{\partial y}\right) - C\frac{\partial \mu}{\partial y}\end{aligned} \tag{5.26}$$

conservation of mass (incompressible)

$$\vec{\nabla} \bullet \vec{V} = 0 \tag{5.27}$$

and the phase field equation

$$\frac{DC}{Dt} = \vec{\nabla} \bullet \left(\kappa \vec{\nabla} \mu\right) \tag{5.28}$$

which is a simplified form of equation 3.67. The solution domain is $\frac{3}{8}cm$ by $\frac{3}{8}cm$. A uniform grid of 16x16 nodes was used (or 17x17 including extra velocity nodes). To maintain a stable interface, κ was set such that the timescale of interface diffusion is less than that of bulk fluid motion. The phase field parameters used were

$$\epsilon = \Delta x \tag{5.29}$$

$$\alpha = \left(\sqrt{18}\right)\gamma\epsilon \tag{5.30}$$

$$\beta = \left(\sqrt{18}\right)\frac{\gamma}{\epsilon} \tag{5.31}$$

$$\kappa = \epsilon^2 \tag{5.32}$$

where $\Delta x = \Delta y$ is the grid spacing. The initial conditions for the simulation are shown in Figure 5.21. The interface is initially sharp and varies from zero to one over a single grid spacing. The drop radius position at an angle of 45deg to the x axis was calculated by interpolating $C = 0.5$. The time evolution of the radius position is shown in Figure 5.22. From the plot, the frequency is approximately 40Hz. The frequency for 16x16 grid of Jacqmin was 40.82Hz (, and for the128x128 grid was 44.98 Hz). Therefore, the code accurately predicts surface tension driven flow. The system at steady state is shown in Figure 5.23. At steady state, the drop is at equilibrium position, $R_{eq} = \frac{3}{8\sqrt{\pi}}cm$, and the interface is smoothed out over about four grid points.

The oscillating 2D drop simulation was repeated for an Fe drop surrounded by FeO. All conditions are the same except for properties (see Appendix 8.1 for properties of Fe-FeO system) . The density and viscosity of Fe and FeO each differ by a factor of two. However, the system is still incompressible for the sharp interface formulation and is modeled as incompressible for the diffuse interface formulation. The initial conditions and the steady state profile are exactly the same as the case above. The time evolution of the radius position is shown in Figure 5.24. From the plot, the frequency is approximately $80Hz$. The increase in frequency is due to the increase

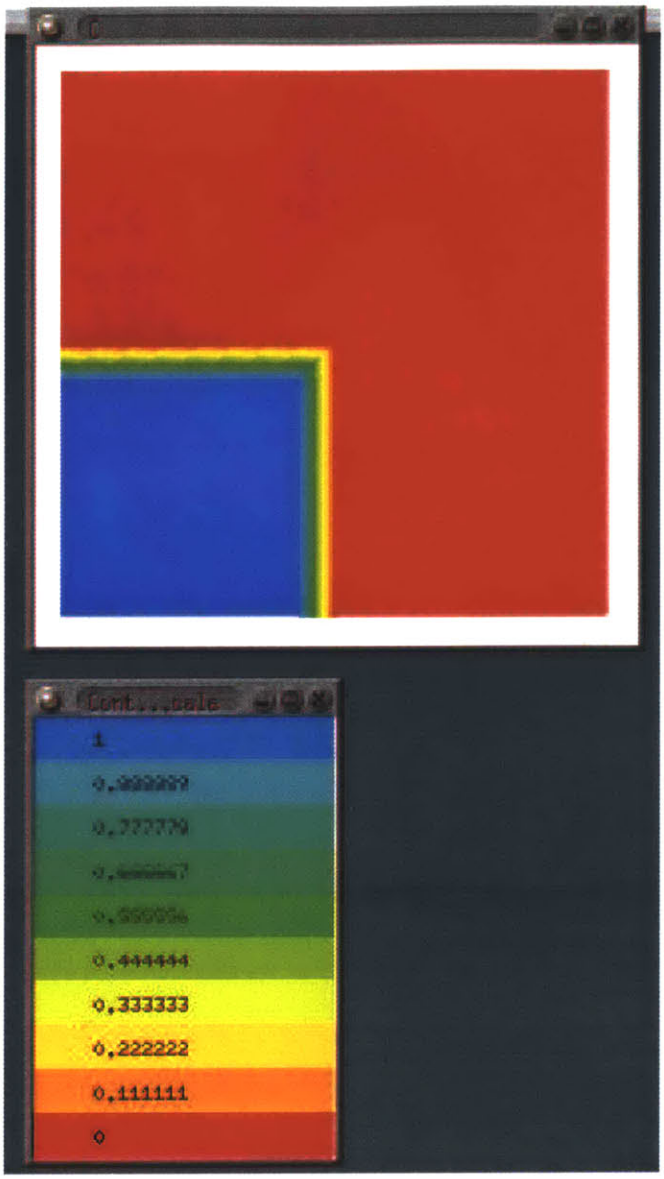

Figure 5.21: C at t=0, 2D drop

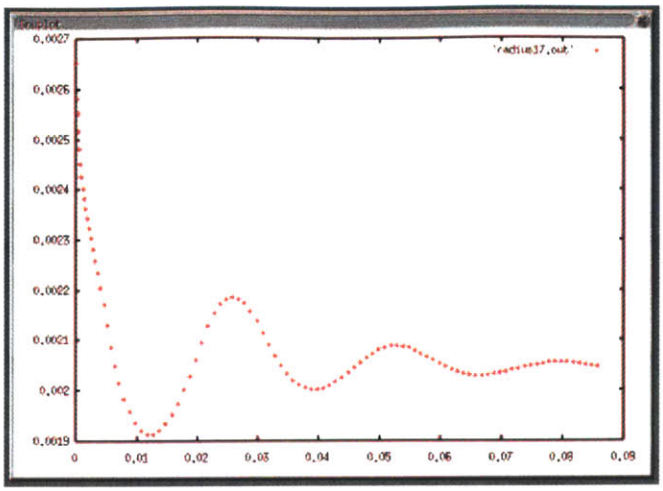

Figure 5.22: Radius (m) @45deg vs time (sec)

in surface tension.

5.5 Diffusion, Gravity and Surface Tension Driven Convection

The Fe drop simulation of the previous section is extended here to include a gravitational field $\overrightarrow{g} = -9.8\frac{m}{s^2}\widehat{j}$. The initial conditions are the same (Figure 5.21). Steady state results are shown in Figure 5.25. Comparing this result to that of $g = 0$ (Figure 5.23), the drop under gravity is slightly compressed in the y-direction. The radial positions at $90deg$ from the x-axis is denoted as h. For the zero g case,

$$h = 5.53mm \tag{5.33}$$

and for the nonzero g case,

$$h_g = 5.08mm \tag{5.34}$$

The compression due to gravity is balanced by surface tension forces. Note that because of the symmetry boundary condition at $y = 0$, the drop has a wetting angle of $90deg$.

The equilibrium configuration of the system can be explained with thermodynamics. Let the

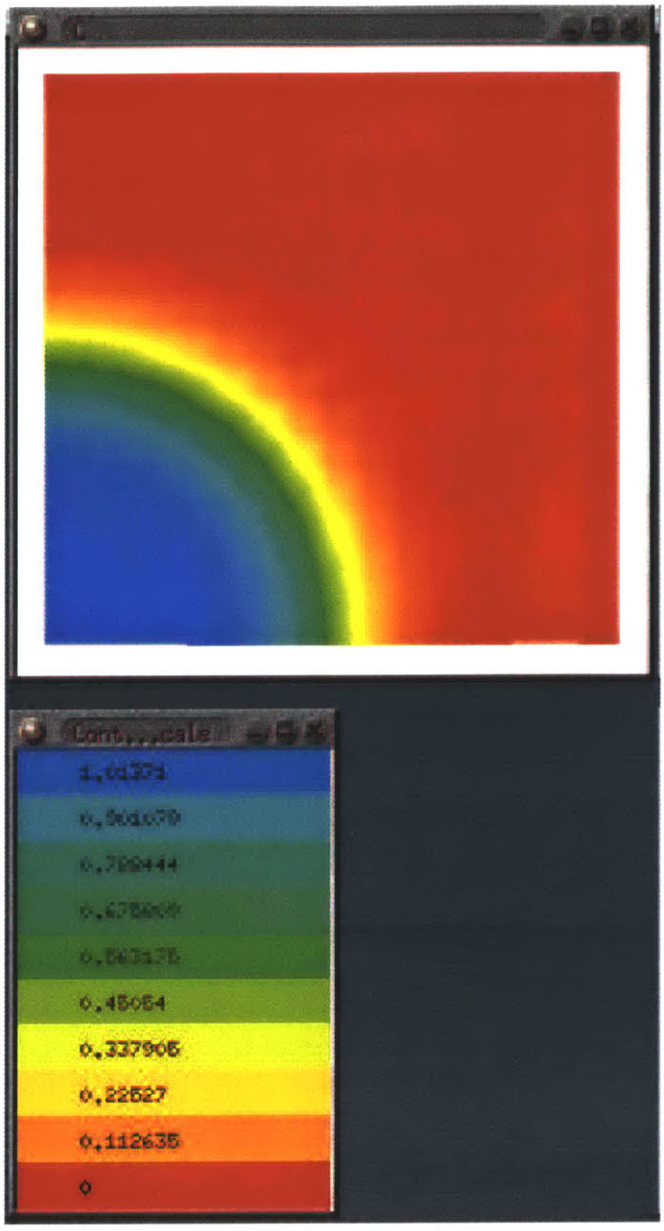

Figure 5.23: C at steady state, 2D drop

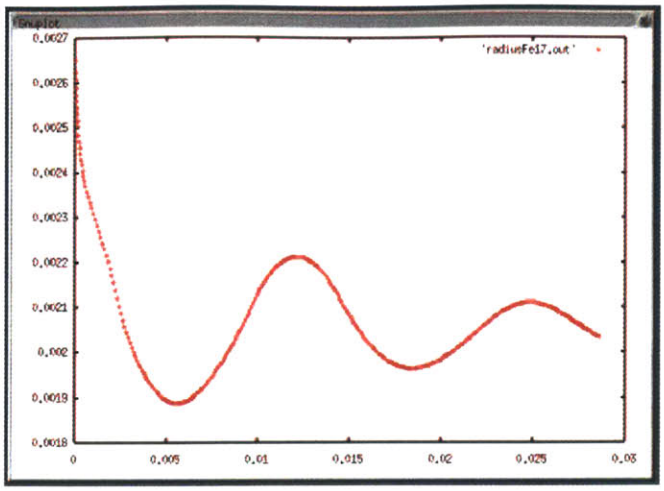

Figure 5.24: ,Radius (m) @45deg vs time (sec)

initial conditions be state 1 and equilibrium be state 2. The system is modeled as an isolated incompressible system (zero flux boundary conditions) undergoing an irreversible run down to equilibrium. The first law reads

$$Q - W = \Delta U + \Delta PE + \Delta KE \tag{5.35}$$

which simplifies to

$$0 = \Delta U + \Delta PE \tag{5.36}$$

Using constitutive relations,

$$0 = mc_v \left(T_2 - T_1\right) + mg \left(\overline{y}_2 - \overline{y}_1\right) + \gamma \left(A_2 - A_1\right) \tag{5.37}$$

where $\overline{y}$ is the center of gravity of the system and A is the surface area of the interface. The final configuration can be found by a force balance at the interface. The first law gives the final temperature of the system. The second law reads

$$\Delta S = S_{in} - S_{out} + S_{gen} \tag{5.38}$$

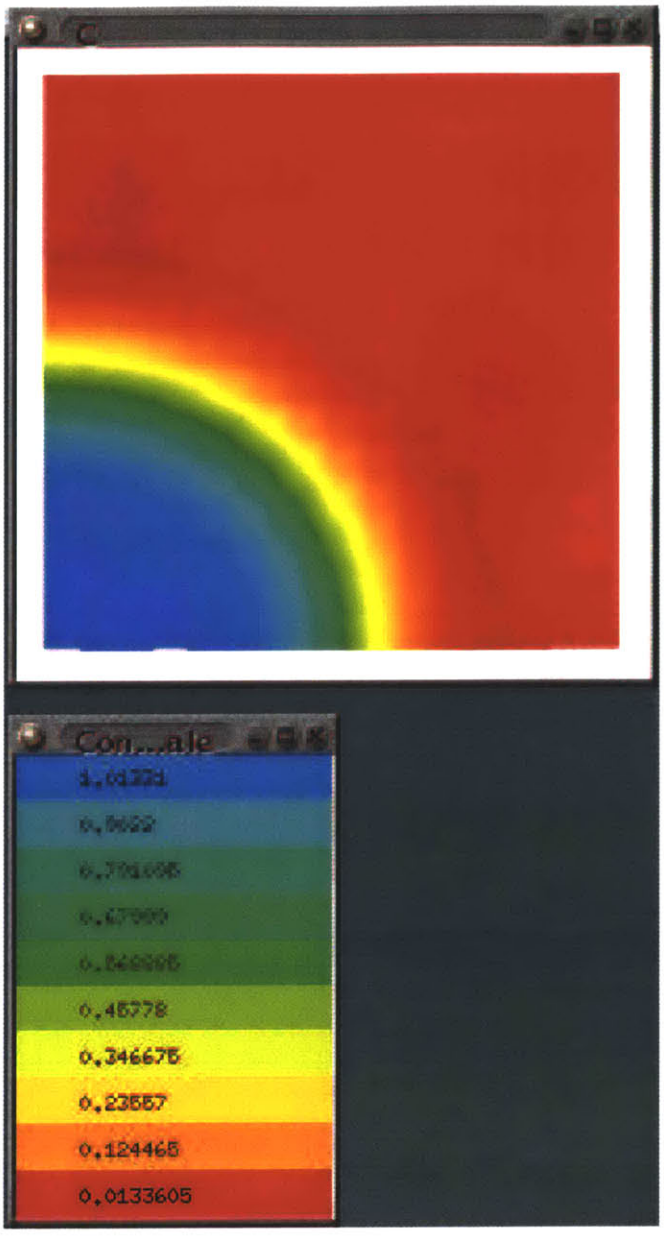

Figure 5.25: C at steady state, 2D drop with gravity

Since the system is thermally insulated, there is no entropy transfer.

$$\Delta S = S_{gen} \tag{5.39}$$

Using constitutive relations,

$$mc_v \ln\left(\frac{T_2}{T_1}\right) = S_{gen} \tag{5.40}$$

The second law gives the entropy generated during the process. The equilibrium state is characterized by a maximum entropy. Looking at the entropy change for the system,

$$\Delta S = mc_v \ln\left(\frac{T_2}{T_1}\right) \tag{5.41}$$

Using the first law,

$$\Delta S = mc_v \ln\left(1 - \frac{mg\Delta\overline{y} + \gamma\Delta A}{mc_v T_1}\right) \tag{5.42}$$

To maximize ΔS is to minimize ΔPE under the constraint of conservation of mass. At state 2,

$$(PE)_2 = mg\overline{y}_2 + \gamma A_2 \tag{5.43}$$

If $g = 0$, then to maximize entropy A_2 is minimized forming a circle. If $\gamma = 0$, then to maximize entropy $\overline{y}_2$ is minimized forming a horizontal interface with Fe on the bottom. For intermediate cases where $g \neq 0$ and $\gamma \neq 0$, there is an optimum balance between the two terms leading to the compressed configuration.

An analytical result for the drop height $h(x = 0)$ is obtained by an overall force balance in the x-direction

$$\gamma w = \int_{y=0}^{y=h} \left(p_{in}\left(y\right) - p_{out}\left(y\right)\right) w dy \tag{5.44}$$

where w is the z-direction width. The pressure inside the drop is related to the pressure outside

the drop by the surface tension and radius of curvature R. The pressures can be written,

$$p_{out}(y) = p_{out}(y = h) + \rho_{out} g (h - y) \tag{5.45}$$

$$p_{in}(y) = p_{out}(y = h) + \frac{\gamma}{|R_h|} + \rho_{in} g (h - y) \tag{5.46}$$

where $R_h = R(x = 0, y = h)$. Substituting for pressure,

$$\gamma = \int_{y=0}^{y=h} \left(\frac{\gamma}{|R_h|} + (\rho_{in} - \rho_{out}) g (h - y) \right) dy \tag{5.47}$$

which simplifies to

$$\gamma = \frac{\gamma h}{|R_h|} + \Delta\rho g \frac{h^2}{2} \tag{5.48}$$

Note that when $h = |R_h|$, $\Delta\rho g = 0$. Therefore, for a circular profile, either $\Delta\rho = 0$ or $g = 0$. Introducing the equilibrium drop radius for $g = 0$, R_{eq}, and rearranging gives,

$$\frac{\Delta\rho g R_{eq}^2}{2\gamma} \left(\frac{h}{R_{eq}} \right)^2 + \frac{R_{eq}}{|R_h|} \left(\frac{h}{R_{eq}} \right) - 1 = 0 \tag{5.49}$$

which is solved with the quadratic equation. For this simulation, $R_{eq} = 5.53mm$, $h(i = 0) = 5.079mm$, $h(i = 1) = 5.052mm$. The radius of curvature is approximated by

$$\frac{1}{R_h} \cong \frac{d^2 h}{dx^2} \cong \left(\frac{h(i = 1) - 2h(i = 0) + h(i = 1)}{(\Delta x)^2} \right) \tag{5.50}$$

using a shadow node. Using this radius of curvature, the force balance gives

$$\left(\frac{h_{analytical}}{R_{eq}} \right) = 0.876 \tag{5.51}$$

The measured value is

$$\left(\frac{h(i = 0)}{R_{eq}} \right) = \frac{5.079}{5.53} = 0.918 \tag{5.52}$$

which gives an error of approximately 5%. Therefore, the model accurately captures the balance between surface tension forces and gravitational forces.

Chapter 6

Discussion

6.1 Introductory Remarks

In this chapter, important assumptions used in the model formulation are revisited, other applications for the model are introduced, and reasons and suggestions for future development of the model are given.

6.2 Assumptions and Limitations

The electrochemical reactions in the model are limited to the transport limited regime. This assumption is valid for electrolysis systems similar to the one described in this thesis. In high temperature systems such as the one discussed here, the mass transfer resistance is much greater than the charge transfer resistance. However, the transport limited regime also corresponds to a zero cation concentration at the cathodic interface. If the full electrochemical current-voltage equations were used, then there would be an exponential response to any significant concentration at the interface, but since the constitutive current-voltage relations are explicitly limited to the transport limited case, the reaction behaves as if the concentration is zero at the interface.

Thy physical slag/metal system is a multi-component system and has a concentration boundary layer. The binary system does not have a concentration boundary layer. Additional cations

are needed to maintain charge neutrality in a concentration boundary layer. One way to capture a diffusion boundary layer would be to extend the formulation to ternary systems. Since there is no boundary layer in the binary system, there is no diffusion resistance associated with the interface motion. Thus with less resistance, the model predicts a larger reaction rate for a given applied voltage than would be expected. However, the model does capture important electrode phenomena such as interface motion and perturbation growth and decay.

The free energy curve was modeled with a polynomial function, and the interface thickness was scaled to a mesoscopic length. Both approximations serve to change the diffusion characteristics of the system. The diffusion flux is proportional the gradient in chemical potential which is a function of the free energy curve. The polynomial approximation captures the interfacial energy of the system, but the exact level of curvature is lost. For example, a large (absolute value of) second derivative of the homogeneous free energy, Ψ'', at $C = 0$ or $C = 1$ corresponds to a large change in free energy for concentrations that stray from equilibrium. Conversely, a small second derivative corresponds to a small free energy change. Since, the driving force for diffusion is a reduction in free energy, each case leads to a different diffusion flux. In the phase field model, α is scaled by ϵ and β is scaled by $1/\epsilon$. Therefore, interface scaling artificially increases α and lowers β. Lowering β lowers the peak in the free energy curve. The implications are a lower Ψ'' near equilibrium concentrations and a lower activation barrier for interface diffusion. α is the gradient penalty coefficient in the free energy equation and acts as a driving force for interfacial gradient minimization. An artificially large α increases this driving force. The surface tension is proportional to $\sqrt{\alpha\beta}$, so it is unaffected by the scaling. Thus, interface scaling leads to a number of issues involving diffusion for systems away from equilibrium, but the model does capture the macroscopic surface tension.

Assuming rapid charge redistribution throughout the system, the conservation of charge equation reduced to an equation for zero divergence of charge flux due to migration. Mathematically speaking, the charge equation reduced to an equation with a single unknown, voltage, significantly reducing the coupling of the equations. The unsteady and convection terms were safely

neglected even in systems with forced convection. However, the diffusion term was not so safely neglected with respect to the migration term. Recall that the representative dimensionless number was on the order of $N_2 \sim 10^{-2}$ (equation 3.87). For the Fe-FeO system analyzed here, this was a conservative estimate but may break down for other systems such as multi-component or aqueous solutions. The concentration difference used was conservative for the binary Cahn-Hilliard system where the mole fraction varied from 1/2 to 1. Other systems may exhibit larger concentration differences which would raise the dimensionless parameter by a factor of 10 or so. Also, the conductivity of slag was used instead of the conductivity of steel. For the binary system, concentration differences characterize the diffuse interface and so coincide with all property differences including conductivity. If the conductivity of steel was used, then N_2 would have decreased by a factor of 1000.

The system modeled was considered to be isothermal. Chemical reactions serve as heat sinks and sources. Also, electrical current and high resistance levels lead to joule heating which is another heat source. The question is whether local variations in temperature have a significant effect on the transport of chemical species. Conservation of energy governs the temperature distribution throughout the system. Transport properties typically have a strong dependence on temperature. The mass and specific heat capacity of the system serve as estimate to the sensitivity of temperature to heat flux, and the heat conductivity serves as a measure of temperature gradients. Another important factor is heat transfer boundary conditions. If the temperature of the surroundings are much lower than the solution, then large temperature differences may exist in the solution. In applying this model to real systems, scaling analysis similar to that in this thesis should be done to ensure that the isothermal approximation is valid.

6.3 Applications

The model developed here would also serve as a useful tool for analyzing existing processes such as magnesium reduction and aluminum reduction. Both are two phase liquid/liquid systems

with transport limited electrochemical reactions. An important feature in the steel refining system is the presence of streamers which complicate cathode dynamics considerably. The model predicts the growth of streamers and could be used in the development of efficient cathode designs. Improving efficiency of refining systems not only improves production but also, just as importantly, significantly reduces the amount of waste.

One system where hazardous waste is particularly problematic is titanium reduction. Current practice involves the use of chlorime gas as apposed to an electrolytic solution. In titanium reduction, ionized titanium exists as Ti^{2+}, Ti^{3+}, and Ti^{4+}. There is a higher thermodynamic driving force for Ti^{4+} to reduce first. The Ti^{2+} and Ti^{3+} build up near the cathode and diffuse away toward the anode and give up electrons and form Ti^{3+} and Ti^{4+}. Then, the Ti^{4+} migrates to the cathode, and the circular pattern continues hindering production rates. (It is worth noting that attemps to reduce hexavalent chromium electrolytically have exhibited the same inefficient circular patterns.) A new method currently being researched at Boston University for avoiding the titanium reoxidation problem is through the use of an anode which is an ionic conductor. The anode is coated with a material that has a high oxide ion diffusivity, a low electron conductivity, and a low titanium diffusivity. Therefore, only the oxide ions are allowed to pass through and be oxidized. The model developed here could be used in developing these new systems which would serve to answer current economic and environmental issues.

6.4 Future Work

The simplified 2D Fe-FeO-Fe system does not capture all phenomena of the physical slag-metal system, but does provide a foundation for a more comprehensive model to be developed in the future. The Cahn-Hilliard model restricts the fluid to two components, eliminating multi-component interactions. The capillary instability is a 3-D phenomenon and does not exist in a 2-D system. For these reasons, a 3-D, multi-component system will need to be developed in future work in order to accurately predict the relationship between design parameters and reaction rate

of the chosen application. However, the the extension of the code to 3-D is straightforward and is a matter of computer storage and speed.

Other more fundamental advances to the model include electrocapillarity, multiphase liquid/solid/gas interactions, magnetic effects, and thermal effects. Electrocapillarity, the variation of surface tension with electric field, affects all interface surface tension related phenomena such as streamer growth, oscillation, and breakup. To include the solid electrode in the computer simulation would be very beneficial to electrode design. Also, many systems like the titanium system described above involve the reduction of a solid metal from a liquid electrolyte, and require fluid/structure (or liquid/solid) interactions for modeling. The oxidation of oxygen in slag systems produces gases such as CO, O_2, H_2O, etc. These gases enhance mass transfer by convection and thus enhance reaction rate. An idea which has not yet been investigated through experimention on electrolytic refining systems is the application of magnetic fields. The general Lorentz force law reads $\vec{F} = q(\vec{E} + \vec{V} \times \vec{B})$, where $\vec{B}$ is the magnetic field vector, q is charge, and $\vec{V}$ is the velocity of charge. Intelligent application of magnetic fields may potentially enhance overall process control. Finally, for systems with relatively low heat capacities and thermal conductivities, the energy equation would allow for more accurate representation of system properties by providing the local temperature.

The finite element method may compliment future developments. Unstructured grids would provide the flexibility needed to increase grid density at a curved interface. Also, Lagrangian descriptions may be used in the development of solid/liquid/gas interactions which would require different meshing schemes in each phase.

Chapter 7

Conclusions

In this thesis, a diffuse interface model for a two component liquid/liquid, isothermal system undergoing transport limited electrochemical reactions was developed. The model was applied to the electric field enhanced smelting and refining of steel process. A representative Fe-FeO system was used as a simplified model. The governing equations were derived for the most general case first. Then, using a series of asymptotic solutions, length, velocity, and time scales were derived. Based on the simple scaling arguments, the governing equations were significantly simplified. In particular, the conservation of charge equation, which governs the voltage field, was reduced from an equation involving concentration, velocity, and voltage with time and space derivatives to an equation involving just voltage with a spatial derivative.

The system of equations were discretized using the finite-difference method and the Crank-Nicholson scheme. Symmetry boundary conditions were used for concentration and were implemented with shadow nodes. The system of nonlinear difference equations were solved using the matrix-free Newton-Krylov method. PETSc was used for distributed array data storage and parallel processing.

A series of case study simulations involving the electrochemical Fe-FeO system were used to display phenomena characteristic of refining systems. The case studies showed that the model accurately predicts:

- Inter-phase diffusion
- Interface motion due to an electric field
- Growth of cathodic interface perturbations into streamers due to an electric field
- Decay of anodic interface perturbations due to a voltage field
- Interface oscillations due to surface tension driven flow
- Interface distortion due external body forces

The simplified 2D Fe-FeO-Fe system does not capture all phenomena of the physical slag-metal system, but does provide a foundation for a more comprehensive model to be developed in the future. The model developed here is general in the sense that it can be used to model any application with similar physical interactions, and the methodology developed here for coupling transport limited electrochemistry with transport equations is fundamental in that the extension to more complex systems is limited only by the development of a free energy model and system properties.

Chapter 8

Appendix

8.1 Properties

$$
\begin{aligned}
D_{Fe^{2+}} &\sim 10^{-6}\frac{cm^2}{s}\text{Ferrous ion diffusivity in slag} \\
\gamma &\sim 1\frac{N}{m}\text{Fe} - \text{FeO interfacial energy} \\
\rho_{metal} &= 7160\frac{kg}{m^3}\text{density of metal} \\
\rho_{slag} &= \frac{\rho_{metal}}{2}\text{density of slag} \\
\eta_{metal} &= 0.006\frac{kg}{m*s}\text{viscosity of metal} \\
\eta_{slag} &= 2\eta_{metal}\text{viscosity of slag} \\
\sigma_{e,metal} &= 7.14*10^5\frac{1}{\Omega*m}\text{electrical conductivity of Fe}
\end{aligned}
$$

8.2 Computer Program

The computer program used for this project can be found at lyre.mit.edu/~dussault.

Bibliography

[1] **Allen J. Bard and Larry R. Faulkner**, *Electrochemical Methods*, John Wiley & Sons, New York ,1980.

[2] **R. Byron Bird, Warren E. Stewart, and Edwin N. Lightfoot**, *Transport Phenomena*, John Wiley & Sons, New York, 1960.

[3] **David J. Griffiths**, *Introduction to Electrodynamics, Second Edition*, Prentice Hall, Upper Saddle River, New Jersey 07485, 1989.

[4] **W.W. Mullins and R.F. Sekerka**, *Morphological Stability of Particle Growing by Diffusion or Heat Flow*, Journal of Applied Physics, Vol. 34, No. 2, pp. 323-329, Feb. 1963.

[5] **W.W. Mullins and R.F. Sekerkam**, *Stability of a Planar Interface During Solidification of a Dilute Binary Alloy*, Journal of Applied Physics, Vol. 35, No. 2, pp. 444-451, Feb. 1964.

[6] **Suhas V. Patankar**, *Numerical Heat Transfer and Fluid Flow*, Washington, Hemisphere Pub. Corp., New York, McGraw-Hill, 1980.

[7] **Lloyd N. Trefethen and David Bau III**, *Numerical Linear Algebra*, Society for Industrial and Applied Mathematics, Philadelphia, 1997.

[8] **Francis B. Hildebrand**, *Advanced Calculus for Applications, Second Edition*, Prentice-Hall, Inc., Englewood Cliffs, New Jersey, 1976.

[9] **David Jacqmin**, *Some Convergence Results for Phase-Field Surface Tension Modeling of Two-Phase Navier-Stokes Flow*, The 1997 ASME Fluids Engineering Divisions Summer Meeting, June 22-26, 1997.

[10] **David Jacqmin**, *An Energy Approach to the Continuum Surface Tension Method: Application to Droplet Coalescences and Droplet/Wall Interactions*, Proceedings of the ASME Fluids Engineering Division, FED-Vol. 234, 1995 IMECE, ASME 1995.

[11] **N. Saunders and A.P. Miodownik**, *CALPHAD, Calculation of Phase Diagrams, A Comprehensive Guide*, Pergamon, 1998.

[12] **E.T. Turkdogan**, *Fundamentals of Steelmaking*, Institute of Materials, London, 1996.

[13] **U.B. Pal, S.A. MacDonald, D.W. Woolley, A.C. Powell and C.P. Manning**, *Enhancing Electrochemical Reactions in Smelting and Refining Operations*, 2001 Electric Furnace Conference Proceedings, ISS publication, pp. 323-336, 2001.

[14] **D.M. Anderson and G.B. McFadden**, *A Diffuse-Interface Description of Fluid Systems*, Applied and Computational Mathematics Division, National Institute of Standards and Technology, Gaithersburg, MD, Report No. NISTER 5887, August 1996.

[15] **J.E. Hilliard**, *Spinoidal Decomposition*, pages 497-560, American Society for Metals Press, Metals Park, Ohio, 1970.

[16] **J. J. Hoyt**, *The Continuum Theory of Nucleation in Multicomponent Systems*, Acta Metall. Mater. ,Vol. 38, No. 8, pp. 1405-1412, 1990.

[17] **Zhiqiang Bi, Robert F. Sekerka**, *Phase-field model of solidification of a binary alloy*, Physica A, pp. 95-106, 1998.

[18] **J.A. Warren and W.J. Boettinger**, *Prediction of Dendritic Growth and Microsegregation Patterns in a Binary Alloy Using the Phase-Field Method*, Acta metall. mater.,Vol. 43, No. 2, pp. 689-703, 1995.

[19] **David Jasnow and Jorge Vinals**, *Coarse-Grained Description of Thermo-Capillary Flow*, Phys. Fluids 8 (3), pp. 660-669, March 1996.

[20] **R. Tonhardt and G. Amberg**, *Phase-Field Simulation of Dendritic Growth in Shear Flow*, Journal of Crystal Growth 194, pp. 406-425, 1998.

[21] **Ravi Chella and Jorge Vinals**, *Mixing of Two-Phase Fluid by Cavity Flow*, Physical Review E, Vol. 53, No. 4, pp. 3832-3840, April 1996.

[22] MIT class notes, class title: Kinetic Processes in Materials, class number: 3.21, Spring 2001.

[23] MIT class notes, class title: Introduction to Numerical Simulation, class number: 2.096, Fall 2001.

[24] MIT class notes, class title: Numerical Methods for Partial Differential Equations, class number: 2.097, Spring 2001.